

POLITECNICO DI TORINO

Collegio di Ingegneria Energetica e Nucleare

Master of Science in Energy and Nuclear Engineering



“Development of a MPC controller for the indoor temperature of a nearly Zero-Energy Building. Application to the CorTau House.”

Supervisors:

Stefano Paolo Corgnati

Andrea Lanzini

Cristina Becchio

Daniele Salvatore Schiera

Candidate:

Vincenzo Ezio Santovito

July 2023

Abstract

The building sector accounts for up to one-third of the EU total final energy consumption, as most European houses and offices were built before 1990 and they did not undergo any major renovation. They show poor thermal insulation capability, and few strategies are implemented today to control and reduce the electricity and heating demands. Almost 40% of the total CO₂ emissions in Europe comes indeed from the building sector, both indirectly during the construction process and directly in the operational lifetime. The set of contaminants, however, also includes hydrofluorocarbons (i.e., greenhouse gases), fine particles (PM_{2.5}/PM₁₀) and toxic dusts, depending on the energy mix of each country. On average, natural gas covers 38.2% of the power demand from the residential stock in OECD countries, while a phasing-out 10% is covered with oil. The high release of pollutants from the building sector could be cut down with on-site renewable generation and an extensive adoption of smart monitoring systems. For this reason, on one side, technologically advanced devices such as hydrogen-fed fuel cells stacks may represent an interesting solution to push down emissions when green H₂ is exploited and, on the other, a reduction in the building energy load can be achieved digitalizing the stock and implementing control strategies for both the electricity and heating demand, keeping in any case high-quality indoor conditions for the household. In this context this study aims at developing a Model Predictive Control (MPC) strategy for the indoor air temperature of a nearly Zero-Energy Building. The heating load will be covered by a Proton Exchange Membrane Fuel Cells (PEMFC) stack. The case study is the CorTau House, a recently renovated single-family house located in Livorno Ferraris, in the province of Vercelli. A co-simulation interface between EnergyPlus and MATLAB is built, as the energy model of the house is developed in EnergyPlus, while both the controller and the fuel cell stack are designed in MATLAB. The schedule of the heating power supply computed by the controller and the corresponding indoor air temperature evolution in the house will be the ultimate results of the co-simulation, in accordance with a temperature setpoint to specify in the controller design phase.

Keywords: Thermal comfort, Building simulation, EnergyPlus, MATLAB, Co-simulation, Model Predictive Control, Proton Exchange Membrane Fuel Cell, Indoor Air temperature, Energy consumption, Digitalization.

Table of contents

1. INTRODUCTION.....	1
1.1. PROJECT MOTIVATION.....	1
1.2. METHODOLOGY.....	3
2. THE ENERGY PERFORMANCE OF BUILDINGS.....	5
2.1. OVERVIEW ON THE EU ENERGY PERFORMANCE OF BUILDINGS DIRECTIVE	5
2.2. FOCUS ON INDOOR THERMAL COMFORT.....	17
2.3. THE NZEB CORTAU HOUSE CASE-STUDY	23
2.3.1. <i>Introduction to the building and thermophysical characterization</i>	<i>23</i>
2.3.2. <i>Development of the EnergyPlus model</i>	<i>27</i>
3. PROTON EXCHANGE MEMBRANE FUEL CELL.....	39
3.1. OVERVIEW ON THE TECHNOLOGY.....	39
3.2. PEMFC BASICS AND MATHEMATICAL MODEL	41
4. MODEL PREDICTIVE CONTROL IMPLEMENTATION	55
4.1. INTRODUCTION TO MODEL PREDICTIVE CONTROL	55
4.2. DESIGN PARAMETERS SPECIFICATION	57
4.3. THE CONTROLLER MATHEMATICAL FORMULATION	60
4.4. MATLAB AND ENERGYPLUS CO-SIMULATION INTERFACE.....	65
4.5. MPC IMPLEMENTATION TO THE CORTAU HOUSE	71
4.5.1. <i>CorTau House performance in normal operation condition</i>	<i>71</i>
4.5.2. <i>CorTau House performance in extreme operations condition</i>	<i>75</i>
4.5.3. <i>Development of the linear model for each heated zone</i>	<i>78</i>
4.5.4. <i>MPC implementation with the control loop closure in MATLAB.....</i>	<i>87</i>
4.5.5. <i>MPC implementation with the control loop closure in EnergyPlus</i>	<i>99</i>
5. TECHNICAL AND ECONOMIC CONSIDERATIONS.....	109
CONCLUSIONS AND FURTHER RESEARCH	119
REFERENCES.....	122
APPENDIX A.....	127
APPENDIX B	131
APPENDIX C	133

List of figures

- Figure 1.1 - Goals and methodologies employed in the building control sector.
- Figure 2.1 - Buildings and construction's share of global energy-related CO₂ emissions, 2020.
- Figure 2.2 - Global direct CO₂ emission reductions through mitigation in the building sector in the 2050 net zero energy scenario.
- Figure 2.3 - Percentage of net imports in gross available energy of EU Member States in 2020 (yellow) and 2022 (blue).
- Figure 2.4 - Final energy consumption by sector in EU, 2020 (percentage of total, based on terajoules).
- Figure 2.5 - Integration of IoT devices into smart homes.
- Figure 2.6 - Example of Energy Efficiency Rating certificate according to Directive 2002/91/EC.
- Figure 2.7 - Example of recommended actions for energy efficiency improvement.
- Figure 2.8 - Annexes 1, 2 and 3 of Directive 2002/91/EC.
- Figure 2.9 - NZEB core and additional features according to EU requirements.
- Figure 2.10 - Example of cost-optimal graph for a building renovation.
- Figure 2.11 - Number of nearly zero energy buildings (nZEB) as of May 2017, by certification.
- Figure 2.12 - Human metabolic rate according to the type of activity in W/ m².
- Figure 2.13 - PMV scale definition.
- Figure 2.14 - Predicted Percentage of Dissatisfied (PPD) as a function of the Predicted Mean Vote index (PMV).
- Figure 2.15 - Sketch of the CorTau House project after the renovation.
- Figure 2.16 - Transversal section of the Cor-Tau house project.
- Figure 2.17 - Building plan subdivision according to the end use of each zone.
- Figure 2.18 - CorTau house east façade in OpenStudio.
- Figure 2.19 - CorTau house north façade in OpenStudio.
- Figure 2.20 - CorTau house south façade in OpenStudio.
- Figure 2.21 - CorTau house west façade in OpenStudio.
- Figure 2.22 - Thermal zones subdivision in the CorTau House building model as implemented in EnergyPlus.
- Figure 2.23 - Occupancy schedules during weekdays for all the thermal zones.
- Figure 2.24 - Occupancy schedules during weekends for all the thermal zones.
- Figure 2.25 - Activity level during weekdays for all the thermal zones.
- Figure 2.26 - Electric equipment schedules during weekdays for all the thermal zones.
- Figure 2.27 - Electric equipment schedules during weekends for all the thermal zones.
- Figure 2.28 - Lighting schedules during weekdays and weekends for all the thermal zones.
- Figure 2.29 - Hourly internal gains for ZT1 Kitchen during weekdays.
- Figure 2.30 - Hourly internal gains for ZT1 Kitchen during weekends.
- Figure 3.1 - Fuel cell schematic with reactants and products flow.
- Figure 3.2 - RedOx reactions for PEM fuel cells.
- Figure 3.3 - Membrane electrode assembly in PEMFC.

- Figure 3.4 - Regions involved in each step of the PEMFC operation.
- Figure 3.5 - Ideal fuel cell and Carnot efficiencies evolution with temperature.
- Figure 3.6 - Example of fuel cell polarization curve with voltage loss regions.
- Figure 3.7 - Curve Fitting Toolbox setting and result for the FCS 7-XXL stack polarization curve.
- Figure 3.8 - Polarization curve and voltage contributions to the stack electrical power and thermal loss depending on the current density.
- Figure 3.9 - FCS 7-XXL stack electrical and thermal power curves evolution.
- Figure 4.1 - Basic Structure of a general Model Predictive Control implementation.
- Figure 4.2 - MPC design parameters and input and output visualization.
- Figure 4.3 - Architecture of the BCVTB with the EnergyPlus client and other clients.
- Figure 4.4 - Evolution of the Heating Load during Winter Design Day for all the thermal zones.
- Figure 4.5 - Evolution of the indoor air temperature in free-running operations condition for all the thermal zones on January 8th.
- Figure 4.6 - Example of optimal overhang depth design.
- Figure 4.7 - Outdoor air drybulb temperature evolution in Turin, January 1st.
- Figure 4.8 - Pre-defined heating power schedule for January 1st.
- Figure 4.9 - Indoor air temperature results from EnergyPlus with the pre-defined heating power schedule.
- Figure 4.10 - Temperature deviation of the linear model from the EnergyPlus simulation in percentage over the latter.
- Figure 4.11 - Indoor temperature linear fitting with the pre-defined schedule.
- Figure 4.12 - MPC control strategy loop adapted to the CorTau House indoor air temperature management.
- Figure 4.13 - Controller development with YALMIP toolbox closing the loop in MATLAB.
- Figure 4.14 - Heating demand computed by the MPC with $\lambda = 0$.
- Figure 4.15 - Indoor temperature response of the building linear model with $\lambda = 0$.
- Figure 4.16 - Heating demand computed by the MPC with $\lambda = 1$.
- Figure 4.17 - Indoor temperature response of the building linear model with $\lambda = 1$.
- Figure 4.18 - Heat demand of ZT1 Kitchen depending on λ .
- Figure 4.19 - Indoor temperature response of ZT1 Kitchen depending on λ .
- Figure 4.20 - Heating demand computed by the MPC with $\lambda = 0.3$.
- Figure 4.21 - Indoor temperature response of the building linear model with $\lambda = 0.3$.
- Figure 4.22 - Co-simulation workflow between MATLAB Toolboxes and EnergyPlus through the MLE+ interface.
- Figure 4.23 - Controller development with YALMIP and MLE+ toolboxes closing the loop in EnergyPlus.
- Figure 4.24 - Heating demand computed by the MPC from the MATLAB and EnergyPlus co-simulation with $\lambda = 0$.
- Figure 4.25 - Indoor air temperature response from the MATLAB and EnergyPlus co-simulation with $\lambda = 0$.
- Figure 4.26 - Heating demand computed by the MPC from the MATLAB and EnergyPlus co-

-
- simulation with $\lambda = 1$.
- Figure 4.27 - Indoor air temperature response from the MATLAB and EnergyPlus co-simulation with $\lambda = 1$.
- Figure 4.28 - Effect of both the external temperature and solar radiation on ZT1 Kitchen indoor air temperature in free-running operation condition.
- Figure 4.29 - Heating demand computed by the MPC from the MATLAB and EnergyPlus co-simulation with $\lambda = 0.6$.
- Figure 4.30 - Indoor air temperature response from the MATLAB and EnergyPlus co-simulation with $\lambda = 0.6$.
- Figure 4.31 - Heating demand computed by the MPC from the MATLAB and EnergyPlus co-simulation with $\lambda = 0.6$ normalized over the floor area.
- Figure 4.32 - Total hydrogen consumption by one NEDSTACK FCS 7-XXL fuel cells' stack according to the heating request computed by the MPC.
- Figure 4.33 - Comparison between the building hourly electrical demand and the generation by one NEDSTACK FCS 7-XXL fuel cells' stack resulting from the heating schedule.
- Figure 4.34 - Position of the stack working points over the polarization and electrical power curves according to the MPC operation.
- Figure 5.1 - Production costs of hydrogen (€/kg) produced via water electrolysis powered with electricity sourced from the national power grid in EU as of March 2022.
- Figure 5.2 - Production costs of renewable hydrogen (€/kg) from PV directly connected to the electrolyser (without grid connection) in EU as of March 2022.
- Figure 5.3 - PV power production from the CorTau House roof panels.
- Figure 5.4 - Electrolyser energy consumption and running cost to meet the H_2 demand from the FC stack.

List of tables

Table 2.1	-	Energy performance efficiencies, parameters and indices for building classification.
Table 2.2	-	Climatic zones definition in Italy according to Presidential Decree No 412/1993.
Table 2.3	-	CorTau house specification.
Table 2.4	-	List of the CorTau House thermal zones with specifications.
Table 2.5	-	HVAC system specifications in the EnergyPlus model.
Table 2.6	-	Shell 175PC Photovoltaics Array Type properties.
Table 3.1	-	Nedstack FCS 7-XXL specifications.
Table 4.1	-	Winter Design Day specifications in the EnergyPlus model.
Table 4.2	-	Maximum hourly heating power from Winter Design Day.
Table 4.3	-	Cooling rate for all the building thermal zones at night.
Table 4.4	-	Pre-defined heating schedule U .
Table 4.5	-	Linear regression coefficients for each heated thermal zone.
Table 4.6	-	Definition of the MPC controller loop variables.
Table 5.1	-	Electrolysis system cost assuming a multi-MW AE system

List of equations

- Eq. (2.1) - Mean Radiant Temperature definition
- Eq. (2.2) - Predicted Percentage of Dissatisfied as function of the Predicted Mean Vote
- Eq. (2.3) - Heating Degree Day definition
- Eq. (3.1) - Carnot cycle limitation on heat engines' efficiency
- Eq. (3.2) - Standard enthalpy of formation of water
- Eq. (3.3) - Standard Gibbs free energy for water
- Eq. (3.4) - Fuel cell thermodynamic efficiency at STP
- Eq. (3.5) - Fuel cell electrical power generation
- Eq. (3.6) - Maximum fuel cell electrical power generation
- Eq. (3.7) - Fuel cell ideal standard potential
- Eq. (3.8) - Butler-Volmer equation for the activation overpotential
- Eq. (3.9) - Voltage loss in the ohmic polarization dominated region
- Eq. (3.10) - Fuel cell polarization curve expression
- Eq. (4.1) - General quadratic cost function formulation for a multi-input and multi-output problem in 2-Norm
- Eq. (4.2) - General quadratic cost function in vectorial notation
- Eq. (4.3) - Constrained Finite-Time Optimal Control problem formulation
- Eq. (4.4) - Linear multi-variable system description
- Eq. (4.5) - Constrained Finite-Time Optimal Control problem in vectorial notation
- Eq. (4.6) - Model Predictive Control problem formulation
- Eq. (4.7) - First element of the optimal input sequence
- Eq. (4.8) - Direct Normal Irradiation according to the ASHRAE Clear Sky model
- Eq. (4.9) - Thermal balance for each CorTau House zone
- Eq. (4.10) - Discretized thermal balance for each CorTau House zone
- Eq. (4.11) - Final expression for the indoor air temperature from the thermal balance
- Eq. (4.12) - Linear model for the building indoor temperature evolution
- Eq. (4.13) - Error introduced by the linear building model
- Eq. (4.14) - General objective function expression in the study
- Eq. (4.15) - Objective function expression for $\lambda = 0$
- Eq. (4.16) - Objective function expression for $\lambda = 1$
- Eq. (4.17) - FCS 7-XXL fuel cells' stack polarization curve expression
- Eq. (4.18) - Thermal power loss from the FCS 7-XXL fuel cells' stack as function of the current density
- Eq. (4.19) - Electrical power generated by the FCS 7-XXL fuel cells' stack as function of the current density
- Eq. (4.20) - Hydrogen consumption by the FCS 7-XXL fuel cells' stack as function of the current density
- Eq. (5.1) - Levelized Cost of Hydrogen (LCOH) definition

List of acronyms

AE	- Alkaline Electrolyser
AFC	- Alkaline Fuel Cell
AMSL	- Above Mean Sea Level
API	- Application Programme Interface
ASHRAE	- American Society of Heating, Refrigerating and Air-Conditioning Engineers
CAD	- Computer-Aided Design
CFTOC	- Constrained Finite-Time Optimal Control
CHP	- Combined Heat and Power
CL	- Catalytic Layer
DBT	- Dry Bulb Temperature
DF	- Daylight Factor
DGI	- Discomfort Glare Index
DM	- Decreto Ministeriale
DMFC	- Direct Methanol Fuel Cells
DNI	- Direct Normal Irradiation
EDA	- Electronic Design Automation
EES	- Energy Efficiency Solution
ENEA	- Energia Nucleare Energie Alternative
EP	- EnergyPlus
EPBD	- Energy Performance of Buildings
EPC	- Energy Performance Certificate
EPW	- EnergyPlus Weather
EU	- European Union
FCHO	- Fuel Cells and Hydrogen Observatory
GHG	- Greenhouse Gas
HDD	- Heating Degree Days
HFTC	- Hydrogen Feed Type Cells
HVAC	- Heating, Ventilation, and Air Conditioning
ICT	- Information and Communications Technology
IDF	- Intermediate Data Format
IEQ	- Indoor Environmental Quality
IoT	- Internet of Things
LCOH	- Levelized Cost of Hydrogen
LEED	- Leadership in Energy and Environmental Design
LoE	- Low Emissivity
MIMO	- Multi-Input Multi-Output
MPC	- Model Predictive Control
NECP	- National Energy and Climate Plan
NZEB	- Nearly Zero Energy Building

PCM	- Phase Change Material
PEMFC	- Proton Membrane Exchange Fuel Cell
PMV	- Predicted Mean Vote
PPD	- Predicted Percentage of Dissatisfied
PV	- Photovoltaic
RES	- Renewable Energy Sources
RH	- Relative Humidity
RHC	- Receding Horizon Control
SDP	- Semidefinite Programming
SeDuMi	- Self-Dual-Minimization
SISO	- Single-Input Single-Output
TPB	- Triple Phase Boundary
ZEB	- Zero Energy Building
ZT	- Thermal Zone (Zona Termica)

1. Introduction

1.1. Project motivation

The renovation and decarbonization of the EU's building stock is among the key objectives of the Green Deal set of initiatives through which the European Commission aims at reaching the ambitious goal of carbon neutrality by 2050. The reasons behind the high effort put in this direction is primarily due to the evidence that this sector is responsible for almost 40% of the total European countries demand for energy according to the DIRECTIVE 2010/31/EU of Energy Performance of Buildings (EPBD) and it is in charge of about 36% of the total EU greenhouse gases (GHG) emissions, with more than 60% of all imported natural gas used to cover houses and offices energy demand. Given that 86% of the housing stock in south Europe was built before 1990 and did not undergo any renovation, an improvement in their energy performance is necessary to drastically reduce their footprint. Poor thermal insulation capability, infrequent implementation of electricity saving strategies and the reliance on fossil fuels for both heating and power demand are the main issues that the building sector needs to face nowadays. Finally, an efficient building performance directly reflects on bills reduction and the improvement of the household living quality, in terms of both thermal and lightning comfort and air quality levels. The amended Energy Efficiency Directive (EU) 2018/2002 updated the Directive 2012/27/EU, setting a target of energy efficiency improvement of at least 32.5% for 2030. The Article 9 of the EPBD introduced the concepts of the Net Zero-Energy Building (NZEB) and nearly Zero-Energy Building (nZEB) [4], whose design is made following bioclimatic architecture principles to cut down the energy request and ensuring that a large amount of the energy demand, both in terms of space heating and electricity, is covered by RES.

Each EU country transposes both directives to their regulation, establishing a 10-year integrated National Energy and Climate Plan (NECP) for 2021-2030 to reach their goals.

A variegated set of actions can be taken to modernize the building stock. These include on one side the improvement of the thermophysical properties of the envelope, for instance adopting PCM material to insulate the building, renovating the windows glazing and sealing connections, but also integrating the newest technologies to produce and supply heat and power on site, reducing the user dependence on the gas

and electricity grids. The implementation of Demand Side Management strategies can push down wasted energy and the costs charged to the house inhabitants. A combination of these expedients can contribute to save on fuel consumption, (between 50-70% reduction), using more efficient heating and cooling equipment to satisfy loads (for instance Fuel Cells) and implementing energy control strategies, i.e., digitalizing the energy systems for buildings. The U.S. Department of Energy states that the integration of both sensors and controls into commercial buildings can lead to an estimated 29% saving in energy consumption, as the building operation would be led by optimized and high-performance scheduled sequences resulting from each controller operation.



Figure 1.1 – Goals and methodologies employed in the building control sector.

Source: U.S. Department of Energy.

Exactly in this context this work aims at developing a control algorithm to integrate a hydrogen Fuel Cell into a residential building located in Livorno Ferraris (VC), to supply heat and electricity in the winter season. Fuel cells are among the most promising technologies in the decarbonization process of all energy intensive sectors, from industry to residential to transport. This is particularly true when the hydrogen employed as energy vector is produced through electrolysis powered by renewables. The advantage of this technology is that it can provide both heat and electricity through an electrochemical process which, as in Proton Exchange membrane Fuel Cells (PEMFC), runs on pure Hydrogen and avoids pollutants emissions.

1.2. Methodology

The first requirement to develop this research is the availability of a building model suited to perform energy balance simulation. EnergyPlus is a whole building energy simulation program that engineers, architects, and researchers use to model both energy consumption for heating, cooling, ventilation, lighting and plug and process loads, and water use in buildings [5].

The building is commonly modelled as an Intermediate Data Format (IDF) file, a format used to interoperate between electronic design automation (EDA) software and solid modelling mechanical computer-aided design (CAD) software [6]. This IDF file contains all the information needed to run energy dynamic simulation, including the geometrical characterization and several functionality and advanced features to make it as similar as possible to the actual building. For instance, it can include occupancy and lightning schedules, HVAC system operation, combined heat and mass transfer models and the building subdivision in thermal zones. The software requires a weather data file in the EPW format, which provides a database of weather data for a given specific location.

The controller is designed in MATLAB, and the YALMIP Toolbox is used to declare both the decision and the output variables and to formulate the core optimization algorithm of the MPC, namely the objective function and the problem constraints.

The main goal would be setting a co-simulation framework between EnergyPlus and the MATLAB environment to implement the Model Predictive Control (MPC) technique. This can be achieved with the aid of advanced MATLAB toolboxes like MLE+ and the Building Controls Virtual Test Bed, to implement a continuous data exchange as input to and output from EnergyPlus. MPC is a powerful feedback control algorithm based on optimization. It uses a model to make predictions about future outputs of a variety of processes. The reasons behind the spread of this powerful control strategy are first its capability of handling multi-input multi-output (MIMO) systems, in which a change on one single output can have an impact on all the others, and secondly the possibility of imposing constraints on the system state, meaning that in principle both the decision and the output variable can be limited within some previously defined boundaries during the controller operation. This is a MPC peculiarity, as for other techniques in which the actuation is thought-out as a continuous variable, in some cases the controller optimization core could compute an

input sequence resulting unfeasible for the real application it refers to. Finally, Model Predictive Control can be implemented for both linear and non-linear models. Even if the linear MPC design is easier and the controller optimizer works faster, many real-world phenomena are intrinsically non-linear, and they are therefore described by non-linear models. If this non-linearity is nonetheless moderate, the so-called Adaptive and Gain Scheduled MPC controllers are the two available methods to couple with a local linearization of the model.

With reference to the methodology developed in this study, starting from an initial plant state (the building indoor air temperature), the main idea is to run forecasts of a simplified model of the plant over a short period, minimizing at each time step the deviation of the plant state from a reference (the indoor temperature deviation from the setpoint for each heated room). The variable over which the optimization is performed is the heat generated by the fuel cell as a by-product of the exothermic H_2/O_2 reaction and the simplified model to feed to the controller would be a linearized energy balance on each confined zone of the building. As the control action sequence is computed, the ultimate result would be the hydrogen rate required to feed a PEMFC stack to ensure the MPC schedule is respected.

2. The energy performance of buildings

2.1. Overview on the EU Energy Performance of Buildings Directive

The great effort put by the European Union in recent years to pursue an organic and effective energy transition set of policies, with an acceleration over the last two decades, is a unicum in the current global context. The Paris Agreement is the international treaty on climate change negotiated at the 2015 UN Climate Change Conference in Paris and it is the general framework in which all the actors involved in the transition process should move. The Agreement clearly states that to keep the global temperature rise below 2°C, a net zero CO₂ emissions goal must be achieved by 2050. As of 2020, the buildings and construction sector accounted for 37% of the global energy-related CO₂ emissions. Figure 2.1 reports the carbon dioxide global emissions from each polluting sector with data calibrated in percentage over the total. The share of building emissions is broken down into residential and non-residential, direct, and indirect. Indirect emissions are those related to the heat and electricity generation. The construction industry emissions are instead those coming from the production of all construction materials supplied to the building sector.

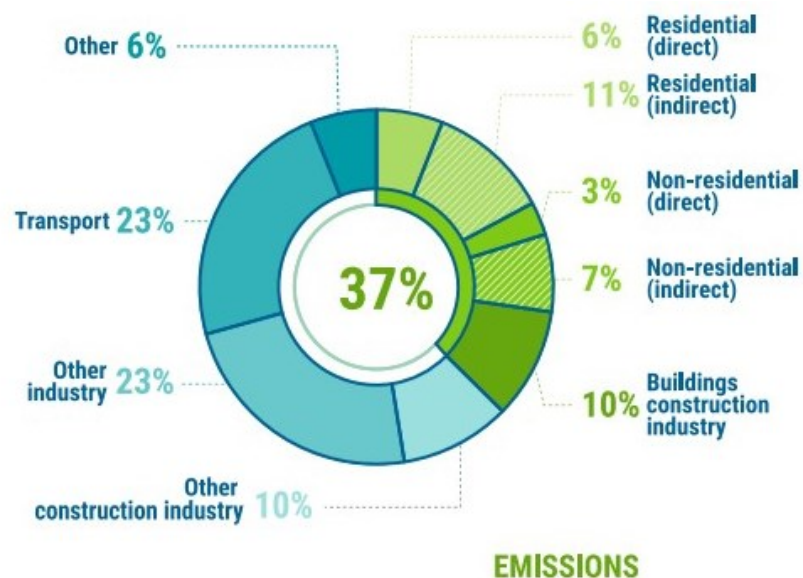


Figure 2.1 – Buildings and construction's share of global energy-related CO₂ emissions, 2020.

Source: IEA 2021a. All rights reserved. Adapted from "Tracking Clean Energy Progress".

In 2021 the International Energy Agency (IEA) proposed a roadmap to reduce the direct CO₂ emissions from the building sector to meet the 2050 Paris Agreement requirements. It included several mitigations measures, and it quantified the impact of each on the global emissions reduction in the 2020-2050 timeframe. The adoption of energy efficiency improvement measures and the complete electrification of the stock would together account for almost 70% of the total CO₂ emissions' reduction required by the Agreement. The IEA predictions are shown in Figure 2.2, in which the "Activity" label stands for the forecasted variation in CO₂ emissions due to increased population and welfare from 2020 to 2030 and from 2030 to 2050.

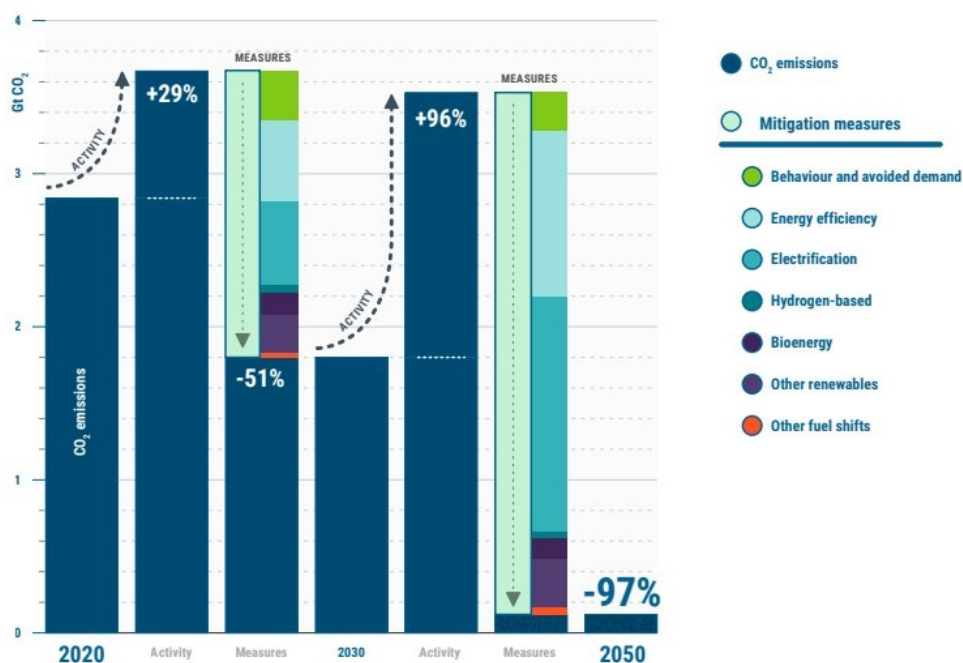


Figure 2.2 – Global direct CO₂ emission reductions through mitigation in the building sector in the 2050 net zero energy scenario.

Source: IEA 2021c, Net Zero by 2050: A Roadmap for the Global Energy Sector.

The long-standing EU's energy dependency issue, especially for what concern fossil fuels such as crude oil, coal, and natural gas, worsened from 2000 to 2020. The energy dependency, quantified as the extent to which each country relies on foreign imports, increased from 56.3% to 57.5% over this 20-year timeframe, and more than a half of the total EU energy needs are thus nowadays covered through foreign countries net inputs

[25]. For instance, EU imported 26.9% of crude oil from Russia as of 2020, a percentage larger than the next three countries combined, being Iraq, Nigeria, and Saudi Arabia. The energy dependence from these countries easily translates into a political and economic one and in fact plans to blackmail Europe over gas supply became reality since the outbreak of war in Ukraine.

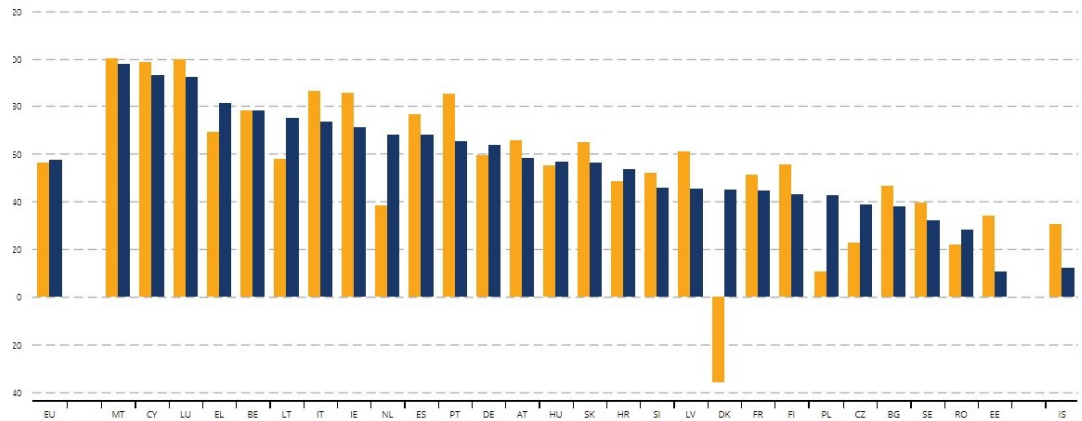


Figure 2.3 – Percentage of net imports in gross available energy of EU Member States in 2020 (yellow) and 2022 (blue).

Source: Eurostat Database, 2022.

For this reason, considering alternative and renewable energy sources, preferably produced on site and especially for sector which could be easily decarbonized such as the building one (apart from the materials production process), is a priority.

The second important pillar of the EU strategy is decreasing the Member States energy demand. The focus is put on the building stock, but attention is also put on transportation. By analysing the final end use of energy in EU in 2019 by sector, transport, households, and industry play a major role, each accounting for about 26-28% of the total consumption as reported in Figure 2.4. The key point here is that there is much room for improvement in the building sector as far as proper legislative actions are taken, incentives for instance.

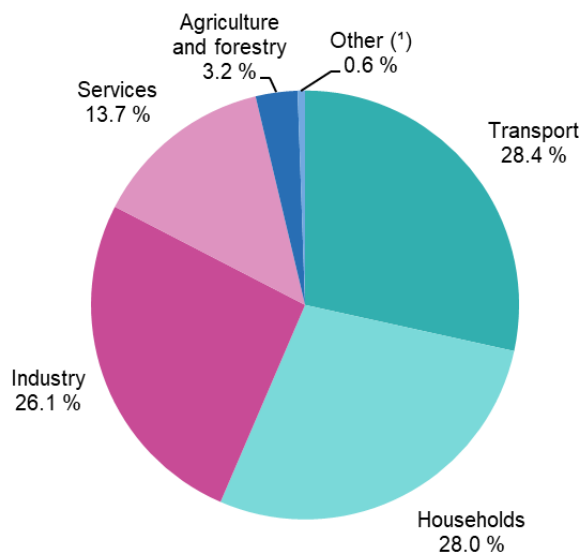


Figure 2.4 – Final energy consumption by sector in EU, 2020 (percentage of total, based on terajoules).

Source: Eurostat Database, 2022.

The renovation of the building stock and the adoption of more efficient energy systems are measures expected to go hand in hand with an increase of the users' awareness on the topic. Demand management strategies and behavioural changes can positively impact the final energy consumption by households, and not to mention, of course, that an energy bill reduction would look appealing also to those least sensitive to the themes of energy and climate change.

Also, the digital transformation is expected to play a key role in the building sector, as a transition towards fully electric buildings is already taking place. Soon a new paradigm is expected to emerge, that is energy will be run by information. The monitoring of all building systems, with systems in charge of ensuring proper indoor quality conditions through sensors and through real-time data exchange with feedback to occupants, is expected to improve the building performance and the life quality of the household. Information and Communications Technology (ICT) and Internet of Things (IoT) are stepping into the sector with solutions for the automatic and remote management of all the systems and objects inside the home, aiming at reducing the consumptions on one side but also improving the comfort and safety of the people. The same idea applies also for instance to the optimization of the water consumption in

what are typically called smart communities.

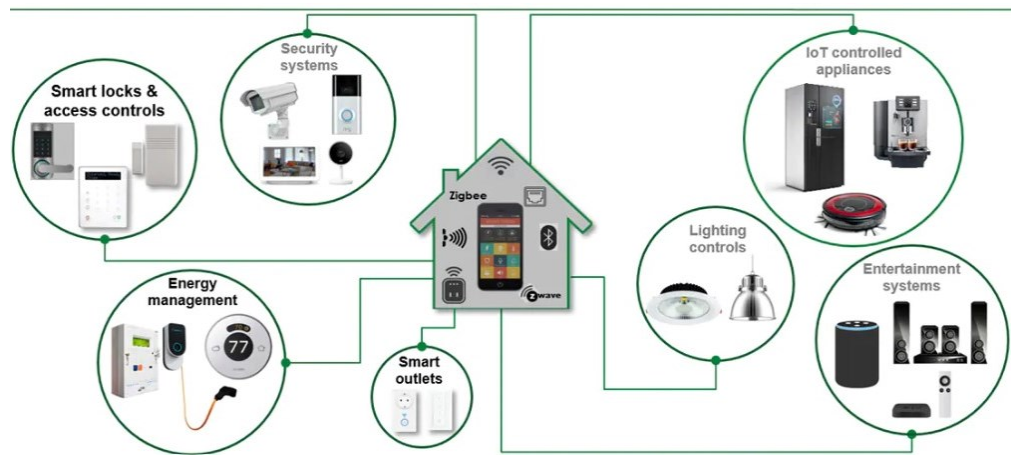


Figure 2.5 – Integration of IoT devices into smart homes.

Source: Littelfuse®.

The Energy Performance of Buildings Directive, commonly referred to as EPBD, is the legislative instrument adopted by the European Union to increase the energy performance in the building sector, acting on residential, commercial, and public premises. The directive provides standards for both new buildings and renovations. A series of recasts was released by the European Commission over the years, as new concerns and needs raised. Each EU Member State adopts the EPBD and implements it in practice in accordance with the features of the country building stock and the climatic zone. This means that different strategies are adopted, and the effort put in the EPBD implementation is still not uniform across the European countries.

The first version of the EPBD, Directive 2002/91/EC, was released on 16th December 2002 and became effective on 4th January 2003. The key point at the time was the introduction of the Energy performance certificates (EPCs), a measure of the building energy performance on a A-G scale. A-rated buildings are highly energy efficient, and they are characterized by the lowest running costs. The opposite holds for G-rated buildings. The certificate first provides the total energy cost of the building including heating, hot water, and lighting. The Energy Efficiency Rating section follows, in which a current rating is given to the building in accordance with its energy efficiency as specified above. The higher the rating the lower the bills are expected to be. A potential rating also provides how the energy efficiency would improve by adopting some

recommended measures, i.e., both internal and external walls insulation. This EPC section provides this set of recommended measures along with an approximate initial investment and the expected savings per year for each single measure.

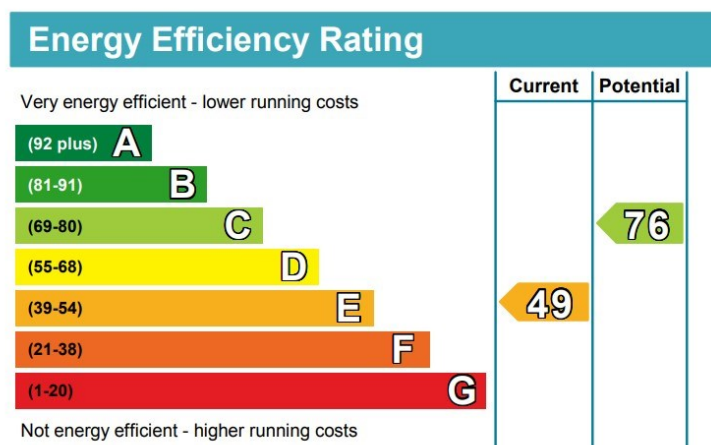


Figure 2.6 – Example of Energy Efficiency Rating certificate according to Directive 2002/91/EC.

Source: Example of an Energy Performance Certificate. Government of the United Kingdom, 2012

Top actions you can take to save money and make your home more efficient			
Recommended measures	Indicative cost	Typical savings over 3 years	Available with Green Deal
1 Increase loft insulation to 270 mm	£100 - £350	£141	✓
2 Cavity wall insulation	£500 - £1,500	£537	✓
3 Draught proofing	£80 - £120	£78	✓

Figure 2.7 – Example of recommended actions for energy efficiency improvement.

Source: Example of an Energy Performance Certificate. Government of the United Kingdom, 2012

EPCs are valid for 10 years from the issue date and they are a well-established instrument to compare buildings' energy performance. The major drawback related to the certificate is that a gap between the certificate and the actual energy expenditure is usually observed as the calculated performance of the building can in principle be quite far from the real one. The household behaviour and the weather are crucial players in this sense.

The Directive also refers to the importance of active solar systems and other heating

and electricity equipment relying on RES. A discussion on the economic feasibility of CHP (combined heat and power) systems is also opened, even if just for new buildings with a total useful area beyond 1000 m².

As mentioned before, each Member State is expected to apply a methodology, set at national or even regional level, to produce one or more indicators on the energy performance of buildings. The main aspects to include are reported in the Directive 2002/91/EC Annexes 1 and 2, while Annex 3 provides a classification on the building typology according to its use.

ANNEX	
General framework for the calculation of energy performance of buildings (Article 3)	
1.	The methodology of calculation of energy performances of buildings shall include at least the following aspects: <ul style="list-style-type: none"> (a) thermal characteristics of the building (shell and internal partitions, etc.). These characteristics may also include air-tightness; (b) heating installation and hot water supply, including their insulation characteristics; (c) air-conditioning installation; (d) ventilation; (e) built-in lighting installation (mainly the non-residential sector); (f) position and orientation of buildings, including outdoor climate; (g) passive solar systems and solar protection; (h) natural ventilation; (i) indoor climatic conditions, including the designed indoor climate.
2.	The positive influence of the following aspects shall, where relevant in this calculation, be taken into account: <ul style="list-style-type: none"> (a) active solar systems and other heating and electricity systems based on renewable energy sources; (b) electricity produced by CHP; (c) district or block heating and cooling systems; (d) natural lighting.
3.	For the purpose of this calculation buildings should be adequately classified into categories such as: <ul style="list-style-type: none"> (a) single-family houses of different types; (b) apartment blocks; (c) offices; (d) education buildings; (e) hospitals; (f) hotels and restaurants; (g) sports facilities; (h) wholesale and retail trade services buildings; (i) other types of energy-consuming buildings.

Figure 2.8 – Annexes 1, 2 and 3 of Directive 2002/91/EC.

Source: Directive 2002/91/EC of the European Parliament and of the Council of 16 December 2002 on the energy performance of buildings, Official Journal L 001, 04/01/2003 P. 0065 – 0071.

Directive 2010/31/EU is the first EPBD recast to date, released on 19th May 2010 and effective starting on 18th June 2010. Various reasons lay behind the needs of a recast of the original Directive. At that time the building sector was responsible of 40% of the total energy consumption in the European Union and, as the sector itself was expanding, new policies and strategies were needed to mitigate its increasing environmental impact. Directive 2010/31/EU was released five years after the Kyoto Protocol entered into force (16th February 2005) and thus it had to comply with its main commitments:

- ➔ Future global warming should be limited below 2°C relative to the pre-industrial temperature level.
- ➔ The total GHG emission should be reduced by 20% as of 2020 with respect to the 1990 levels.

The recast also aimed at reducing the large gap between the Member States' results in improving the energy performance of their own building stock that had risen since the release of Directive 2002/91/EC.

The concept of nearly Zero-Energy Building (nZEB) was introduced here for the first time. Such buildings are characterized by a high energy performance, and the low amount of energy that is however required is largely covered by RES, preferably produced on-site or nearby.

According to the Directive, all new buildings should meet the nZEB requirements by 31 December 2020, and the Member States should also promote the refurbishment of the pre-existing stock in the same direction. The nZEB definition is task of each Member State and is quantified in a numerical indicator of primary energy use expressed in kWh/m² per year. The nZEB design, however, should be carried out not only focusing on energy related matters but also considering economic aspects.

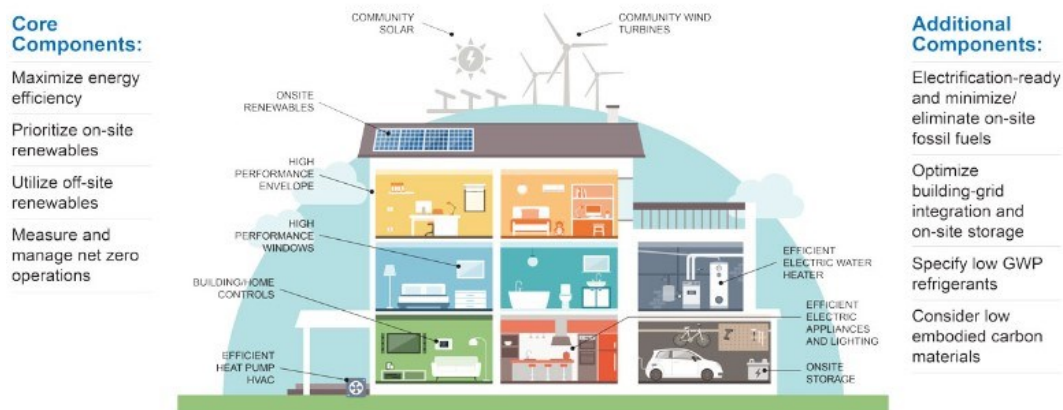


Figure 2.9 – nZEB core and additional features according to EU requirements.

Source: S. Hobart, M. Schantz, The Time for a Net-Zero Building Boom is Now, UrbanLand, March 26, 2021

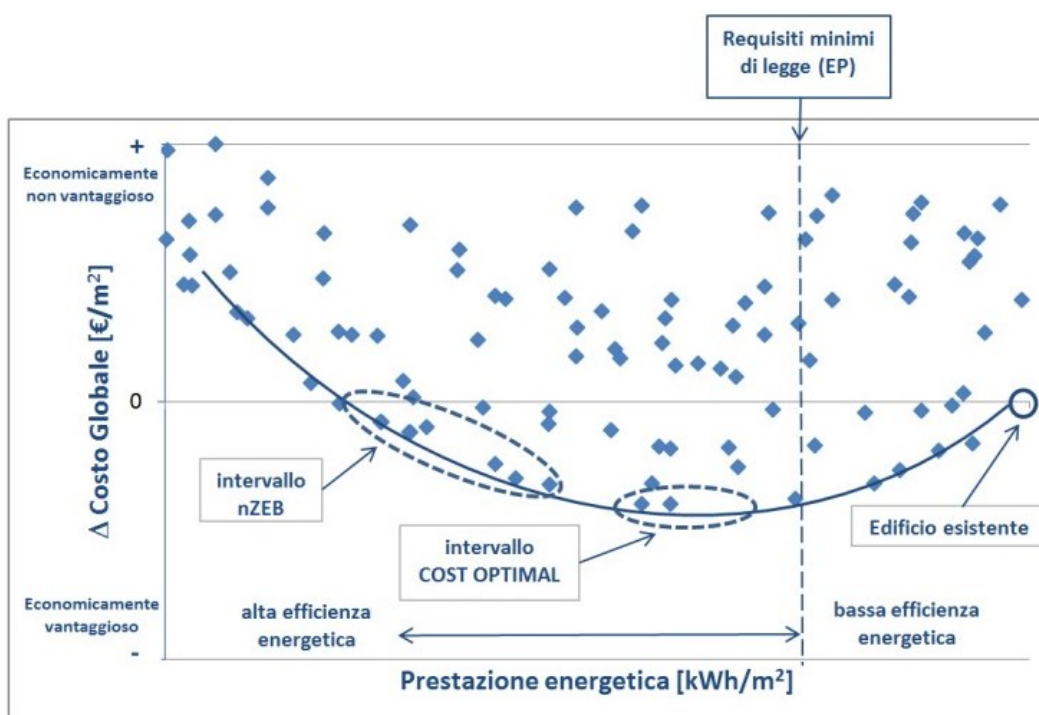


Figure 2.10 – Example of cost-optimal graph for a building renovation.

Source: Riquilificazione energetica degli edifici pubblici esistenti: direzione nZEB, V. Corrado, I. Ballarini, G. De Luca, E. Primo, D. Iatauro, ENEA, Report RdS/PAR2016/252.

The Directive encourages to follow a cost-optimal approach, pursuing the best compromise between the initial investment on the energy equipment and the savings expected throughout the building lifetime. In general, higher investments on the energy systems and on the thermal envelope solutions are expected to bring higher energy efficiencies and probably less maintenance costs over the years. The cost-optimal analysis takes into consideration a set of possible Energy Efficiency Solutions (EESs) including building envelope EES, HVAC/Energy Systems EESs and renewable energy sources EESs. At the design stage of the new construction or the renovation process these solutions are combined in a matrix form and displayed over a cost-optimal graph. This diagram shows the primary energy consumption (kWh/m²/year) versus global cost (€/m²) for each combination. The cost-optimal range gathers the EESs combinations with the best compromise between the investment cost and the yearly energy demand. Figure 2.10 shows an example of the cost/energy performance resulting trend.

Directive 2018/844/EU, released on 30th May 2018 and effective starting on 19th June 2018, pushes further the requirements on new buildings refurbishments. The European Commission emphasizes the need to decarbonise the building stock and pushes to 40% the reduction of the total GHG emission with respect to 1990 levels by 2030. The energy poverty issue is addressed, and each Member State oversees adopting proper actions to alleviate the problem in the weakest portion of the national building stock. Emphasis is also put on digitalisation, particularly on what concerns renewables integration and smart grids, but also on the consumer increased attention on monitoring emissions and indoor quality parameters like indoor air temperature. The integration of automatic controls is also encouraged to ensure efficient and safe building operations. Real-time energy monitoring can in fact reduce the gap between the calculated and the real energy performance of the building by driving a more conscious behaviour in the user.

As of 2020, the implementation of the EPBD Directive and its recasts in Italy is mainly focused on renovations rather than new buildings, as the construction rate is quite low. The Italian regulation for nZEBs is contained in the Ministerial Decree “Applicazione delle metodologie di calcolo delle prestazioni energetiche e definizione delle prescrizioni e dei requisiti minimi degli edifici”, which was released on 26th June 2015 and is commonly referred to as “DM Requisiti Minimi”. The parameters and indices

reported in Table 2.1 are taken from the Decree Annex 1 and are those required for new buildings but also major renovations to meet the nZEB requirements in Italy, starting from 2019 for public buildings and from 2021 for all the others.

Table 2.1 – Energy performance parameters for building classification.

H'_T [W/m ² K]	Global average heat transfer coefficient per unit of building surface area.
$A_{sol,est} / A_{sup\ utile}$ [-]	Ratio of the buildings' summer solar radiation surface to useful surface area.
$EP_{H,nd}$ [kWh/m ²]	Thermal performance index of heating.
η_H [-]	Average seasonal efficiency of air conditioning system during winter season.
EP_H [kWh/m ²]	Energy performance index of air conditioning system during winter season, expressed as non-renewable or total primary energy.
$EP_{W,nd}$ [kWh/m ²]	Thermal performance index of domestic hot water production.
EP_W [kWh/m ²]	Energy performance index of domestic hot water production, expressed as non-renewable or total primary energy.
η_w [-]	Average seasonal efficiency of domestic hot water system.
EP_v [kWh/m ²]	Energy performance index of ventilation, expressed as non-renewable or total primary energy.
$EP_{C,nd}$ [kWh/m ²]	Thermal performance index of cooling.
η_c [-]	Average seasonal efficiency of air conditioning system during summer season (eventually including humidity control).
EP_c [kWh/m ²]	Energy performance index of air conditioning system during summer season, expressed as non-renewable or total primary energy.
EP_L [kWh/m ²]	Energy performance index of artificial lighting, expressed as non-

	renewable or total primary energy.
EP_T [kWh/m ²]	Energy performance index of people and objects transport (elevators, sidewalks, and escalators), expressed as non-renewable or total primary energy.
$EP_{gl} = EP_H + EP_W + EP_V + EP_C + EP_L + EP_T$ [kWh/m ²]	Global energy performance index of the building, expressed as non-renewable or total primary energy.

Source: Decreto interministeriale 26 giugno 2015 - Applicazione delle metodologie di calcolo delle prestazioni energetiche e definizione delle prescrizioni e dei requisiti minimi degli edifici.

The nearly Zero-Energy Buildings certified in Italy as of May 2017 are grouped in Figure 2.11 according to the certification, with LEED and CasaClima ones leading.

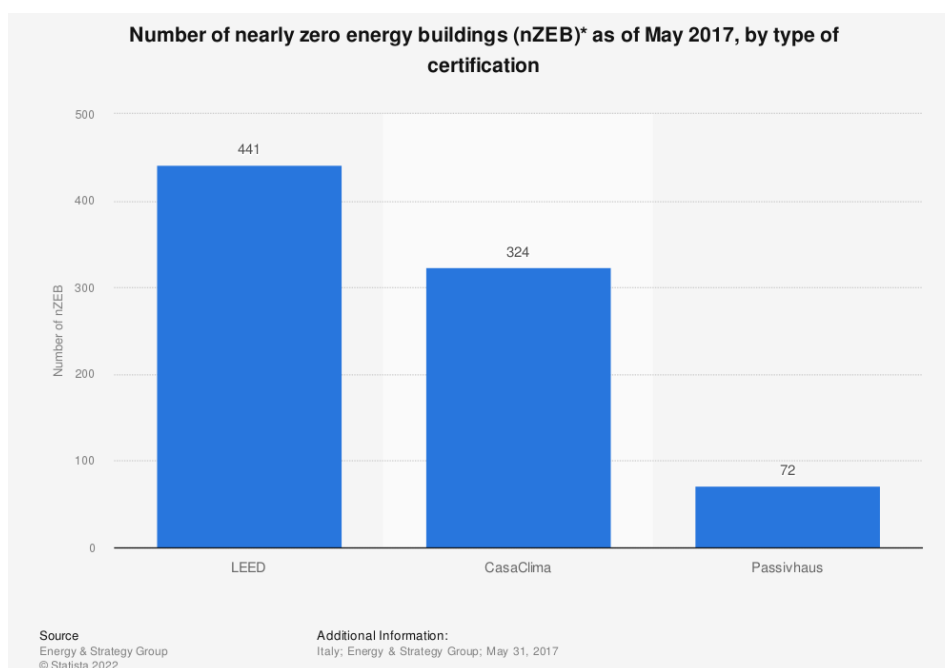


Figure 2.11 - Number of nearly zero energy buildings (nZEB) as of May 2017, by certification.

Source: Energy & Strategy Group. (July 26, 2017). Number of nearly zero energy buildings (nZEB)* as of May 2017, by type of certification [Graph]. In Statista.

The most recent revision of the EPBD was proposed by the European Commission on 15th December 2021 and it included:

- Obligation for all member states to establish national building renovation plans.
- Establishment of minimum energy performance standards (MEPS), requiring the worst energy performant (non-residential) buildings to reach at least class F by 2030 and class E by 2033.
- Introduction of new financial mechanisms to incentivize banks and mortgage holders to promote energy efficient renovation (mortgage portfolio standard).
- Obligation to ensure new buildings are solar ready and to install solar energy equipment on pre-existing ones.

2.2. Focus on indoor thermal comfort

The Indoor Environmental Quality IEQ of a building is interpreted as the quality of a building's indoor environment related to the health of the occupants. This item is a critically important credit category in the LEEDTM (Leadership in Energy and Environmental Design) rating system. Various aspects are considered in literature to assess what influences the IEQ of an indoor environment, with the main ones reported here:

- Thermal quality or comfort.
- Visual quality or comfort (taking into account the Daylight Factor DF and the Discomfort Glare Index DGI).
- Acoustic quality or comfort.
- Air quality.
- Hygroscopic quality.

Thermal comfort and satisfaction is nowadays the key parameter to focus the attention on when designing a new building or retrofitting an already existing construction. This

is due to the fact that the household's health and well-being is primarily influenced by their thermal sensation, and this has a direct impact on their everyday life and productivity. The UNI EN ISO 7730:2006 norm defines thermal comfort as "that condition of mind which expresses satisfaction with the thermal environment", or, in other words, that condition in which neither a too hot nor a too cold thermal sensation is experienced by the household. Defining a general and unique parameter to assess whether an environment is comfortable or not in terms of temperature is quite hard, as this is extremely dependent on each individual sensitivity and several environmental (i.e., external) and personal (i.e., internal) factors. Thermal comfort is regulated by the already mentioned ISO 7730 but also by the ASHRAE Standard 55 (2017).

The main environmental factors, the most important are:

- Air Temperature T_a , defined as the dry bulb temperature (DBT) of the air in contact with the body.
- Mean Radiant Temperature T_{mr} , defined as the uniform temperature of a hypothetical spherical surface surrounding the person that would exchange the same net radiative energy as the real environment. It can be computed as the temperature of all the surfaces surrounding the person weighted on the surfaces themselves:

$$T_{mr} = \frac{\sum_i T_i A_i}{\sum_i A_i} \quad (2.1)$$

- Relative humidity RH , defined as the ratio between the actual water content in air and the maximum amount it can hold at that temperature, expressed in percentage.
- Air velocity w , the velocity of the air in contact with the person, measured in m/s. Higher air velocity means higher heat exchange between the person and the air (i.e., the environment).

Both T_a and T_{mr} can be controlled by increasing the energy performance of the walls.

For the subjective parameters, the attention is typically focused on:

- Metabolic Rate or Level of Activity, described as the heat produced by the person accordingly to the activity they are doing. Some examples are reported in Figure 2.12.

Activities	W/m ²
Resting	
Sleeping	40
Reclining	45
Seated, quiet	60
Standing, relaxed	70
Walking (on level surface)	
3.2 km/h (0.9 m/s)	115
4.3 km/h (1.2 m/s)	150
6.4 km/h (1.8 m/s)	220
Office activities	
Reading, seated	55
Writing	60
Typing	65
Filing, seated	70
Filing, standing	80
Walking about	100
Lifting/packing	120

Figure 2.12 – Human metabolic rate according to the type of activity in W/m².

Source: ASHRAE Handbook Fundamentals, 2005.

- Clothing level, directly controlled by the person.

Thermal comfort can be maintained only when the heat produced by the metabolism equals the heat expelled by the person.

Even though different models have been developed to deal with the thermal comfort issue, the one proposed by Povl Ole Fanger is the most famous and the one generally employed to draft regulation on this topic. The Fanger theory provides a method to predict whether a certain thermal environment would be acceptable to a large group of people and thus deals with the thermal comfort issue with a statistical approach. A

deep description of the whole Fanger theory is out of the scope of this study. The main result is that the theory reduces to the definition of two parameters:

- PMV, Predicted Mean Vote, which predicts the subjective ratings of the environment in a group of people. This index is based on the seven-point thermal sensation scale provided by the ASHRAE and its scale is reported in Figure 2.13.

No.	Definition	Numerical value
1	Cold	-3
2	Cool	-2
3	Slightly cool	-1
4	Neutral	0
5	Slightly warm	+1
6	Warm	+2
7	Hot	+3

Figure 2.13 – PMV scale definition.
Source: ASHRAE Handbook Fundamentals, 2005.

The value of PMV, in the range (-3; +3), is directly related to a thermal sensation definition through the scale from cold to hot.

- PPD, Predicted Percentage of Dissatisfied, an indicator of the percentage of the people in the indoor environment under analysis that would not be thermally satisfied as a function of the PMV.

$$PPD = 100 - 95 \cdot e^{(-0.03353 \cdot PMV^4 - 0.219 \cdot PMV^2)} \quad (2.2)$$

The evolution of the PPD as a function of the PMV expressed in Eq. (2.2) is sketched in Figure 2.14. It is worth pointing out that even at thermal neutrality (i.e., $PMV = 0$) about 5% of the people in the room may still be dissatisfied, in line with the high variability of each individual sensitivity to the environment in terms of temperature. This means that the design objective should be exploring a range of acceptable thermal conditions rather than a single puntual one, or, in other words, how much the indoor conditions could deviate from the optimum without drastically increasing the percentage of dissatisfied people.

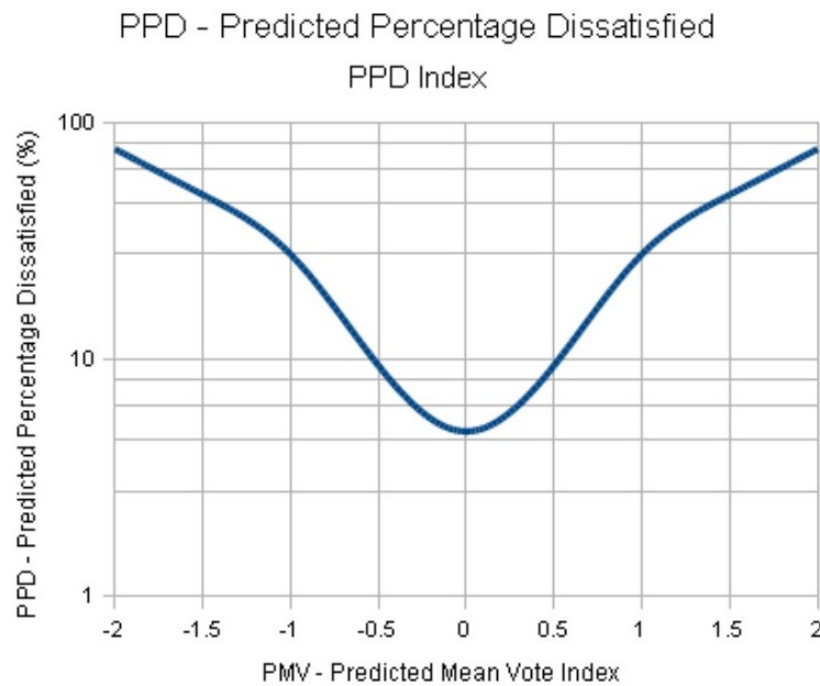


Figure 2.14. – Predicted Percentage of Dissatisfied (PPD) as a function of the Predicted Mean Vote index (PMV).

Source: The Engineering Toolbox.

For what concerns the heating season and regardless of each individual sensitivity to the temperature (the application of the Fanger theory is in this sense sufficient), the Italian legislation and more specifically the Presidential Decree No 412/1993 sets an indoor temperature lower limit of 18 °C for industrial environments and 20 °C in residential buildings, offices, and schools. A tolerance of 2 degrees in the latter is generally accepted. The Presidential Decree divides the country into six climatic zones, and it establishes the starting date and the duration of the heating season for each of them. The subdivision into climatic zones is based on the number of heating degree days HDD and it is independent from the geographical location. The HDD number is defined as the sum over the entire year of the difference (only if positive) between the reference indoor temperature, conventionally fixed to the residential 20°C winter setpoint, and the average daily outdoor temperature. The higher will be this number, the colder is the location. The expected heating demand is directly linked to it.

$$HDD = \sum_{i=1}^{365} (20 - \bar{T}_{outdoor})$$

(2.3)

The Ministry of Ecological transition adopted a set of emergency measures to face the energy crisis that followed the outbreak of war in Ukraine. These are collected in the “Piano nazionale di contenimento dei consumi di gas naturale”. For residential buildings the indoor temperature limit is lowered to 19 °C, while the heating season and the number of daily heating hours is reduced by 15 days and 1 hour respectively. The measures are implemented starting from winter 2022/2023 and the consequent annual savings of natural gas are expected to reach 2.697.249.794 SCM [26].

Table 2.2 – Climatic zones definition in Italy according to Presidential Decree No 412/1993.

ZONE	DEGREE DAYS	HEATING SEASON	DAILY HEATING HOURS
A	Less than 600	December, 1st – March, 15th	6
B	Between 600 and 900	December, 1st – March, 31st	8
C	Between 901 and 1400	November, 15th – March, 31st	10
D	Between 1401 and 2100	November, 1st – April, 15th	12
E	Between 2101 and 3000	October, 15th – April, 15th	14
F	More than 3001	All year	No limitation

Source: Authors' elaboration.

2.3. The nZEB CorTau House case-study

2.3.1. Introduction to the building and thermophysical characterization

Within the context of the implementation of the DIRECTIVE 2010/31/EU of Energy Performance of Buildings (EPBD) and thus the development and construction of nZEB, the CorTau House is a significative project developed in Livorno Ferraris, a municipality in the Province of Vercelli in the Italian region of Piedmont, located about 40 kilometers northeast of Turin and about 25 kilometers west of Vercelli. The project consisted in the full recovery and renovation of a typical rural building of the Piedmont region called “curmà”, which begun in March 2014 and ended in 2016.



Figure 2.15 – Sketch of the CorTau House project after the renovation.

Source: S.P. Corgnati, C. Guala, M. Luciano, ‘The challenge of designing and building nZEBs: a single-family house in Italy’, REHVA Journal – November 2014.

The CorTau House experience, as a renovation of a typical Piedmont rural building, can be extended to a variety of already existing constructions, complying with the requirements of the Italian nZEB legislation, increasing the independence from fossil fuels as the house completely electric and self-sufficient in terms of energy production, with the on-site energy production sustained by PV panels on the roof and the heat extraction from groundwater.

Table 2.3 - CorTau house specifications.

Site	Livorno Ferraris (VC)
Latitude	45°17'6''00 N
Longitude	08°4'42''60
Height above mean sea level (AMSL)	188 m
Intervention	Retrofit of a traditional rural building
Intended use	Residential
Typology	Single-family house
Climatic Zone	E
Heating Degree-Days	2549

Source: Author's elaboration.



Figure 2.16 – Transversal section of the Cor-Tau house project.

Source: S.P. Corgnati, C. Guala, M. Luciano, 'The challenge of designing and building nZEBs: a single-family house in Italy', REHVA Journal – November 2014

The building has a ground usable surface of 130 m² and a volume of 390 m³ subdivided in both a living area and a night area. The main idea driving the building renovation process was improving the interaction with the environment by applying bioclimatic architecture principles to the construction. For instance, the largest fenestrations are located on the south façade to benefit from free solar gains in the winter season. Shading devices are however installed above the windows to limit this effect in summer, as to prevent possible internal spaces overheating.



Figure 2.17 – Building plan subdivision according to the end use of each zone.

Source: David Simula. Qualità dell'aria e comfort termico in un edificio NZEB: analisi CFD di possibili strategie di ventilazione = Indoor Air Quality and thermal comfort in a NZEB building: CFD analysis of possible ventilation strategies. Tesi di laurea. 2019.

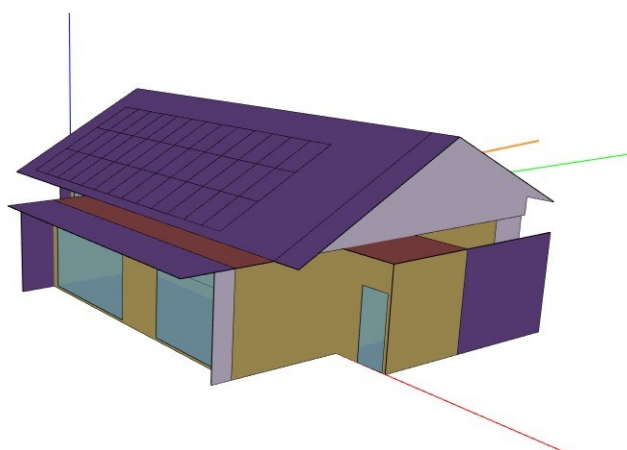


Figure 2.18 – CorTau house east façade in OpenStudio.

Source: Author's elaboration.

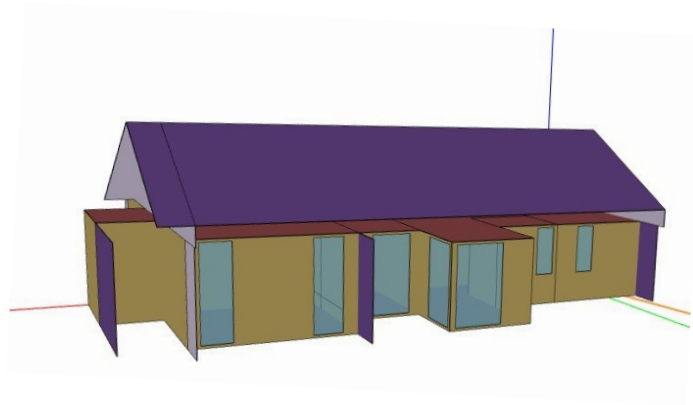


Figure 2.19 – CorTau house north façade in OpenStudio.

Source: Author's elaboration.



Figure 2.20 – CorTau house south façade in OpenStudio.

Source: Author's elaboration.

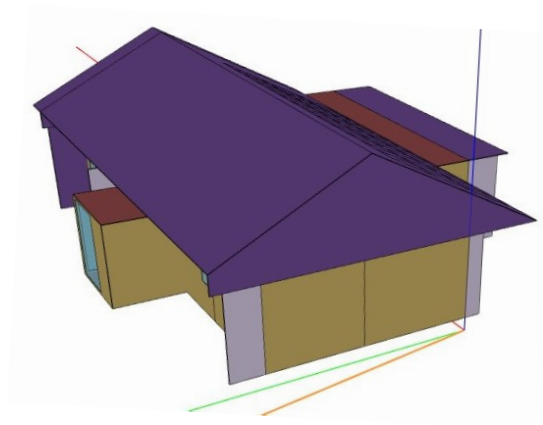


Figure 2.21 – CorTau house west façade in OpenStudio.

Source: Author's elaboration.

A summary on the material layers and thermal properties of both the opaque envelope and the fenestration is available in Appendix A.

As far as the transparent envelope is concerned, triple-pane glass windows filled with Argon gas are mounted on the external wall, as they represent a valid cost effective, soundproof and energy-efficient alternative to normal windows. The three glasses are coated with a Low Emissivity (LoE) layer, thin and nearly colorless. The great advantage of this technology is that the glass allows most of the visible fraction of natural light to enter through the window while reflecting the long-wave radiation. While in summer the long-wave radiation coming from the sun is reflected outside, avoiding an increase of the cooling load on the building, in winter the same happens at the indoor side, helping in the reduction of the heating demand from the building.

2.3.2. Development of the EnergyPlus model

The puntual and detailed description of the CorTau House modelling process in EnergyPlus is out of the scope of this study. However a focus on the aspects directly affecting the MPC design and response is needed to fully understand how the MATLAB and EnergyPlus co-simulation actually works, and which are the major factors influencing the indoor air temperature evolution. The CorTau House is subdivided in eight thermal zones, and the controller will work independently on each of the heated ones. The entrance bush will not be included in the simulation as no heating equipment is neither installed nor modelled in EP. Figure 2.22 and Table 2.4 show the plan subdivision and the relative floor area.

To define each thermal zone the software requires first the orientation with respect to the North direction and the zone dimensions, thus the ceiling height, the internal volume and the floor area.

Once this is completed, the next step would be detailing all the surfaces characteristics in a dedicated `BuildingSurface:Detailed` EP object. Here the outdoor wall for the kitchen is reported as an example, assigned to the ZT1 Kitchen zone and the `External Wall` construction objects.

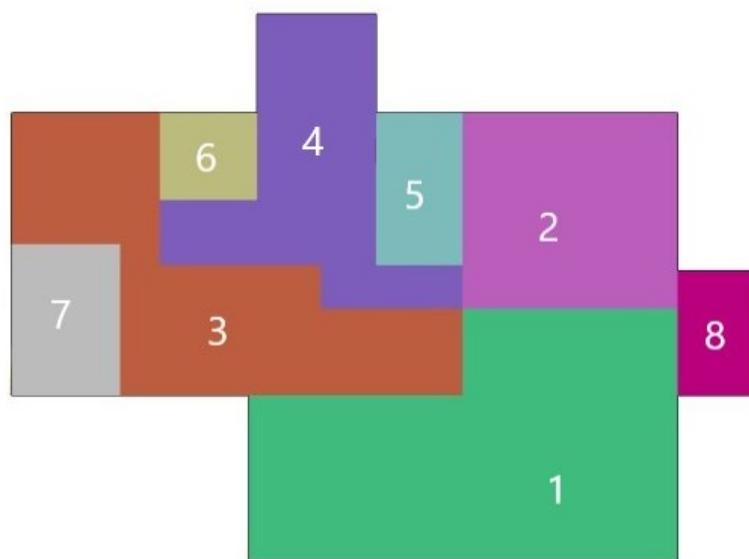


Figure 2.22 – Thermal zones subdivision in the CorTau House building model as implemented in EnergyPlus.

Source: Author's elaboration.

Table 2.4 – List of the CorTau House thermal zones with specifications.

Zone Name	Floor Area (m ²)	Heating
ZT 1 Kitchen	48,7	YES
ZT 2 Living Room	19,1	YES
ZT 3 Night Area	27,4	YES
ZT 4 Studio	20,5	YES
ZT 5 Bathroom1	5,3	YES
ZT 6 Bathroom2	3,5	YES
ZT 7 Bathroom3	6,9	YES
ZT 8 Entrance bush	5	NO

Source: Author's elaboration.

```
!- ===== ALL OBJECTS IN CLASS: BUILDINGSURFACE:DETAILED =====
```

```
BuildingSurface:Detailed,

  ZT1P1,                !- Name

  Wall,                 !- Surface Type

  External Wall,        !- Construction Name

  ZT 1 Kitchen,         !- Zone Name

  ,                     !- Space Name

  Outdoors,             !- Outside Boundary Condition

  ,                     !- Outside Boundary Condition Object

  SunExposed,           !- Sun Exposure

  WindExposed,          !- Wind Exposure

  autocalculate,        !- View Factor to Ground

  autocalculate,        !- Number of Vertices

  5.52,0,3.15,          !- X,Y,Z ==> Vertex 1 {m}

  5.52,0,0,             !- X,Y,Z ==> Vertex 2 {m}

  5.52,-3.85,0,         !- X,Y,Z ==> Vertex 3 {m}

  5.52,-3.85,3.15;     !- X,Y,Z ==> Vertex 4 {m}
```

The `Construction` object includes all the material layers, whose physical properties are in turn defined in a corresponding `Material` object. The examples for the `External Wall` and its coating are reported below.

```
!- ===== ALL OBJECTS IN CLASS: CONSTRUCTION =====
```

```
Construction,

  External Wall,        !- Name

  EW - RIV. EST.,       !- Outside Layer

  EW - ISOL.,           !- Layer 2

  EW - LAT.,            !- Layer 3
```

```
EW - CART.,                !- Layer 4

EW - INT.;                 !- Layer 5

!-  =====  ALL OBJECTS IN CLASS: MATERIAL  =====

Material,

EW - RIV. EST.,            !- Name

MediumRough,              !- Roughness

0.004,                    !- Thickness {m}

45,                       !- Conductivity {W/m-K}

7680,                    !- Density {kg/m3}

840;                      !- Specific Heat {J/kg-K}
```

Various parameters can be extracted by running the EnergyPlus IDF File through the EP-Launch, the official software launcher that manages input and output files and performs batch simulations. Among the various thermal zone object outputs, the Zone Mean Air Temperature is the one of interest in the controller design.

```
!-  =====  ALL OBJECTS IN CLASS: OUTPUT:VARIABLE  =====

Output:Variable,

*,                        !- Key Value

Zone Mean Air Temperature, !- Variable Name

timestep;                 !- Reporting Frequency
```

The model requires the introduction of a set of schedules to consider the effects of the occupancy, the electric equipment, and the lighting system on the building thermal balance, as they all constitute an internal heat source affecting the indoor temperature level. Different schedules are built for weekdays and weekends, as explained in the following.

- The occupancy pattern is derived from UNI 10339 and a significant difference between day and night hours can be observed.

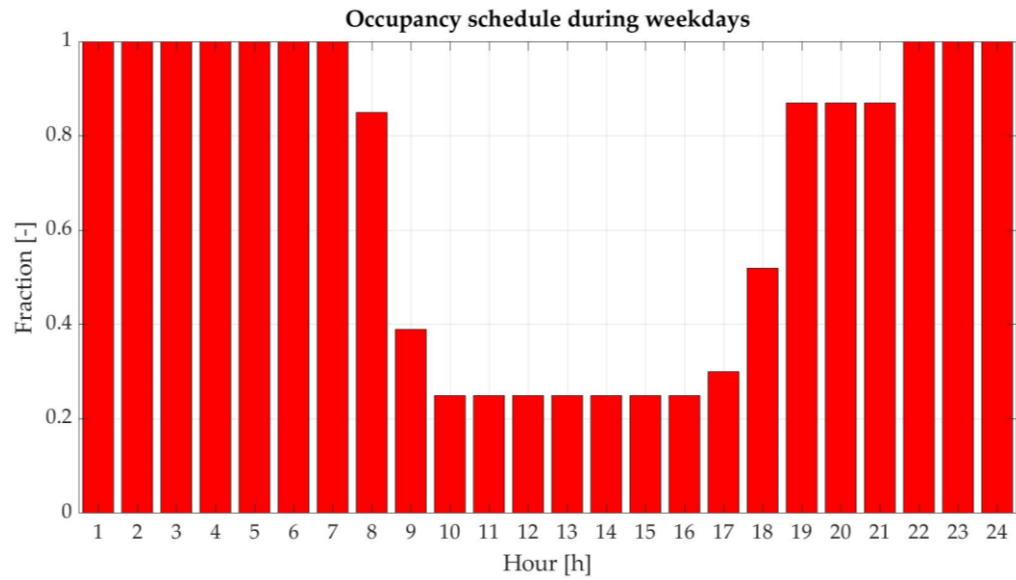


Figure 2.23 - Occupancy schedules during weekdays for all the thermal zones.
Source: Author's elaboration.

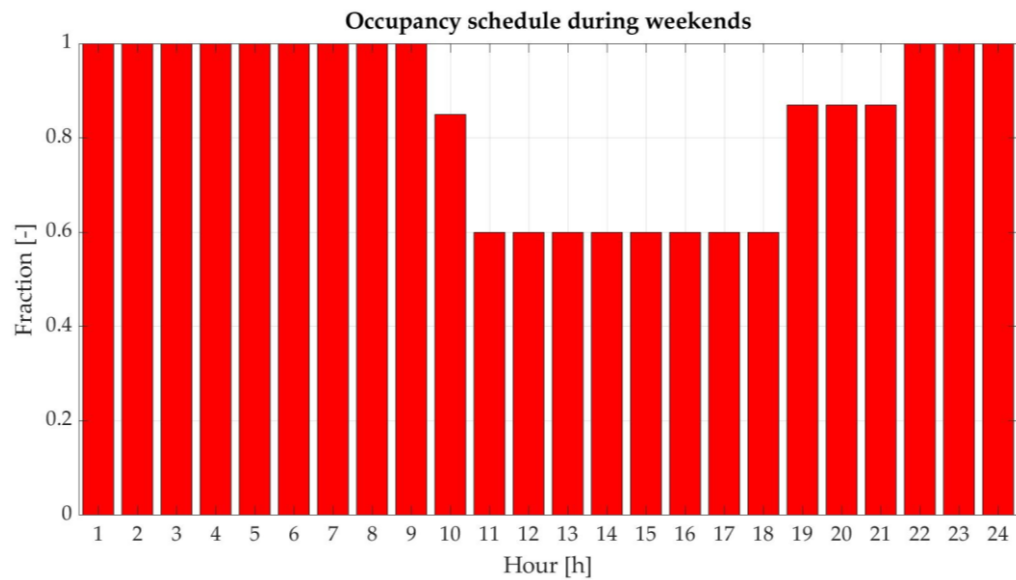


Figure 2.24 - Occupancy schedules during weekends for all the thermal zones.
Source: Author's elaboration.

People are expected to be mostly outside between 9:00 and 17:00, especially on weekdays.

For the actual trend of the internal gains due to the building occupancy a specific value of 0.04 person/m² is assumed in all the confined zones except for the bathrooms, where a null value reflects the fact that these zones are not significantly occupied during the day. The occupancy is coupled with the activity level, which provides the hourly evolution of the metabolic rate in the occupied zone in W/person. In this case a value of 82.8 W/person heat release is assumed while sleeping and 126 W/person for the rest of the day. The same trend is expected for weekdays and weekends as this parameter only depends on the activity that is carried out and the correlated metabolic energy expenditure.

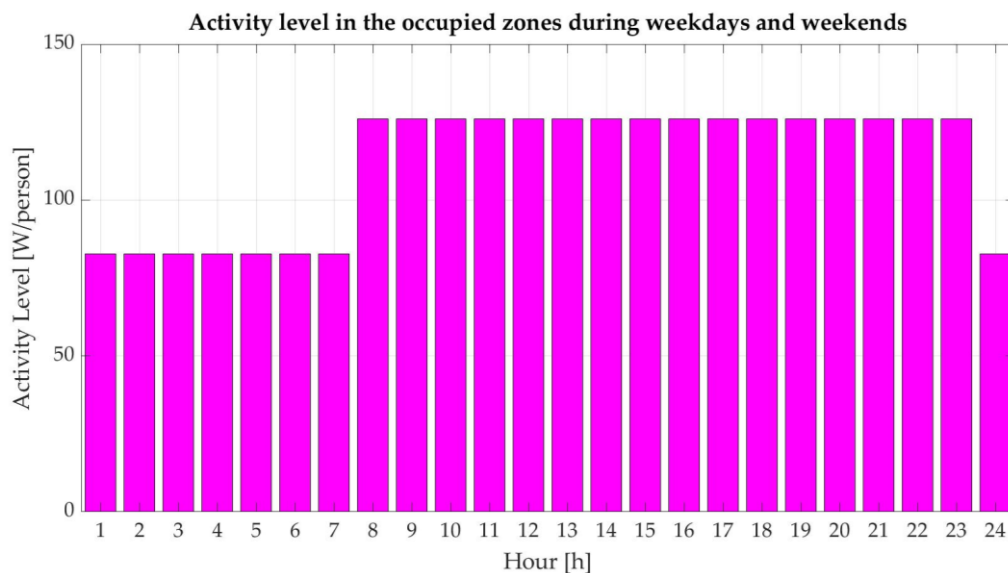


Figure 2.25 - Activity level during weekdays for all the thermal zones.

Source: Author's elaboration.

The product of the occupancy schedule, the building occupancy in person/m², the activity level and the zone floor area provide the hourly thermal power gain to each zone.

- For the electric equipment, a specific value of 5.38 W/m^2 is introduced in the model, according to the ASHRAE 90.1 Standard. The schedule is differentiated for weekdays and weekends as a different equipment usage is expected.

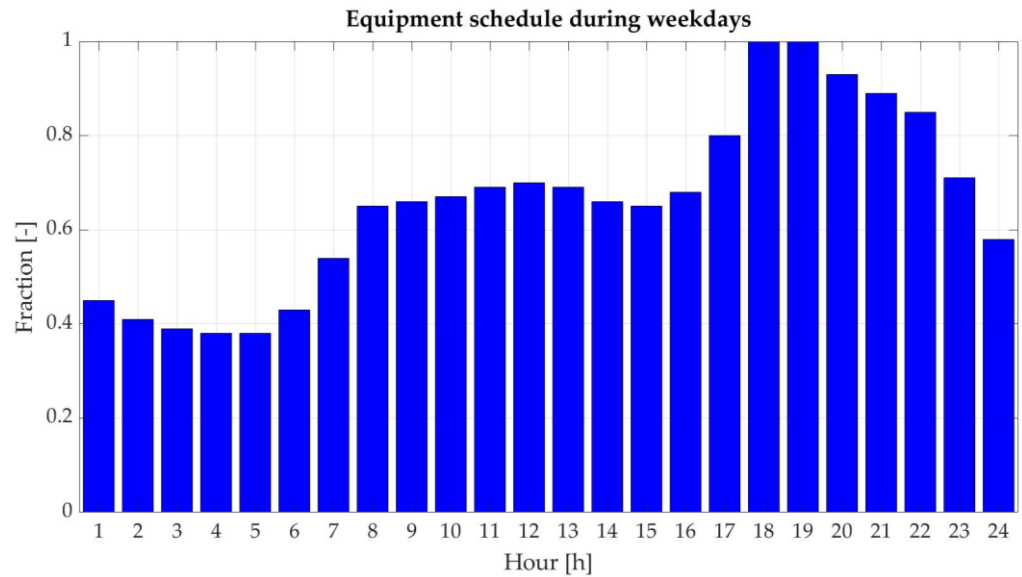


Figure 2.26 - Electric equipment schedules during weekdays for all the thermal zones.
Source: Author's elaboration.

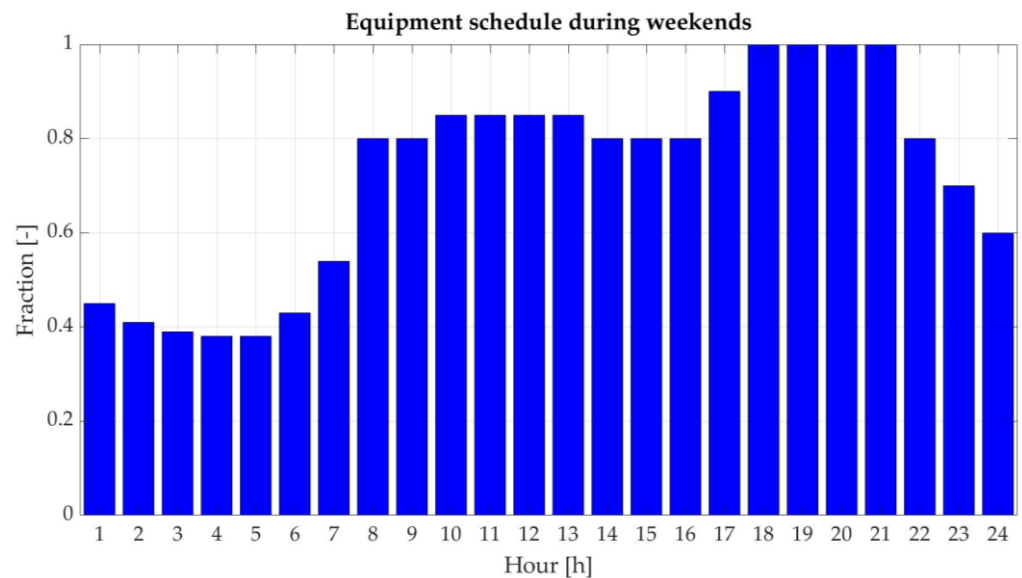


Figure 2.27 - Electric equipment schedules during weekends for all the thermal zones.
Source: Author's elaboration.

- The ASHRAE 90.1 Standard provides an average internal heat source due to lighting system equal to 3.88 W/m^2 . The schedule adopted for the CorTau House is reported in Figure 2.28, with a peak in the morning as the occupants are waking up and leaving the house and the other in the evening, when they get back home from work.

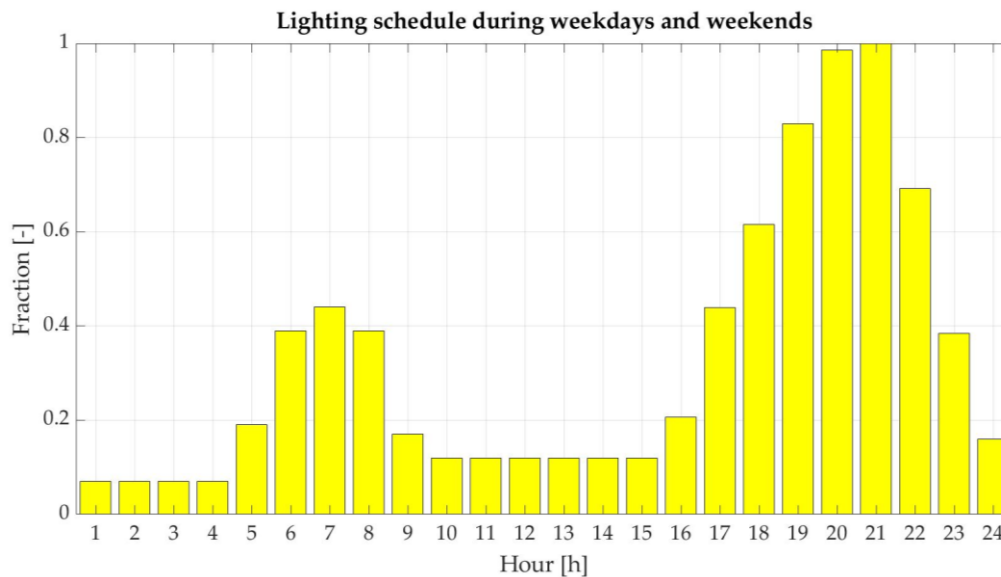


Figure 2.28 - Lighting schedules during weekdays and weekends for all the thermal zones.
Source: Author's elaboration.

The heat gains due to the occupants' metabolic rate and the lighting and equipment systems are summed up to obtain the total internal gains for each room. Figures 2.29 and Figure 2.30 show the resulting total hourly internal gains for ZT1 Kitchen, for weekdays and weekends respectively, broken down into each of the above-mentioned items.

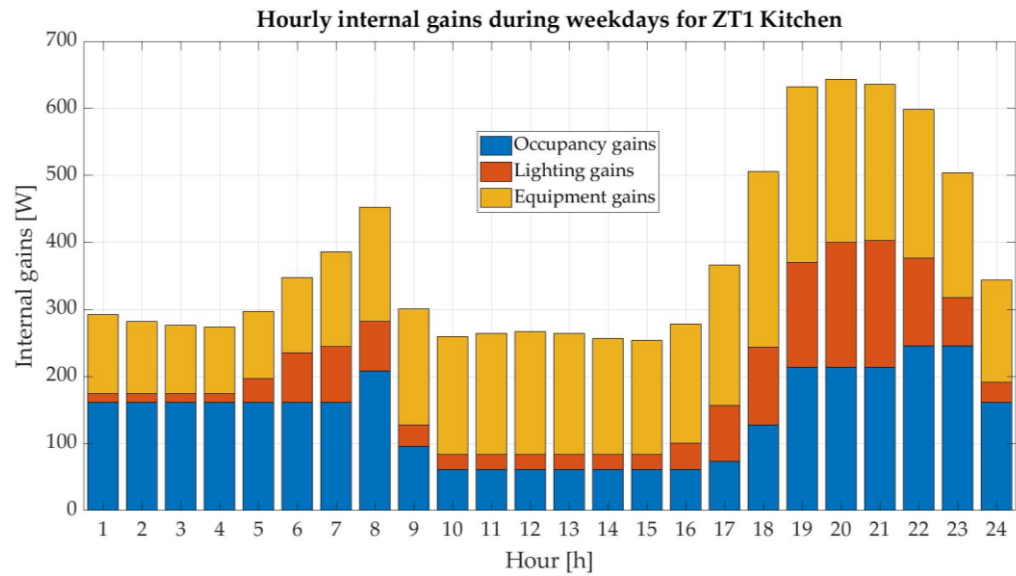


Figure 2.29 - Hourly internal gains for ZT1 Kitchen during weekdays.
Source: Author's elaboration.

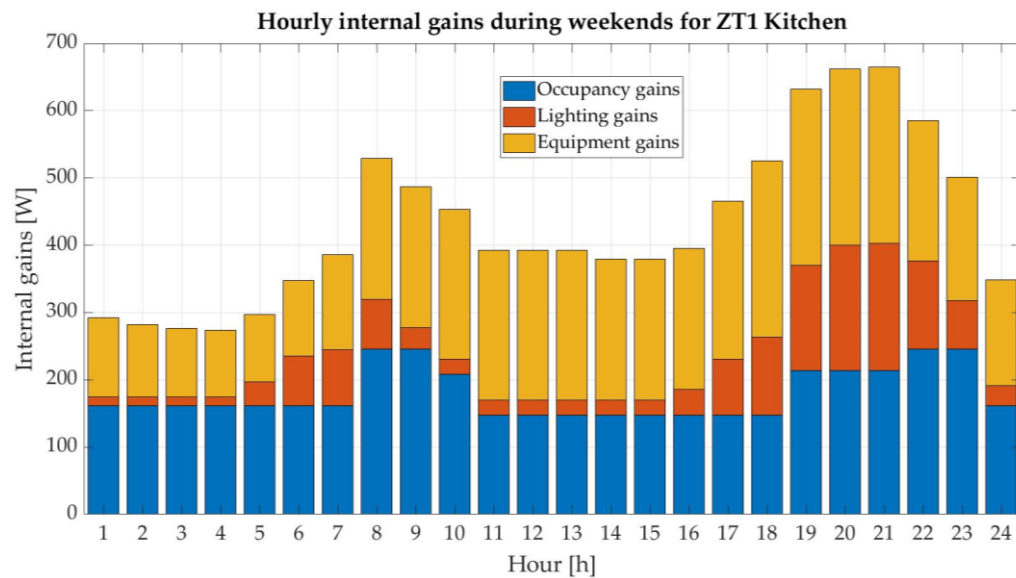


Figure 2.30 - Hourly internal gains for ZT1 Kitchen during weekends.
Source: Author's elaboration.

The EnergyPlus model of the CorTau house is equipped with a model for an ideal HVAC system. The `ZoneHVAC:IdealLoadsAirSystem` input object corresponds to a zone HVAC unit, meaning that the object does not provide a central air handling unit,

but instead heating or cooling air is supplied singularly to each zone to meet the temperature setpoint specified in the model. Options for humidity control, outdoor air, economizer, demand-controlled ventilation, and heat recovery are all available in the system. The HVAC specifications are set equal for all the thermal zones, and they are reported in Table 2.5. No limits on the air flow rate (m^3/s) and the sensible heating or cooling capacity (W) are set, the sensible heat ratio is constant and specified below and no economizer, demand-controlled ventilation nor heat recovery strategies are implemented in this case.

Table 2.5 – HVAC system specifications in the EnergyPlus model.

Maximum Heating Supply Air Temperature	50 °C
Minimum Cooling Supply Air Temperature	13 °C
Maximum Heating Supply Air Humidity Ratio	0.0156 $\text{kg}_{\text{Water}}/\text{kg}_{\text{DryAir}}$
Minimum Cooling Supply Air Humidity Ratio	0.0077 $\text{kg}_{\text{Water}}/\text{kg}_{\text{DryAir}}$
Cooling Sensible Heat Ratio	0.7

Source: Author's elaboration.

As the CorTau House is a nearly Zero-Energy Building, most of its energy needs must be met by in-situ renewable generation. For this reason, 39 crystalline silicon PV panels are installed on the house roof. The photovoltaic modules are modeled using an equivalent one-diode circuit in EnergyPlus and the array type is the Shell 175PC, whose properties are reported in Table 2.6.

Table 2.6 – Shell 175PC Photovoltaics Array Type properties.

Number of Cells in Series	72	[-]
Active Area	1.125	[m ²]
Transmittance Absorptance Product	0.95	[-]
Semiconductor Bandgap	1.12	[eV]
Shunt Resistance	1000000	[Ω]
Short Circuit Current	5.43	[A]
Open Circuit Voltage	44.6	[V]
Reference Temperature	25	[°C]
Reference Insolation	1000	[W/m ²]
Module Current at Maximum Power	4.95	[A]
Module Voltage at Maximum Power	35.4	[V]
Temperature Coefficient of Short Circuit Current	0.0008	[A/K]
Temperature Coefficient of Open Circuit Voltage	-0.145	[V/K]
Nominal Operating Cell Temperature Test Ambient Temperature	20	[°C]
Nominal Operating Cell Temperature Test Cell Temperature	45.35	[°C]
Nominal Operating Cell Temperature Test Insolation	800	[W/m ²]
Module Heat Loss Coefficient	30	[W/(m ² K)]
Total Heat Capacity	50000	[J/(m ² K)]

Source: EnergyPlus Documentation.

3. Proton Exchange Membrane Fuel Cell

3.1. Overview on the technology

The fuel cell technology is nowadays among the most promising in the framework of energy transition. The high interest put in this direction by the scientific community is primarily because most fuel cells are hydrogen-fuelled devices able to supply clean electrical and thermal power thanks to electrochemistry. The first attempt to exploit hydrogen as an energy vector dates to 1839, when Sir William Grove developed a rudimental fuel cell with a combination of sheet iron, copper and porcelain plates, and a solution of sulphate of copper and dilute acid [8].

Several sectors found in fuel cells an interesting alternative to more standard solutions throughout the years, with the first commercial use being the deployment of an Alkaline Fuel Cell (AFC) in a manned flight of the NASA Gemini 5 space program in 1965. With the development and spread of other fuel cell types, the focus shifted from niche applications to stationary power production, terrestrial transportation, powering portable devices and meeting residential and non-residential demands for electricity.

An electrochemical cell is converting the chemical energy of a fuel, often but not always hydrogen H_2 , into electricity through RedOx reactions with oxygen O_2 . The performance is strictly related to the technology but, in general, the conversion efficiencies reach values way above those observed in classical heat engines based on combustion. The thermal energy obtained as a secondary product can be either expelled or employed in a variety of applications, as in this case building heating.

The main difference between traditional combustion devices and this technology is that while in the first the reduction and oxidation reactions occur at the same place and time, in fuel cells they are separated in space, letting the resulting electron flow supply a load connected to the cell's terminals.

While the temperature difference ΔT is the thermodynamic driver for the gas-turbine engines operation, this is not the case for fuel cells, where the thermodynamic driver is the chemical potential difference between the species involved in the RedOx reactions. In addition to this, the electricity is produced directly from electrochemistry avoiding the multiple conversion steps needed for power production in traditional combustion

engines. Finally, fuel cell output scales with the surface area and not the device volume. This means that, differently from heat engines, they can be made efficient at small sizes.

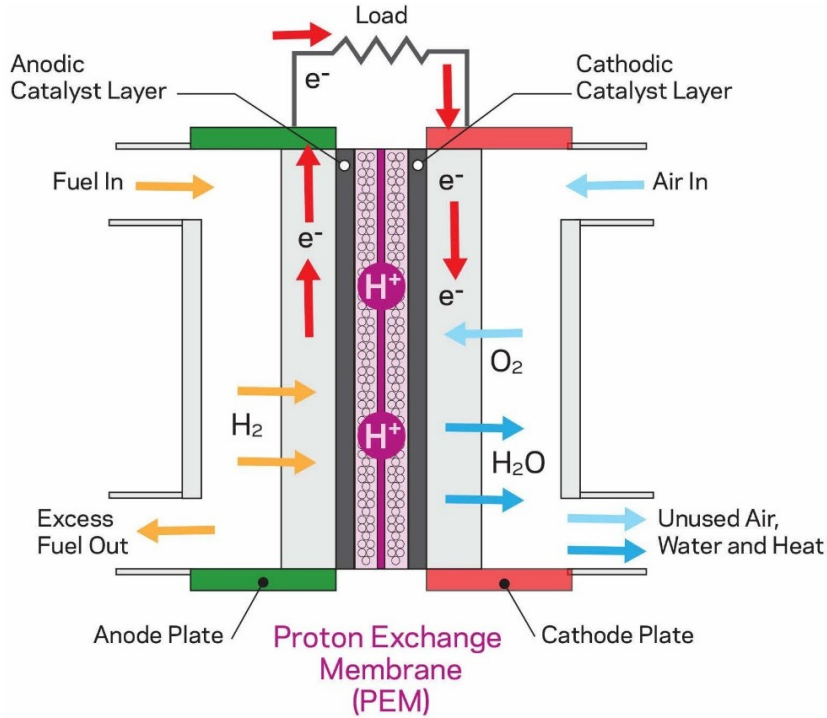


Figure 3.1– Fuel cell schematic with reactants and products flow.

Source: Piatkowski, Piotr, Iwona Michalska-Pozoga, and Marcin Szczepanek. 2022. "Fuel Cells in Road Vehicles" *Energies* 15, no. 22: 8606. <https://doi.org/10.3390/en15228606>.

All the heat engines are subject to the Carnot cycle limitation on the efficiency.

$$\eta_{th,rev} = 1 - \frac{T_C}{T_H}$$

(3.1)

and similarly, also fuel cells are subject to an efficiency limitation coming from the analysis of their ideal reversible operation [9], as better explained in the following section.

3.2. PEMFC basics and mathematical model

Proton-exchange membrane fuel cells (PEMFC) are one of the most promising technology due to their light weight, the low pressure and temperature ranges of operation and the fact that they can employ pure hydrogen and oxygen to produce primarily electricity but also water and heat as by-products. H_2 undergoes the oxidation half reaction at the anode side while oxygen undergoes reduction at the cathode side.

Electrochemical reaction		E^0/V
Anode	$H_2 \rightarrow 2H^+ + 2e$	0.000
Cathode	$2H^+ + 2e + \frac{1}{2}O_2 \rightarrow H_2O(\text{liquid})$	1.229
Overall reaction	$H_2 + \frac{1}{2}O_2 \rightarrow H_2O(\text{liquid})$	1.229

Figure 3.2 – RedOx reactions for PEM fuel cells

Source: Andrey, Yaroslavtsev & Dobrovolsky, Yurii & Shaglaeva, N & Frolova, L & Gerasimova, Ekaterina & Sanginov, E.. (2012). Nanostructured materials for low-temperature fuel cells. Russian Chemical Reviews. 81. 191. 10.1070/RC2012v081n03ABEH004290.

The fuel cell theoretical potential as computed for the overall reaction is 1.23 V. The measured voltage during real cell operation reduces due to loss sources. Specific materials are required to extract electricity from the H_2/O_2 reaction taking place inside the fuel cell. The device is built as a membrane electrode assembly (MEA), constituted of a thin proton-exchange membrane (PEM, generally Nafion™) permeable to hydrogen ions (protons, H^+) but impermeable to electronic flows and two electrodes (the cell anode and cathode) physically separated by the PEM with a carbon supported catalyst layer on both.

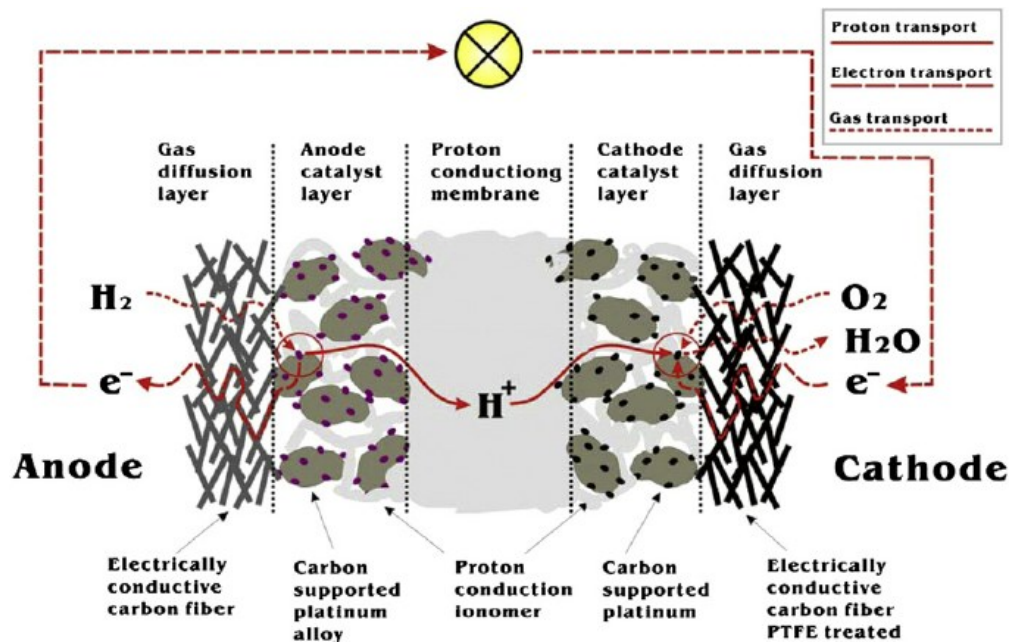


Figure 3.3 – Membrane electrode assembly in PEMFC.

Source: Andersen, Shuang & Chen, Qian & Joergensen, Fleming & Stein, Paul & Skou, Eivind. (2007). F-19 NMR studies of Nafion (TM) ionomer adsorption on PEMFC catalysts and supporting carbons. Solid State Ionics. 178. 1568-1575. 10.1016/j.ssi.2007.10.007.

○ Proton-Exchange Membrane

It is made of a fluorocarbon polymer backbone on which sulfonic acid groups SO_3 have been bonded through a chemical process, as in the fluoropolymer NafionTM commercialized by DuPont. The membrane is designed to let ionic flows from the cathode side to the anode while acting as an electronic insulator. The main functions of the membrane are thus the separation of the two RedOx semi-reactions and avoiding the recombination of H^+ and e^- (i.e., cell short circuit occurrence), therefore acting as a barrier to the crossover mixing of the fuel and the oxidant. An external circuit connected to the load is provided as the electrons current path [10].

The membrane must provide both mechanical and chemical stability, the latter as to bear the oxidizing and the reducing environments at the two electrodes' sides. The PEM characterization is accomplished through three main parameters [11]:

- Proton conductivity σ .

- Methanol permeability P (as the membrane is also employed in Direct Methanol Fuel Cells DMFC).
- Thermal stability.

The Nafion® membrane, the most common proton exchange membrane employed in fuel cells applications, shows a proton conductive resistance that is inversely proportional to the membrane water content [12] and thus a specific hydration level of the electrolyte membrane is required to ensure a proper ionic flows through it. The water management issue is crucial in PEMFC performance and a recirculation from the reaction site towards the membrane to keep it at the correct level of water content is possible. This could be both active (involving additional external elements) or passive (by means of pressure and concentration gradients along the electrolyte). A water layer management at the cathode side is typically added to the fuel cell structure to increase the water flow resistance towards the external environment and therefore to promote its passive back flow to the anode.

○ Catalytic Layer

The catalytic layer CL is the most active sublayer of the MEA, being its main functions the increase of the reaction rates at both electrodes but also the selectivity towards the desired products. The materials and alloys that can be employed include PtM, M=Ru, Pd, Ni, Rh, V, Mo, W at the anode side and PtN, N=Co, Fe or Mn at the cathode, among others.

The catalyst design is key to the cell performance. In the most common configuration for PEMFC, Pt nanoparticles with a diameter of about 5 nm are supported on a carbon structure able to provide a wide surface area, good electrical conductivity, and inertness as far as the chemical reactions taking place in the cell are concerned. The catalyst loading and utilization is typically in the range of 0.3-0.4 mg/cm² on both electrodes. The CL is designed as a 3D network to maximize the contact between the ionic conductor (i.e., the electrolyte), the electron conductor (i.e., the electrode) and the gas phase in what is called Triple Phase Boundary TPB, the electrochemically active sites where the reaction truly takes place.

Half of the total FC cost is due to the need of precious metals in the catalytic layer [13].

For this reason, a high effort is put in finding alternative solutions to make PEMFC economically favourable over other technologies. The other main issue related to the catalyst is that the cell voltage, and thus the power production, is greatly reduced when the CL is poisoned by carbon monoxide CO or sulphur S. Nowadays the hydrogen production still massively relies on steam reforming of light hydrocarbons, whose product is a gas mixture containing hydrogen but also poisoning species. Additional fuel processing is required when this hydrogen is feeding a PEMFC, as high purity levels are required by such devices.

- Collector and Gas diffusion layer

The collector plate on one side provides a pathway for the reactant gases and the product water ensuring a uniform gas distribution over the electrode active area, and on the other gives the assembly mechanical support and structural rigidity. The gas diffusion section instead is a porous structure made of carbon fibre-based material composed of two sublayers, one being the electrode and the other being the proper microporous layer. They allow the flow of both the reactants and the water produced in the reaction, and they must be both electrically and thermally conductive to dissipate the heat generated during the cell operation towards either the external environment or a heat recovery system.

Figure 3.4 gives an idea on how and where the various steps of the FC operation process, listed right below it, take place.

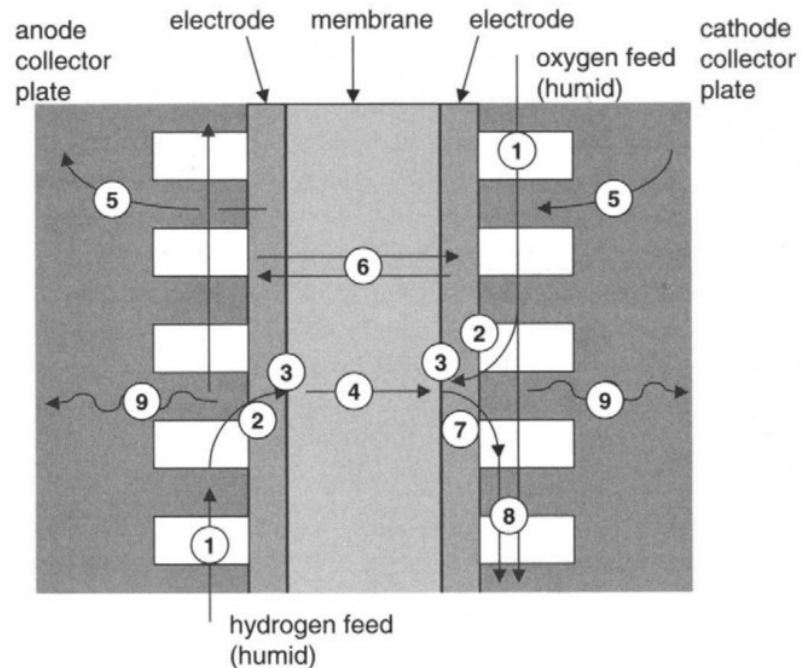


Figure 3.4 – Regions involved in each step of the PEMFC operation.

Source: Borkovski, Stefan & Erkechova, Maja. (2020). Control approaches of pem fuel cells: a review. 5.

126.

1. H_2 and O_2 gaseous flow through the collector plates' channels.
2. Gas diffusion through the electrodes' porous media.
3. Electrochemical reactions at the catalyst layer.
4. H^+ proton transport through the proton-conductive polymer membrane.
5. Conduction of electrons through the external electrically conductive circuit connected to the load.
6. H_2O liquid water transport through the Proton-Exchange Membrane.
7. Water transport through both the catalyst and the gas diffusion layers towards the external environment.
8. Flow of the unused gas carrying water droplets.
9. Heat dissipation through the collector plate.

Care is needed when talking about the fuel cell efficiency, as the efficiency of the electrochemical reaction is commonly referred to as *fuel stack efficiency*, but the real cell efficiency considering all the loss sources is presented in literature as *fuel cell system efficiency*.

For what concerns the stack efficiency, the enthalpy of reaction ΔH^0 quantifies the amount of energy released in the exothermic water formation reaction at Standard Condition (25 °C and atmospheric pressure). Part of this is unavoidably lost as entropy and is not available to do useful work. The Gibbs free energy ΔG^0 quantifies the amount of enthalpy of reaction that is not lost and that can be converted into electricity.

$$\Delta H_{(l)}^0 = -286 \text{ kJ/mol}_{H_2O} \quad (3.2)$$

$$\Delta G^0 = \Delta H^0 - T\Delta S = -237 \text{ kJ/mol}_{H_2O} \quad (3.3)$$

The enthalpy of reaction measures the heat that would be theoretically released in the hydrogen combustion reaction, while the Gibbs free energy is the electrical energy produced when the cell is operated reversibly (i.e., in ideal operation conditions).

Therefore, for a generic H_2/O_2 fuel cell operated at STP, the stack efficiency can be computed as:

$$\eta_{FC,rev} = \frac{\Delta G^0}{\Delta H^0} = \frac{-237 \text{ kJ/mol}_{H_2O}}{-286 \text{ kJ/mol}_{H_2O}} = 0.83 \quad (3.4)$$

The following diagram shows the ideal reversible operation efficiencies of both the fuel cell and the Carnot cycle depending on the operating temperature.

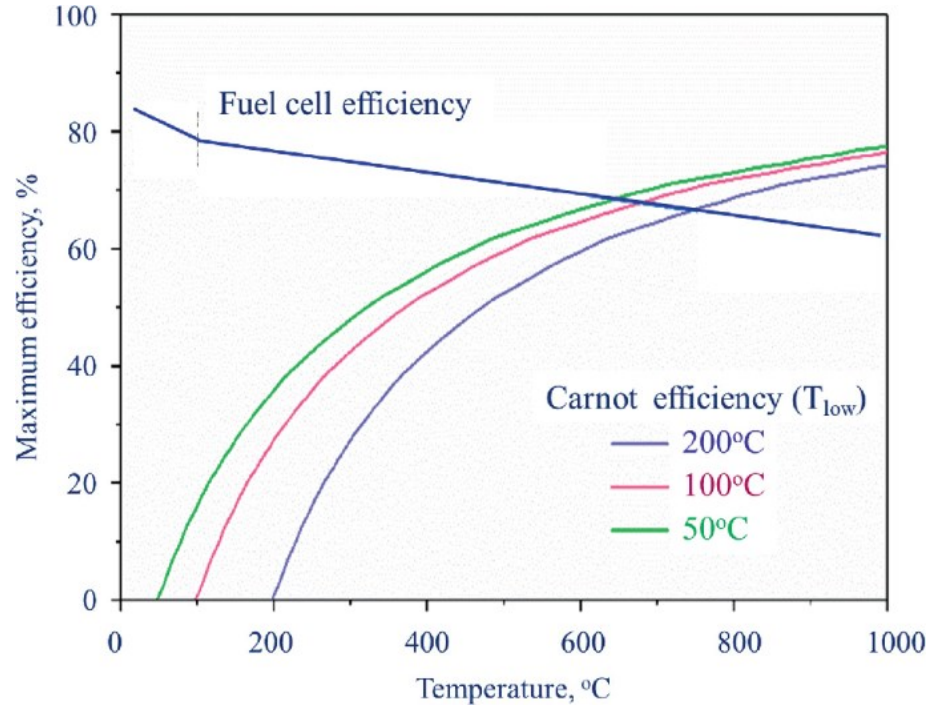


Figure 3.5 – Ideal fuel cell and Carnot efficiencies evolution with temperature.

Source: Jiang, S.P., Li, Q. (2022). Fuel Cell Thermodynamics. In: Introduction to Fuel Cells. Springer, Singapore. https://doi.org/10.1007/978-981-10-7626-8_2

The electrical power generated by the cell can be evaluated as

$$W_{electrical} = q_{el} \cdot E_{cell} = n \cdot N_{Av} \cdot q_{el} \cdot E_{cell} = n \cdot F \cdot E_{cell} \quad (3.5)$$

where

- n is the mole of electrons involved in the reaction, and by looking at the anode and cathode semi-reactions two electrons are exchanged for the formation of a single water molecule. This means $n = 2 \text{ mol e}^-$.

- $N_{av} = 6.023 \times 10^{23} \text{ mol}^{-1}$ is the Avogadro number.

- E_{cell} is the FC potential in V.

- $q_{el} = 1.602 \times 10^{19} \text{ C}$ is the electron charge.

- $F = N_{Av} q_{el} = 96\,500 \text{ C / mol } e^-$ is the Faraday constant.

As already mentioned, ΔG^0 quantifies the maximum amount of chemical energy that can be converted in electricity by the fuel cell through the reaction.

$$W_{electrical,maximum} = -\Delta G^0 \quad (3.6)$$

The maximum voltage that the fuel cell can supply is therefore evaluated as:

$$\begin{aligned} E_{cell}^0 &= \frac{W_{electrical,maximum}}{n \cdot F} = \frac{-\Delta G^0}{n \cdot F} = \\ &= \frac{-237 \text{ kJ}}{\text{mol}_{H_2O}} \cdot \frac{1000 \text{ J}}{1 \text{ kJ}} \cdot \frac{\text{mol}_{H_2O}}{2 \text{ mol}_{e^-}} \cdot \frac{\text{mol}_{e^-}}{96\,500 \text{ C}} = 1.23 \text{ V} \end{aligned} \quad (3.7)$$

In the end, a single H_2/O_2 fuel cell at STP conditions can generate a maximum theoretical voltage $E^0 = 1.23 \text{ V}$, also referred to as ideal standard potential. However, various sources of losses are affecting both the cell voltage and efficiency during real operation. For this reason, the cell characteristic curve, generally referred to as polarization curve, relates the cell voltage to the generated current, showing the real performance of the FC in its operating range. The curve shows the displacement of the cell voltage from the theoretical maximum as resulting from the thermodynamics analysis above.

As better shown in Figure 3.6, the evolution of the output cell voltage varies throughout the current range as three regions can be distinguished, each dominated by one specific voltage loss source. Fuel cells' current data are often scaled to the cell cross section, especially for comparison purposes. For this reason, current density (A/cm^2) values rather than current ones (A) are reported.

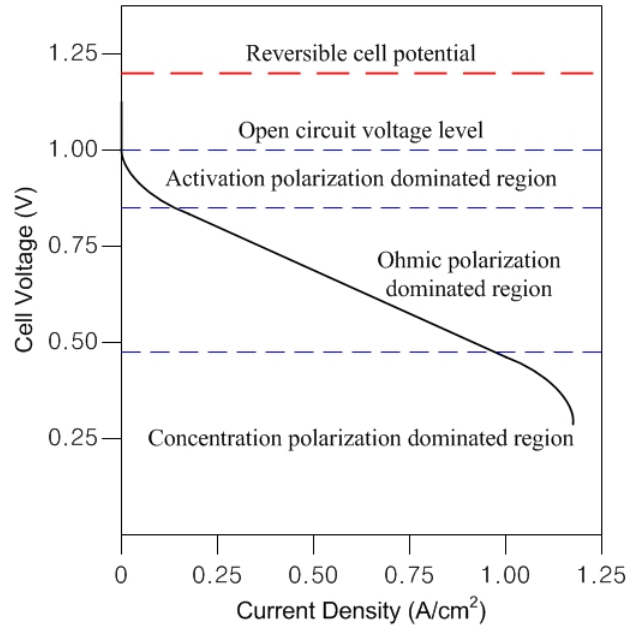


Figure 3.6 – Example of fuel cell polarization curve with voltage loss regions.

Source: Jung, Jee-Hoon & Ahmed, Shehab. (2010). Dynamic Model of PEM Fuel Cell Using Real-time Simulation Techniques. Journal of Power Electronics. 10. 10.6113/JPE.2010.10.6.739.

1. Activation polarization dominated region

The main source of voltage loss observed in the low current density region is related to the energy barrier that the reactants need to overcome to start the chemical reaction (i.e., the activation energy) at the catalyst site. Part of the electrode voltage is lost to compensate the lack of catalytic activity; this FC potential decrease quantifies the performance of the catalyst to reduce the energy barrier and increase the reaction rate, but it cannot be pushed to zero due to the intrinsic slowness of the oxygen semi-reaction.

According to the Butler-Volmer equation, the activation overpotential can be expressed as

$$\Delta V_{act} = \frac{RT}{\alpha_a F n} \ln \left(\frac{j}{j_0} \right) \Big|_{anode} + \frac{RT}{\alpha_c F n} \ln \left(\frac{j}{j_0} \right) \Big|_{cathode} \quad (3.8)$$

- n is the number of protons exchanged per each mole of reactant.
- $R = 8.314 \text{ J}\cdot\text{K}^{-1}\cdot\text{mol}^{-1}$ is the gas constant.
- j (mA/cm^2) is the current density.
- j_0 (mA/cm^2) is the reaction exchange current density, a measure of the reaction rate.
- α_a and α_c (-) are the charge transfer coefficients at the anode and the cathode side respectively.
- F is the Faraday constant.
- T is the fuel cell operating temperature.

For PEMFC the cathodic contribution to the activation polarization is dominating as the anode exchange current density is much higher than the cathode one.

2. Ohmic polarization dominated region

The PEMFC components alternatively involved in the protons and electrons conduction intrinsically show an electrical resistance and thus a voltage loss in the form of an ohmic polarization. This is particularly relevant within the electrolytic membrane (ionic conduction), the electrodes (both electronic and ionic conduction) and finally at the cell terminals due to the electrons current towards the load.

The collector plates and the electrodes obey to the Ohm's law, and in fact the voltage drop is observed to increase linearly with the current density.

$$\Delta V_{ohmic} = j \cdot R_{ohmic} = j \cdot (R_{elec} + R_{ionic}) \quad (3.9)$$

The ionic resistance R_{ionic} term is usually dominating over the electronic one R_{elec} as the H^+ transport through the Nafion™ membrane is quite harder than the electrons transfer through the electrodes and the external circuit. Both are expressed in $\Omega \text{ cm}^2$.

3. Concentration polarization dominated region

This voltage loss source is dominating in the high current density region, roughly above 1 A/cm². This is due to an undesired accumulation of the species involved in the cell operation both at the reactants and at the products side, due to the mass transfer effects, and it specifically originate at the reactant delivery site and at the product removal one.

When the fuel cell is demanded to generate a too high current, almost outside of its operating range, the reactants consumption rate overcomes the supply rate on one side, while on the other the products are accumulated at a higher rate than the removal one. This inevitably leads to a dramatic drop in the cell voltage output and performance. As this kind of loss occurs outside of the FC operating range, it will not be included in the analysis.

A generally accepted expression for the polarization curve of a single cell is formulated as the theoretical voltage of 1.23 V diminished by both the concentration and ohmic losses as a function of the current density j (mA/cm²).

$$\begin{aligned}
 V_{FC} &= V_{theoretical} - \Delta V_{act} - \Delta V_{ohmic} = \\
 &= 1.23 \text{ V} - \frac{RT}{\alpha_c F n} \ln \left(\frac{j}{j_0} \right) \Big|_c - j \cdot R_{ohmic} = \\
 &= 1.23 \text{ V} - (a + b \cdot \ln(j)) - j \cdot R_{ohmic}
 \end{aligned}
 \tag{3.10}$$

In this study, a PEM fuel cell stack available on the market is intended to cover the heating demand resulting from the controller operation. The details on the methodology are reported in Chapter 4. Nedstack provides a variety of PEM fuel cells options even for the built environment, with solutions that combine electricity and heat generation through Hydrogen Feed Type Cells (HFTC). The FCS 7-XXL fuel cell stack produced by Nedstack is intended to operate in the domestic CHP sector, among others. The stack is made of 48 PEM fuel cells with a total rated power of 6.8 kWe at

the beginning of life. The set of voltage (V) and current (A) data included in the FCS 7-XXL stack datasheet is used here to fit the polarization curve expression as formulated in (3.10) through the MATLAB Curve Fitting Toolbox. The open circuit stack voltage would be 47 V in accordance with the datasheet provided by Nedstack and available in Appendix B.

Table 3.1 – Nedstack FCS 7-XXL specifications.

n_{cell}	Weight	Size	$P_{\text{H}_2, \text{max}}$	$P_{\text{air}, \text{max}}$	$T_{\text{H}_2, \text{inlet}}$	$T_{\text{air}, \text{inlet}}$
	(kg)	(mm)	(mbarg)	(mbarg)	(°C)	(°C)
48	26	351 x 196 x 288	250	200	50-60	55-60

Source: PRODUCT DATA SHEET FCS 7-XXL Gen 2.9. Revision 01, 05-07-2022. Nedstack PEM FUEL CELLS.

The values of the three fitting parameters a, b and R_{ohmic} obtained for the polarization curve are:

- $a = 7.157 \text{ V}$.
- $b = 0.5747 \text{ V}$.
- $R_{\text{ohmic}} = 8.639 \Omega \text{cm}^2$, total internal resistance of the FC stack.

The results on the fitting fall inside a 95% confidence interval and the value of the R^2 parameter reaches 0.9986, at least far from the open circuit 47 V level. The stack voltage decreases almost linearly with increasing current as expected in the ohmic polarization dominated region.

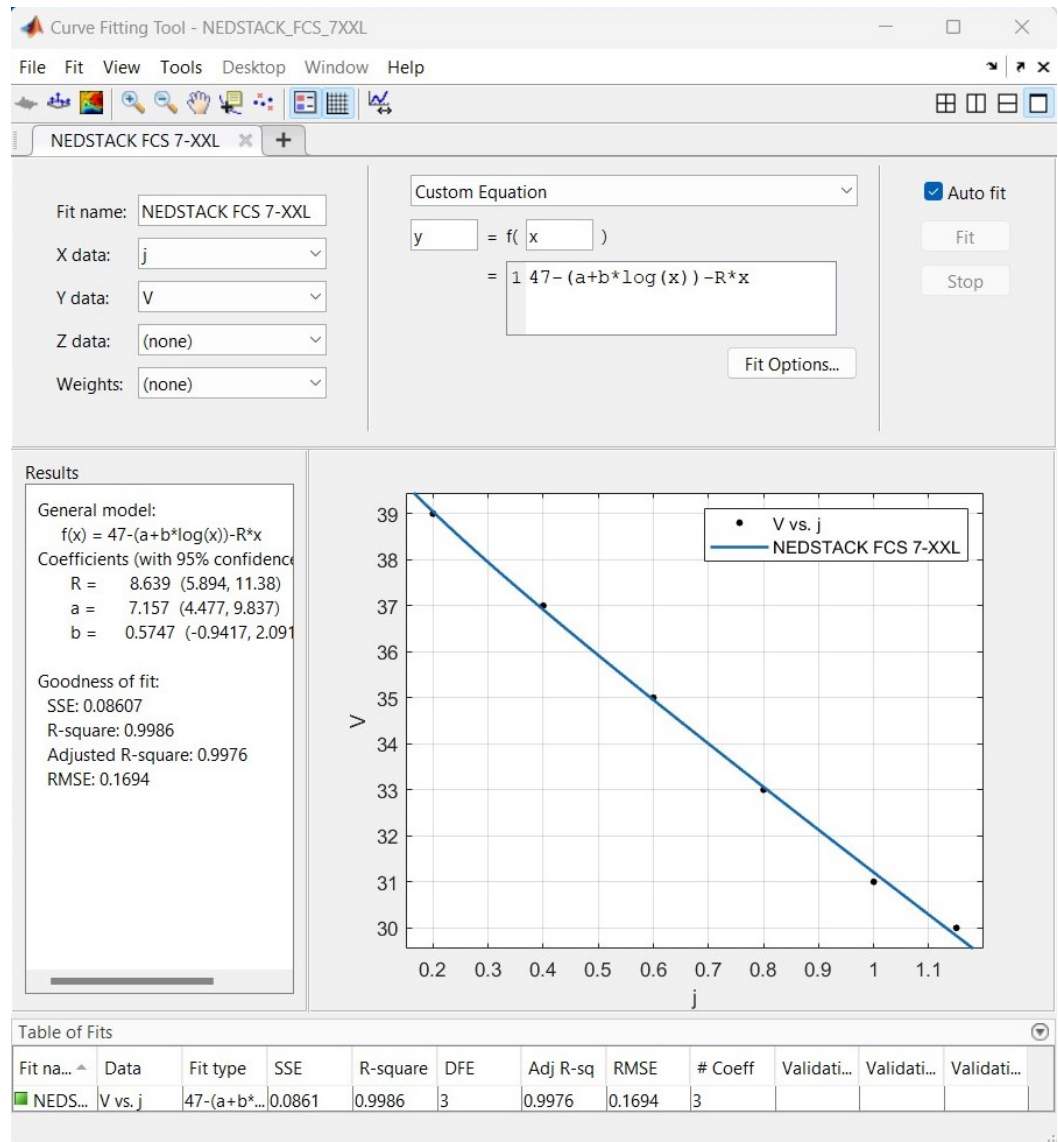


Figure 3.7 – Curve Fitting Toolbox setting and result for the FCS 7-XXL fuel cell's stack polarization curve.

Source: Author's elaboration.

As far as the power production is concerned, the electrical generation would simply be the product of the voltage at the stack terminal and the generated current, while the thermal loss would be the difference between the electrical generation in ideal and real conditions, accounting for the voltage loss terms described previously.

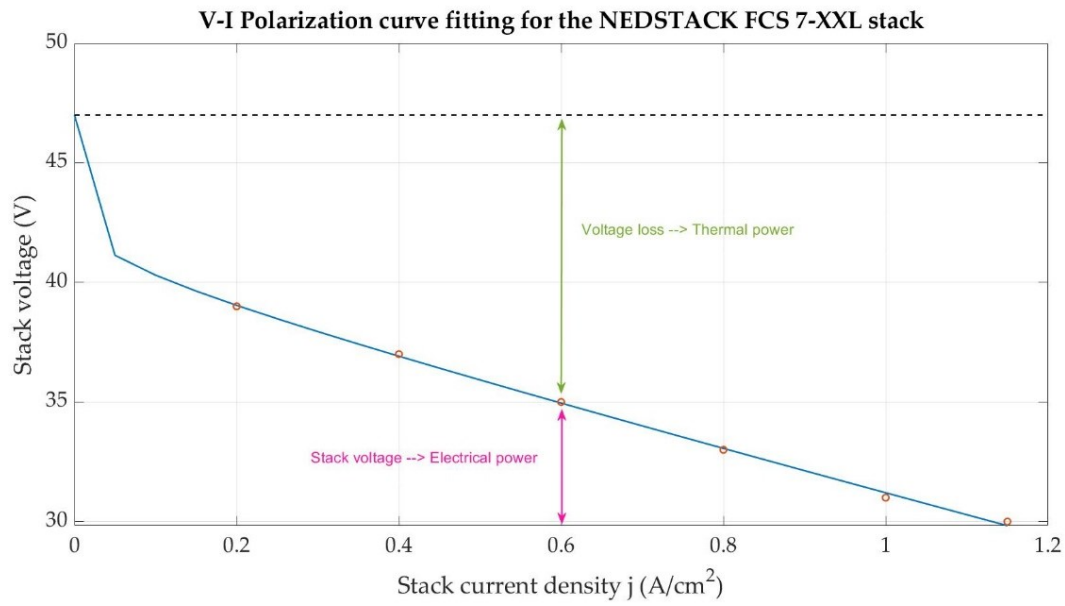


Figure 3.8 – Polarization curve and voltage contributions to the stack electrical power and thermal loss depending on the current density.

Source: Author's elaboration.

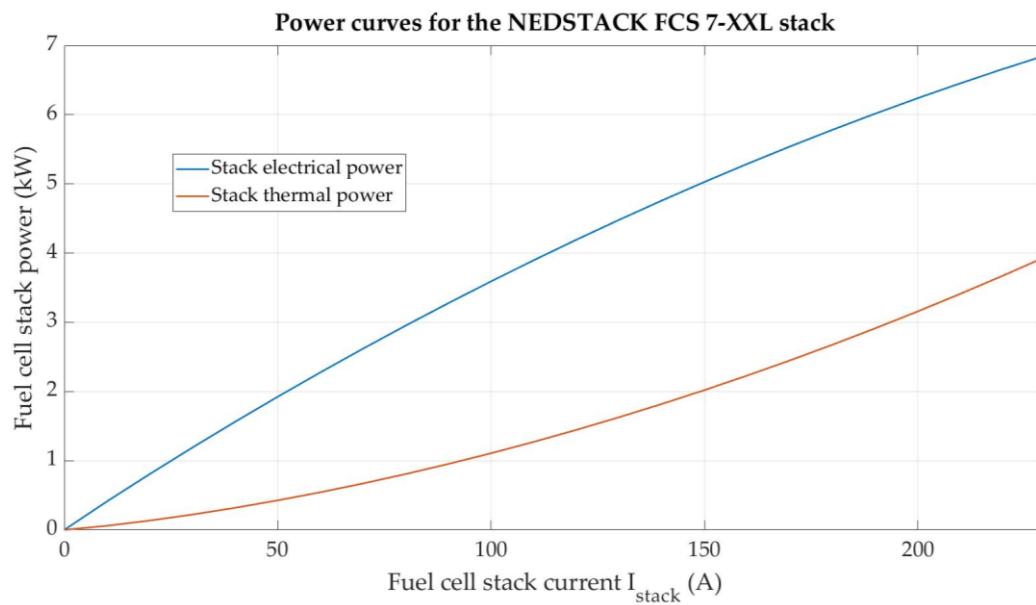


Figure 3.9 – FCS 7-XXL stack electrical and thermal power curves evolution as function of the stack current.

Source: Author's elaboration.

4. Model Predictive Control implementation

4.1. Introduction to Model Predictive Control

Model Predictive Control, commonly abbreviated to MPC, is a control strategy widely employed in various sector, from autonomous vehicles to industry automatization to building integration, based on an iterative and finite-horizon optimization of a plant simplified model. It first appeared in literature in the late 1970s, but its implementation gained popularity in the Chemical Process Industry sector in the 1980s. The feedback algorithm which the controller is based on takes advantage of an already defined dynamic model. In this way predictions of the effect of future actions on the plant output are possible [17].

Model Predictive Control is also commonly known as Receding Horizon Control (RCH) because of the forward-moving nature of the control timeframe.

One of the strengths of MPC is its capability to handle multi-input multi-output systems (MIMO), meaning it can manage more than just one single parameter receiving instead more inputs and therefore performing multi-dimensional optimizations. Such multivariable controller can act simultaneously on more than just one output taking into account the interaction between all the involved variables. In MIMO plants the variation of a single output might influence all the others.

MPC implements the optimization of an objective function that includes the plant variables to control. Such optimization is performed at each time step of the prediction horizon p , which is the entire period of time through which the controller operates. Once a plant simplified mathematical model and a reference for the output are established, a forecast of the plant behavior is performed forward in time over a shorter timeframe that is the control horizon c . When the simulation starts running, the controller receives the measured plant state, its initial condition. In this study that would be the initial indoor air temperature for each of the thermal zones. A first optimization of the objective function, which naturally includes the current plant state, the setpoint and a decision variable (in this case the heating power released to the zone) is carried out. Once the latter is obtained from the optimization, its value is sent to the plant and an updated system condition is recorded. The cycle ends with the variables

updating, the control horizon shifting and the problem reinitialization.

The indoor air temperature is compared with the setpoint in the objective function. The deviation of the predicted output from the goal temperature setpoint is the quantity that the optimizer will primarily minimize but additional requirements on both the plant input (heating power delivery) and output (indoor temperature) can be included.

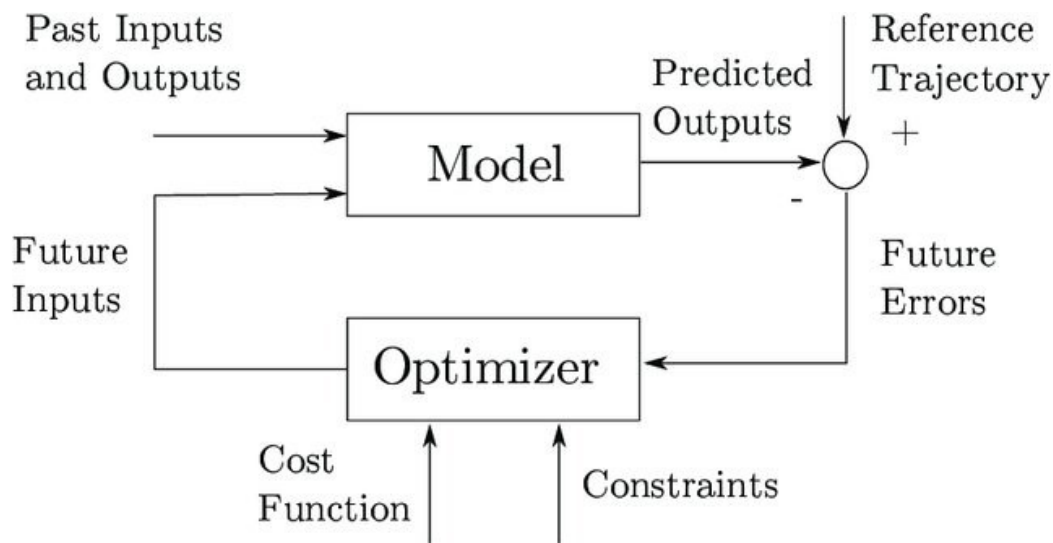


Figure 4.1 – Basic Structure of a general Model Predictive Control implementation.

Source: Pendleton, Scott & Andersen, Hans & Du, Xinxin & Shen, Xiaotong & Meghjani, Malika & Eng, You & Rus, Daniela & Jr, Marcelo. (2017). Perception, Planning, Control, and Coordination for Autonomous Vehicles. Machines. 5. 6.

Another reason behind the wide spread of MPC controllers is the chance to impose constraints on both the plant state and the decision variable. The introduction of such constrained monitoring ensures that the variables of interest never fall out of specified ranges. Imposing constraints in the optimization algorithm can be extremely important, as for instance in this application the indoor temperature should not fall out of the ± 2 °C tolerance proposed at the end of Section 2.2. An upper limit for the heating power delivery to each zone can also be introduced but care must be taken as the input and the output constraints could theoretically conflict and make the optimum search fail.

The whole process can get computationally expensive when a multi-variable control strategy is implemented. A compromise between the accuracy of the optimization result and the machine computational effort is asked for but the development of increasingly fast computers and hardwares are expected to alleviate the issue in the future.

At this point, it is necessary to remark that MPC requires a plant simplified model to include in the minimization core of the control algorithm. Linear models are easily controllable, while non-linear ones often require a local linearization procedure and more advanced solving algorithms.

Summarizing, at each time step the controller evaluates what would be the value of the decision variable to send as input to the plant so that its state variable reaches as fast as possible a target reference depending on its initial condition. The way Model Predictive Control carries out this quite simple idea is actually predicting the future plant output with a mathematical simplified model that mimics the real system response. On a general view, the accuracy of the model response and its complexity go hand in hand, and it is the task of the designer to decide which variables are worth to include.

4.2. Design parameters specification

The first task to accomplish in the design process of the MPC controller is the parameters setting. A careful selection of their values, also with the aid of a trial and error method, can result in a higher quality of the controller operation schedule and a reduced computational cost of the algorithm. The three parameters to focus the attention on are listed below.

- Sample time t_s

The sample time t_s is the time step at which the MPC is actuated. It sets the rate at which the control algorithm is executed. On one hand, if the sample time is too large the controller may be unable to record higher frequencies disturbances possibly interfering with the system while, on the other, in case it is too small an increased computational cost is expected and, even worse, high fluctuations in the controller

schedule could generate if the plant state varies with a significantly slower rate.

- Prediction horizon p

The time window over which the controller is intended to operate is called prediction horizon p . The corresponding number of time steps is indicated with N_p . For building application p is commonly set in the range of days or weeks, subordinate to the availability and reliability of weather data. The external temperature, the solar radiation, the indoor and outdoor air humidity and the wind speed all affect the system state (i.e. the internal temperature T_{indoor}) through heat exchange processes between the outdoor and the indoor ambient.

- Control horizon c

The optimizer in the controller core operates over a more or less wide timeframe called control horizon c . The corresponding number of time steps is indicated with N_c . This parameter can naturally range between the sample time t_s and the entire prediction horizon p . At each time step the optimization algorithm works over the entire c providing a set of control actions u_k, \dots, u_{k+N_c} . Usually they are all discarded except for u_{k+1} , the one related to the immediate subsequent time step. This control action is recorded, actuated and finally the plant response is used to reinitialize the loop. The control horizon is then shifted one step forward in time. The smaller is c , the less are the control actions that the optimizer has to compute at each time step k . The significance of the control moves results beyond u_{k+1} is quite low, as for all of them the earlier plant state would necessarily come from the simplified model rather than the real plant. A good rule of thumb for the control horizon c is to set it to around $10 \div 20$ % of p but covering at least 2-3 time steps.

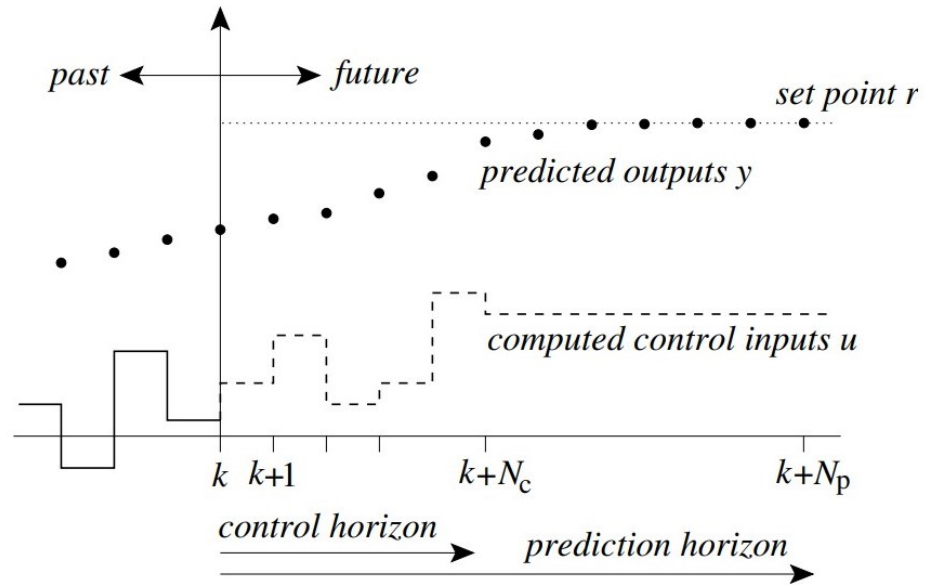


Figure 4.2 – MPC design parameters and input and output visualization.

Source: Negenborn, R.R. & De Schutter, Bart & Wiering, Marco & Hellendoorn, J. (2022). Experience-based model predictive control using reinforcement learning.

As mentioned above, MPC can incorporate constraints on the input and output values but also on the inputs' rate of change. This means that a limitation on the variation of the value of the control action u from one time step to the subsequent can be included along with the minimization of the output deviation from the setpoint. This directly translates into the chance of limiting the variation in time of the thermal power delivery to the building, as steep changes may infatuate the household comfort. A classification on the variables' constraints categorized them into hard or soft ones, according to whether a violation of the threshold is possible (even if not desirable) or not. Having hard constraints on both inputs and outputs is not advisable since they could conflict one with each other, causing the optimum search to fail or lead to unrealistic results.

The MPC controller looks for the output evolution in time that gets as fast as possible to the set target, but, again, a set of smooth control moves is desirable from the user perspective in order to avoid abrupt changes in the plant state. The way to achieve this is weighing the input rate of change and the output deviation from the reference setpoint in the optimization objective function J , usually also referred to as cost function. Its expression varies depending on the application. It can be a sum of squared

errors, a sum of absolute errors, the worst error over time or an economic objective. J expression would be a weighted squared sum of the predicted errors on the plant output and the input variation in this work. While searching for the cost function minimum at the current time step, the MPC controller also checks that both inputs and outputs stay within the constraints, as already mentioned.

The input sequence u_k, \dots, u_{k+N_c} is then the result of the cost function J minimization over c . At the current time step k the controller records only the first value of such input sequence found by the algorithm erasing all the others. After sending u_{k+1} to the system, the controller records a new measurement of its state as a result of the combination of the input control action and the disturbances on the plant. The evolution of the plant state is expected to differ from the prediction computed over c by the controller, based on the simplified model.

4.3. The controller mathematical formulation

Optimization is the core of MPC. How the controller searches for the optimal set of input values at each time step strongly depends on the mathematical formulation of the system model, and the chance of linearizing it as the major discriminating factor. If the model is linear, it has linear constraints and a quadratic cost function J is built, then the system can be controlled by a linear time-invariant MPC. In this case the cost function is naturally convex, showing one single global optimum. The algorithm goal will therefore be finding it, knowing its existence is ensured when all the properties listed above are verified.

If the system is instead non-linear, a linear MPC strategy can be in principle implemented, but only if a linearized model of the plant can be built, keeping all the benefits of the convex problem optimization. The adaptive and gain-scheduled MPC controllers are the two available methods for this kind of problem. Adaptive MPC, for instance, updates at each time step the plant non-linear model with its linearized version. The optimization problem keeps the same mathematical formulation from each time step to the subsequent over the entire prediction horizon, and so do the constraints. A gain-scheduled MPC strategy is commonly adopted if instead a tracking on the operating condition is needed to modify the constraints. A local linearization of

the model is performed offline in this case for each of the operating point. In other words, a specific controller is designed at each time step and each is equipped with its own set of variables' constraints. The algorithm needs a portion of code to be able to switch between controllers when the plant operating conditions change.

Gain-scheduled MPC evidently requires a larger memory to store all the pre-defined controller versions. The general recommendation is to resort to the adaptive method when the plant model can be locally linearized, and the constraints are fixed independently from the system state.

In case of non-linear system that cannot be represented at all with linearized models (not even locally), then non-linear Model Predictive Control is required. The system modeling can be highly realistic and as a consequence the controller prediction can be extremely accurate. Solving the optimization problem for a non-linear cost function can get however quite tough when non-linear constraints are set on the variables, since J may not be convex anymore, showing multiple local minima. Finding the global one among them is not an easy numerical task at all and much more sophisticated algorithms are needed to accomplish for the task.

The general quadratic cost function formulation for a multi-input and multi-output problem in 2-Norm is

$$J_0(x(0), U_0) = x'_{N_c} P x_{N_c} + \sum_{k=0}^{N_c-1} (x'_k Q x_k + u'_k R u_k) \quad (4.1)$$

where

- N_c is the time control horizon.

- $U_0 \triangleq [u'_0, \dots, u'_{N_c-1}]'$ is the input sequence.

- $x'_{N_c} P x_{N_c}$ and $(x'_k Q x_k + u'_k R u_k)$ are Squared Euclidean Norms.

- $P, Q \geq 0$ are positive semi-definite weighting matrices.

- $R > 0$ is a positive definite weighting matrix.

The cost function expression can be rearranged in vectorial form as

$$\begin{aligned}
 J_0(x(0), U_0) = & x_0' Q x_0 + \begin{bmatrix} x_1 \\ x_2 \\ \vdots \\ x_{N_c-1} \\ x_{N_c} \end{bmatrix}' \begin{bmatrix} Q & 0 & 0 & \dots & 0 \\ 0 & Q & 0 & \dots & 0 \\ \vdots & \vdots & \ddots & \vdots & \vdots \\ 0 & \dots & 0 & Q & 0 \\ 0 & 0 & \dots & 0 & P \end{bmatrix} \begin{bmatrix} x_1 \\ x_2 \\ \vdots \\ x_{N_c-1} \\ x_{N_c} \end{bmatrix} \\
 & + \begin{bmatrix} u_0 \\ u_1 \\ \vdots \\ u_{N_c-1} \end{bmatrix}' \begin{bmatrix} R & 0 & \dots & 0 \\ 0 & R & \dots & 0 \\ \vdots & \vdots & \ddots & \vdots \\ 0 & \dots & 0 & R \end{bmatrix} \begin{bmatrix} u_0 \\ u_1 \\ \vdots \\ u_{N_c-1} \end{bmatrix}
 \end{aligned} \tag{4.2}$$

A Constrained Finite-Time Optimal Control (CFTOC) problem can be formulated as a minimization of the cost function over N_c .

$$J_0^*(x(0)) = \min_{U_0} [J_0(x(0), U_0)] \tag{4.3}$$

The mathematical expression for the simplified plant model follows.

$$x_{k+1} = Ax_k + Bu_k, \quad k = 0, \dots, N_c - 1$$

$$x_k \in \mathcal{X}, \quad k = 0, \dots, N_c - 1$$

$$u_k \in \mathcal{U}, \quad k = 0, \dots, N_c - 1$$

$$x_{N_c} \in \mathcal{X}_f$$

$$x_0 = x(0)$$

(4.4)

At the following time step $k+1$ the plant state x_{k+1} is predicted to be a linear combination of the current state x_k and input u_k . \mathcal{X} , \mathcal{U} and \mathcal{X}_f are polyhedral regions, the variables' domains in multi-dimensional application. The constraints are included in their definition. For SISO models, they naturally translate into intervals in \mathbb{R} . Also in this case it is possible to expand the linear model in vectorial notation.

$$\begin{bmatrix} x_1 \\ x_2 \\ \vdots \\ x_{N_c-1} \\ x_{N_c} \end{bmatrix} = \begin{bmatrix} B & 0 & \dots & 0 \\ AB & B & \dots & 0 \\ \vdots & \vdots & \ddots & \vdots \\ A^{N_c-1}B & A^{N_c-2}B & \dots & B \end{bmatrix} \begin{bmatrix} u_0 \\ u_1 \\ \vdots \\ u_{N_c-1} \end{bmatrix} + \begin{bmatrix} A \\ A^2 \\ \vdots \\ A^{N_c} \end{bmatrix} x_0$$

(4.5)

For Model Predictive Control (i.e. Receding Horizon Control), coupled with a linear model as defined as in (4.4), a CFTOC is solved in the form of

$$J_t^*(x(t)) = \min_{U_{t \rightarrow t+N_c|t}} \left[p(x_{t+N_c|t}) + \sum_{k=0}^{N_c-1} q(x_{t+k|t}, u_{t+k|t}) \right]$$

$$x_{t+k+1|t} = Ax_{t+k|t} + Bu_{t+k|t}, \quad k = 0, \dots, N_c - 1$$

$$x_{t+k|t} \in \mathcal{X}, u_{t+k|t} \in \mathcal{U}, \quad k = 0, \dots, N_c - 1$$

$$x_{t+N_c|t} \in \mathcal{X}_f$$

$$x_{t|t} = x(t)$$

(4.6)

where

- $U_{t \rightarrow t+N_c|t} = \{u_{t|t}, \dots, u_{t+N_c-1|t}\}$ is a generic input sequence.
- $x_{t|t}$ is the system state at time t .
- $x_{t+k|t}$ is the state of the plant model at time $t+k$, predicted at time t computed applying to the linearized system model $x(t+1) = Ax(t) + Bu(t)$ the input sequence $u_{t|t}, \dots, u_{t+k-1|t}$, starting from the current state $x_{t|t} = x(t)$.
- $u_{t+k|t}$ is the input value at time $t+k$, predicted at time t .

The minimization algorithm searches for the optimal input sequence solution over the control horizon $U_{t \rightarrow t+N_c|t}^* = \{u_{t|t}^*, \dots, u_{t+N_c-1|t}^*\}$ but only the first element is applied to the plant, so that

$$u(t) = u_{t|t}^*(x(t)) \quad (4.7)$$

The peculiarity of the MPC formulation with respect to the general CFTOC one is that the minimization of the cost function is performed at each time step of the control horizon, then throughout $t \rightarrow t + N_c$.

Summarizing, the controller implements and solves at each time step a CFTOC problem over the whole control horizon but only the optimal input found in $[t, t+1]$ is sent to the plant. At $t+1$, the CFTOC problem is solved again but on a control horizon shifted by one sampling time and with the updated system state. The procedure is reiterated throughout the prediction horizon length.

The sequence of the MPC controller operation steps follows.

1. Measure of the current state x_k .
2. Solve the CFTOC problem, obtaining the solution $U_{t \rightarrow t+N_c|t}^* = \{u_{t|t}^*, \dots, u_{t+N_c-1|t}^*\}$.

3. The first element of the solution vector $u(t) = u_{t|t}^*$ is sent to the plant, while all the others are discarded.
4. Update the time step $k + 1 \rightarrow k$ and repeat the loop.

4.4. MATLAB and EnergyPlus co-simulation interface

The MPC technique implementation requires, on one side, the definition of the plant mathematical model and, on the other, the proper control algorithm. Various software are commercially available to run building energy simulation. The choice falls on EnergyPlus for the purpose of this analysis as it is free and open source, but also due to the availability of a comprehensive software documentation available for any version of the software. The MATLAB environment is a reasonable choice for the development of the MPC algorithm and the fuel cell stack modeling.

The two software need to run simultaneously and exchange information at each time step; thus a co-simulation interface must be thought out. A first solution could be resorting to the Building Controls Virtual Test Bed, an interface which allows the coupling of a bunch of simulation programs. It is based on the Ptolemy II software environment, and it was developed by the University of California at Berkeley [21].

EnergyPlus provides a co-simulation object called `ExternalInterface`, which is originally intended to run with the BCVTB. However, the communication protocol is open and can be used by other interfaces devoted to co-simulation. In particular, MLE+ is a MATLAB toolbox explicitly developed to transfer information with building energy simulation running on EnergyPlus, relying on the BCVTB architecture but allowing an easier communication between the two softwares for non-expert users who are familiar with MATLAB and Simulink. The direct coupling via the BCVTB can get quite complex, requiring the user to learn the Ptolemy II programming language to let the BCVTB call MATLAB as a client. MLE+ is instead called and executed in a traditional MATLAB workspace, therefore enabling code generation and debugging, low-level co-simulation API (Application Programming Interface) and the integration of other useful toolboxes.

In this study the MLE+ toolbox is tested with the EnergyPlus 9.6.0 and MATLAB R2020a releases. Its full functionality with future software releases needs to be verified.

The MLE+ interface is implemented as a loose coupling co-simulation architecture between clients [22] (MATLAB and EP in this case) in order to reduce the risk that a change made within one software will cause unanticipated changes within the other. This can help in simplifying the simulation testing and fixing.

Each software performs its simulation autonomously and exchange data at a fixed synchronization time step without any communication in-between two subsequent time instants. This means that EP runs the simulation at a fixed time step and pauses, sends information through the MLE+ external interface to MATLAB, which will compute the control action to be sent back to EP.

The MLE+ Toolbox provides a set of functions and classes to implement the co-simulation. Those required to enable the communication between the two softwares are listed below.

- `mlep.idfFile` to specify the IDF building simulation configuration file
- `mlep.epwFile` to specify the EPW weather file
- `mlep.initialize` to load and parse all input files, make interface I/O configuration
- `mlep.start` to start the EnergyPlus process and establish connection
- `mlep.read` to read outputs from the EnergyPlus simulation.

Syntax: `[outputs, time] = read(obj)`

Outputs:

`outputs` - Vector of real values sent by EnergyPlus.

`time` - Time mark sent by EnergyPlus simulation.

- `mlep.write` to write inputs to the EnergyPlus simulation.

Syntax: `write(inputs, time)`

Inputs:

`inputs` - Vector of real values to be sent to EnergyPlus.

time - Time mark to be send to the EnergyPlus simulation.

- `mlep.stop` to close communication and stop the EnergyPlus process. Close socket connection.

Even if in principle the MLE+ toolbox does not require the BCVTB to be installed, the EP `ExternalInterface` object actually does in order to export and import data. The MLE+ and the BCVTB manuals provide a detailed tutorial for both the installation and configuration process of the two.

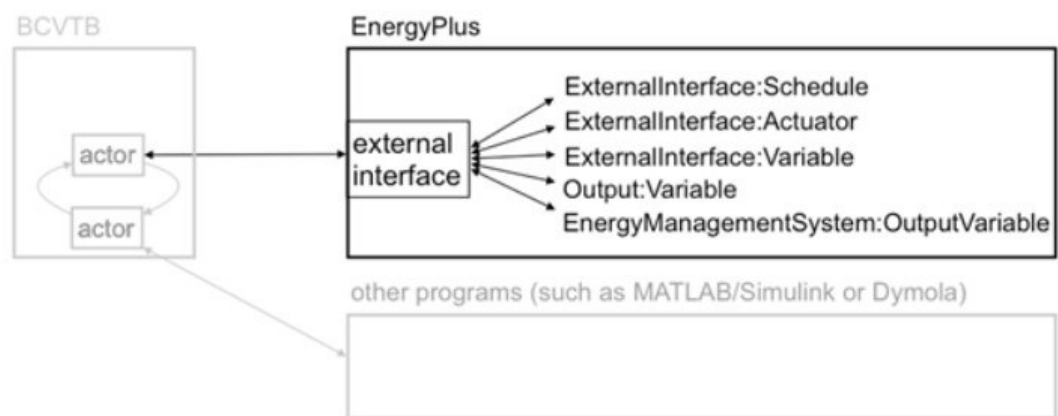


Figure 4.3 – Architecture of the BCVTB with the EnergyPlus client and other clients.

Source: EnergyPlus Documentation.

The IDF file needs to be updated to allow the data exchange by introducing this `ExternalInterface` object. The name of the external interface is the only required input, being in this case `PtolemyServer`.

```
!- ===== ALL OBJECTS IN CLASS: EXTERNALINTERFACE =====

ExternalInterface,

    PtolemyServer;          !- Name of External Interface
```

All the variables, schedules or actuators set directly by the external interface (i.e., output from the MATLAB code and input to EnergyPlus) need to be declared at this point with a `ExternalInterface:Variable`, `ExternalInterface:Schedule` or `ExternalInterface:Actuator` object. An example for ZT1 Kitchen taken from the code follows.

```
!- ===== ALL OBJECTS IN CLASS: EXTERNALINTERFACE:SCHEDULE =====  
  
! Heating schedule. This schedule is set directly by the external  
interface.  
  
    ExternalInterface:Schedule,  
  
    HeatingRatePower1,          !- Name  
  
    FRACTION,                   !- Schedule Type Limits Name  
  
    0;                          !- Initial Value
```

A configuration .xml file to name variables.cfg needs to be created in the same directory of the building simulation Input Data File and the MATLAB code. This file specifies all the input and output variables to and from EnergyPlus and their order. The .xml file must be written following a rigid syntax set of rules, otherwise the communication is failing. In particular the file shows the header

```
<?xml version = "1.0" encoding = "utf-8"?>  
  
<!DOCTYPE BCVTB-variables SYSTEM "variables.dtd">
```

followed by the exchanging variables mapping.

Such list is structured in-between the lines

```
<BCVTB-variables><!--INPUT to E+-->
```

and

```
</variable><!--OUTPUT from E+-->
```

and

```
</BCVTB-variables>
```

as a set of three lines for each of those variables.

The first of these three lines set will be

```
<variable source = "Ptolemy"> in the first block
```

or

```
<variable source = "EnergyPlus"> in the second block
```

depending on whether the interface is sending an input to EP (i.e. Ptolemy is the variable source, which actually first collects the data from MATLAB) or getting an output from it (i.e. EP is the variable source).

The second line is written as

- `<EnergyPlus actuator = "NAME"/>`
for `ExternalInterface:Actuator`, where `NAME` is the EnergyPlus actuator name.
- `<EnergyPlus schedule = "NAME"/>`
for `ExternalInterface:Schedule`, where `NAME` is the EnergyPlus schedule name.
- `<EnergyPlus variable = "NAME"/>`
for `ExternalInterface:Variable`, where `NAME` is the EnergyPlus Energy Runtime Language (Erl) variable name.

The third and last line would simply close the variable definition with

```
</variable>
```

The IDF file needs to be updated to also include the delivery of the amount of heat as computed by the controller to each ambient. For simplicity, this can be done with an `OtherEquipment` object by simply providing the control action from the Ptolemy interface. Such object configures a heating power gain or loss directly to the zone and without the need of designing an entire HVAC system. The portion of code for the ZT1 Kitchen follows.

```
!- ===== ALL OBJECTS IN CLASS: MPC =====

OtherEquipment,

    HeatZT1,                !- Name

    ,                      !- Fuel Use Type

    ZT1 Kitchen,           !- Zone Name

    HeatingRatePower1,     !- SCHEDULE Name

    EquipmentLevel,        !- Design Level calculation method

    1117,                  !- Design Level {W}

    ,                      !- Power per Zone Floor Area {watts/m2}

    ,                      !- Power per Person {watts/person}

    0,                     !- Fraction Latent

    0,                     !- Fraction Radiant

    0,                     !- Fraction Lost

    1.2E-7,                !- Carbon Dioxide Generation Rate

    ;                      !- End-Use Subcategory
```

The schedule for the `OtherEquipment` object is asked as a fraction of the `Design Level {W}` entry. The values of such maximum heating power levels for each zone are found in Section 4.5.1.

4.5. MPC implementation to the CorTau house

4.5.1. CorTau House performance in normal operation condition

Two preliminary simulations are carried out before the implementation of the MPC technique, with the first being a EP energy building simulation in so-called normal operation condition, in which the HVAC system operation is governed by the thermostat setpoint. As already mentioned, a weather file in the EPW format is required by EP to correctly run the simulation. The International Weather for Energy Calculations (IWEC) data file for Turin is used here, which is the result of the ASHRAE Research Project 1015 by Numerical Logics and Bodycote Materials Testing Canada for ASHRAE Technical Committee 4.2 Weather Information.

The unit is modelled with a `ZoneHVAC:IdealLoadsAirSystem` object.

```
!- ===== ALL OBJECTS IN CLASS: ZONEHVAC:IDEALLOADSAIRSYSTEM =====

ZoneHVAC:IdealLoadsAirSystem,

    ZT1 Kitchen Ideal Loads Air System,    !- Name

    ,                                     !- Availability Schedule Name

    ZT 1 Cucina Ideal Loads Supply Inlet,    !- Zone Supply Air Node Name

    ,                                     !- Zone Exhaust Air Node Name

    50,                                     !- Maximum Heating Supply Air Temperature {C}

    13,                                     !- Minimum Cooling Supply Air Temperature {C}

    0.0156,    !- Maximum Heating Supply Air Humidity Ratio {kgWater/kgDryAir}

    0.0077,    !- Minimum Cooling Supply Air Humidity Ratio {kgWater/kgDryAir}

    NoLimit,                                     !- Heating Limit

    ,                                     !- Maximum Heating Air Flow Rate {m3/s}

    ,                                     !- Maximum Sensible Heating Capacity {W}

    NoLimit,                                     !- Cooling Limit

    ,                                     !- Maximum Cooling Air Flow Rate {m3/s}
```

```
,                                !- Maximum Total Cooling Capacity {W}

,                                !- Heating Availability Schedule Name

,                                !- Cooling Availability Schedule Name

ConstantSensibleHeatRatio,      !- Dehumidification Control Type

0.7,                             !- Cooling Sensible Heat Ratio {dimensionless}

None,                             !- Humidification Control Type

,                                !- Design Specification Outdoor Air Object Name

,                                !- Outdoor Air Inlet Node Name

None,                             !- Demand Controlled Ventilation Type

NoEconomizer,                   !- Outdoor Air Economizer Type

None,                             !- Heat Recovery Type

0.7,                             !- Sensible Heat Recovery Effectiveness {dimensionless}

0.65;                            !- Latent Heat Recovery Effectiveness {dimensionless}
```

For what concerns the internal gains, their contribution is always taken into consideration throughout the year in the energy balance of the thermal zones except for two specific days, which are called Heating Design Day and Cooling Design Day or alternatively Winter Design Day and Summer Design Day. The sizing of the HVAC system is based on the energy needs of the building during these two days as the worst climatic conditions for the heating season and the cooling season are observed. The Design Day Outdoor Air Temperature is evaluated according to the criteria proposed in the ASHRAE Handbook of Fundamentals. In particular, a high and a low pair of dry-bulb temperatures and a range multiplier are used to build the daily profile of the external temperature in Design Day. However, the user can provide a different profile in accordance with other methodologies or even historical meteorological data. Solar irradiance on the building envelope is the other physical quantity along with the outdoor temperature playing a major role on the evolution of the building heating and cooling loads, with the ASHRAE Clear Sky being the EP default solar model. The Direct Normal Irradiation DNI is evaluated as follows.

$$DNI = A \cdot e^{-\frac{B}{\sin(\alpha)}} \quad (4.8)$$

Where

- A is the solar radiation beyond the atmosphere, or in other words, the apparent solar irradiation at air mass $m = 0$.
- B is the atmospheric extinction coefficient.
- α is the solar altitude.

January 21st is the Winter Design Day for the the CorTau House based on the data available in the EPW file for Turin.

Table 4.1 – Winter Design Day specifications in the EnergyPlus model.

Maximum Dry-Bulb Temperature	-6 °C
Daily Dry-Bulb Temperature Range	0 °C
Wetbulb or DewPoint at Maximum Dry-Bulb	- 6 °C
Barometric Pressure	97924.0 Pa
Wind Speed	0.4 m/s
Wind Direction	300 deg
Solar Model Indicator	ASHRAE Clear Sky

Source: Author's elaboration.

The EP simulation of the CorTau House in normal operation condition is executed, and the results of the the heating load evolution to meet the setpoint in Winter Design Day is shown in Figure 4.4. For each thermal zone, the load peak will be used as the upper constraint on the decision variable for the future implementation of the controller. Both the sensible and the latent fractions are included in the heating load.

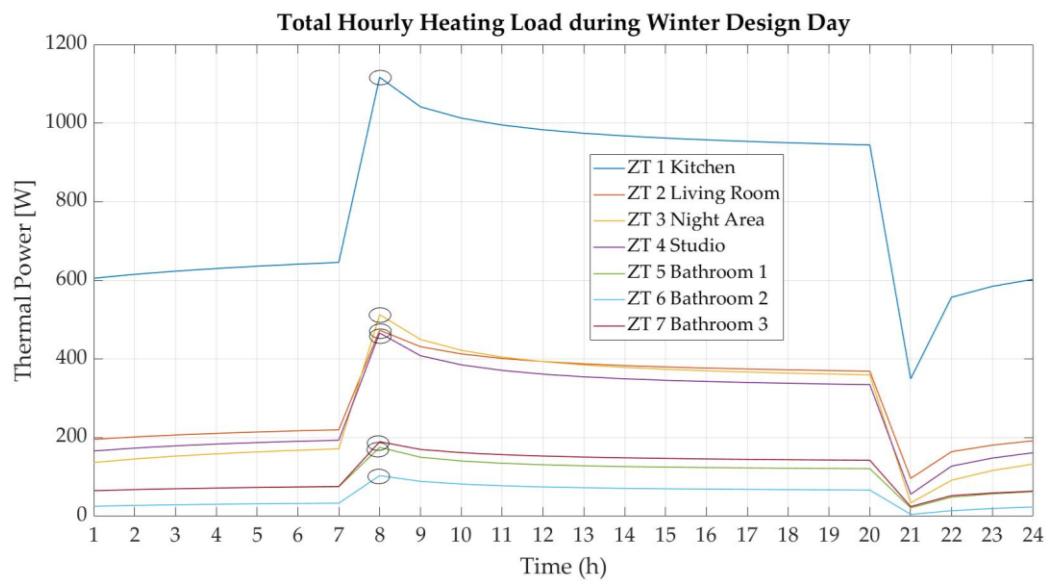


Figure 4.4 – Evolution of the Heating Load during Winter Design Day for all the thermal zones.

Source: Author's elaboration.

Table 4.2 – Maximum hourly heating power from Winter Design Day.

	Heating Power [W]
ZT 1 Kitchen	1117
ZT 2 Living Room	474
ZT 3 Night Area	513

ZT 4 Studio	467
ZT 5 Bathroom1	176
ZT 6 Bathroom2	104
ZT 7 Bathroom3	190

Source: Author's elaboration.

4.5.2. CorTau House performance in extreme operations condition

The second preliminary simulation required to configure the MPC controller involves the building free-running operation condition, in which the HVAC system is turned OFF and all the internal gains to the thermal zones are erased from the simulation. In other words, the idea is to observe the performance of the building envelope when subject to critical conditions in winter. As a result, the indoor temperature is set free and will only depend on how the building envelope responds to the external weather condition. In this way it is possible to quantify how well the building reacts to a heating supply shortage. As all the internal gains are set to zero, the free-running operation condition let the designer quantify how fast the indoor temperature would decrease when no free gain appears in the thermal balance of each zone. A cooling rate in °C/h can be computed. This information is quite useful to understand what a suitable time step for the development of the controller could be. As a rule, the controller time step should be in the order of magnitude of the time required to observe a significative variation in the indoor temperature.

A possible strategy to implement such extreme operation condition in EP is by modifying the schedule of the heating system to turn it off when desired. Although this is in principle sufficient, a very low fictitious setpoint temperature (for instance -100 °C) is also set in the heating season, to guarantee that even if for some reasons the heating system would unexpectedly turn on, such redundant condition on the setpoint guarantees that no heat will be however supplied.

The rationale behind this preliminary simulation is to keep the original setpoint and setback temperatures of 20 °C and 18 °C and the HVAC system ON from January 1st to January 7th, and then forcing the extreme operation condition on January 8th with the methodology described above.

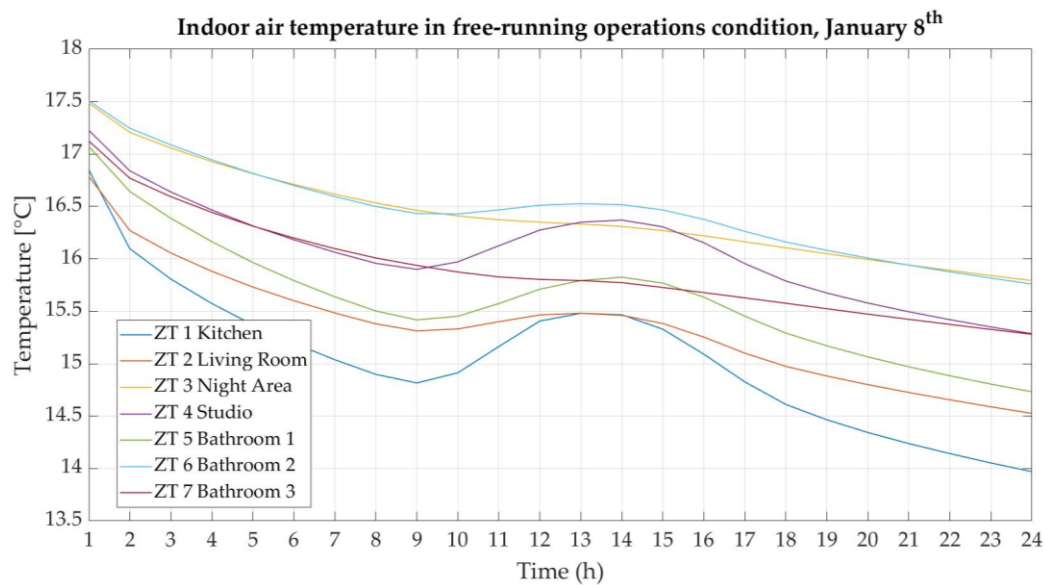


Figure 4.5 – Evolution of the indoor air temperature in free-running operations condition for all the thermal zones on January 8th.

Source: Author's elaboration.

The common trend observed for all the thermal zones is a monotonous decrease in the indoor air temperature until approximately 9:00, as the HVAC system is turned OFF and the internal gains are erased from the thermal balance. An increase follows throughout the central hours of the day for all the zones except for ZT3 Night Area and ZT7 Bathroom 3, with a bell-type trend that can be reasonably ascribed to the effect of the solar radiation reaching the building, which is, indeed, the only contribution to the thermal balance that cannot be erased in this kind of simulation. Major increases are observed in ZT1 Kitchen, ZT4 Studio and ZT5 Bathroom 1, as they are characterized by the highest amounts of fenestration per floor area. Even if overhangs are installed to limit the impact of the sun radiation, the design is typically performed in the summer season to prevent overheating, and, consequently, the overhang depth

is not shadowing the entire window in winter when the solar altitude is notably lower. In addition, the effect of both reflected and diffuse radiation components cannot be avoided at all adopting such protection devices.

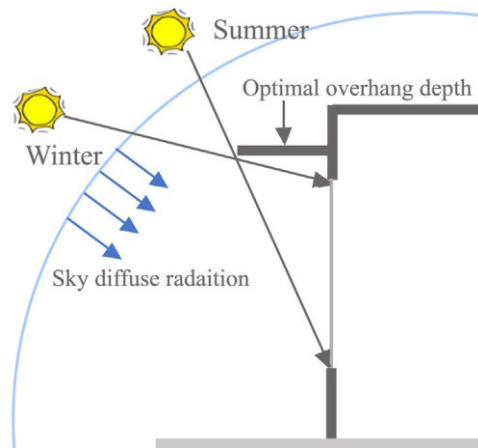


Figure 4.6 – Example of optimal overhang depth design.

Source: Yao, Jian. (2014). An investigation into the impact of movable solar shades on energy, indoor thermal and visual comfort improvements. *Building and Environment*. 71. 24–32.

Focusing on the initial temperature decrease observed at night, ZT1 Kitchen accounts for the greatest drop. This is mainly due to, again, the amount of fenestration (usually characterized by higher values of thermal transmittance with respect to the opaque envelope), but also to the fact that most of the zone perimeter is external and directly exposed to the outdoor environment. This is not the case for ZT3 Night Area for instance, as it is in contact with the adjacent building on the west-oriented side of the CorTau House and a significantly lower fraction of its perimeter is external.

The choice of a simulation time step $t_s = 1$ h for the controller seems reasonable as significant plant state variations can be appreciated after one or more hours in free-running conditions. All the building zones experience at least a 1 °C drop in indoor air temperature at night on January 8th, and the effect is expected to be amplified in case the external temperatures are lower, reminding that the day chosen for this simulation is not the Winter Design Day, as it could conflict with the need of turning OFF the HVAC system.

As expected, the building envelope performance in free-running operation is quite satisfactory as the design choices adopted in the renovation process were expected to guarantee an excellent thermal performance of the house. The cooling rate associated to ZT1 almost doubles the value measured in other zones.

Table 4.3 – Cooling rate for all the building thermal zones at night.

	Cooling rate [°C/h]
ZT 1 Kitchen	0.23
ZT 2 Living Room	0.16
ZT 3 Night Area	0.11
ZT 4 Studio	0.15
ZT 5 Bathroom1	0.18
ZT 6 Bathroom2	0.12
ZT 7 Bathroom3	0.13

Source: Author's elaboration.

4.5.3. Development of the linear model for each heated zone

Following the two preliminary simulations which involved exclusively EnergyPlus, the idea is to set now a first co-simulation interface with MATLAB to build the simplified thermal model of the house. This will be later employed in the optimization core of the MPC.

In these simulations the controller is intended to operate for a limited time horizon to easily check the correct working of the communication between the two software avoiding an excessively long execution time. A one-day long simulation is sufficient

for this scope, avoiding the Winter Design Day for the same reasons as in Section 4.5.2. As any other day can be selected, the choice falls on January 1st for the sake of simplicity, as EP simulations commonly begin on this date. The evolution of the daily external air drybulb temperature is reported in Figure 4.7.

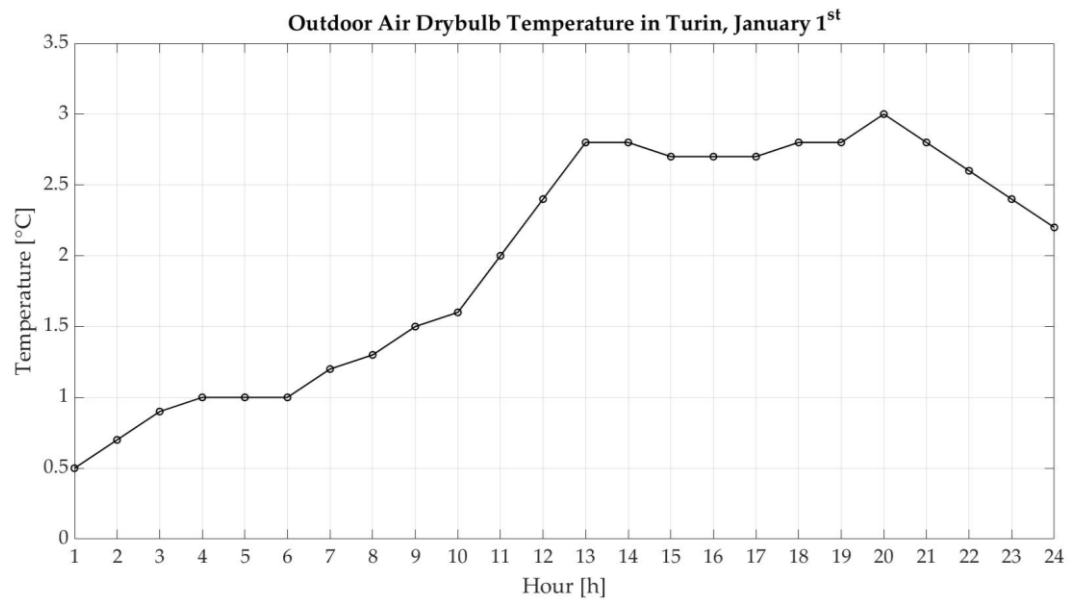


Figure 4.7 - Outdoor air dry bulb temperature evolution in Turin, January 1st.

Source: Author's elaboration.

After loading the IDF and the EPW files, a pre-defined heating schedule $U = u_1, \dots, u_{24}$ is sent from MATLAB to the EP `OtherEquipment` object, first to check if the communication interface works and if the T_{indoor} response is satisfactory, and then to use both the heating schedule and the resulting response to fit a linear model for each thermal zone.

The same heating power fraction schedule U is sent to all the thermal zones of the CorTau House IDF model with an hourly time step in accordance with the final considerations from Section 4.5.2.

The idea is to feed the `OtherEquipment` object with a heating power schedule expected to produce both increases and decreases in the indoor air temperature throughout the day, mimicking what would happen in reality.

Table 4.4 – Pre-defined heating schedule U .

Time interval	Power Fraction wrt nominal [-]
01:00 – 03:00	1
04:00 – 05:00	0.2
06:00	0.6
07:00 – 09:00	0.7
10:00 – 12:00	0.8
13:00	0.2
14:00 – 16:00	0.3
17:00	0.2
18:00 – 20:00	1
21:00 – 22:00	0.7
23:00 – 24:00	0.4

Source: Author's elaboration.

Figures 4.8 and Figure 4.9 show the evolution of the input and output to the EnergyPlus model throughout January 1st.

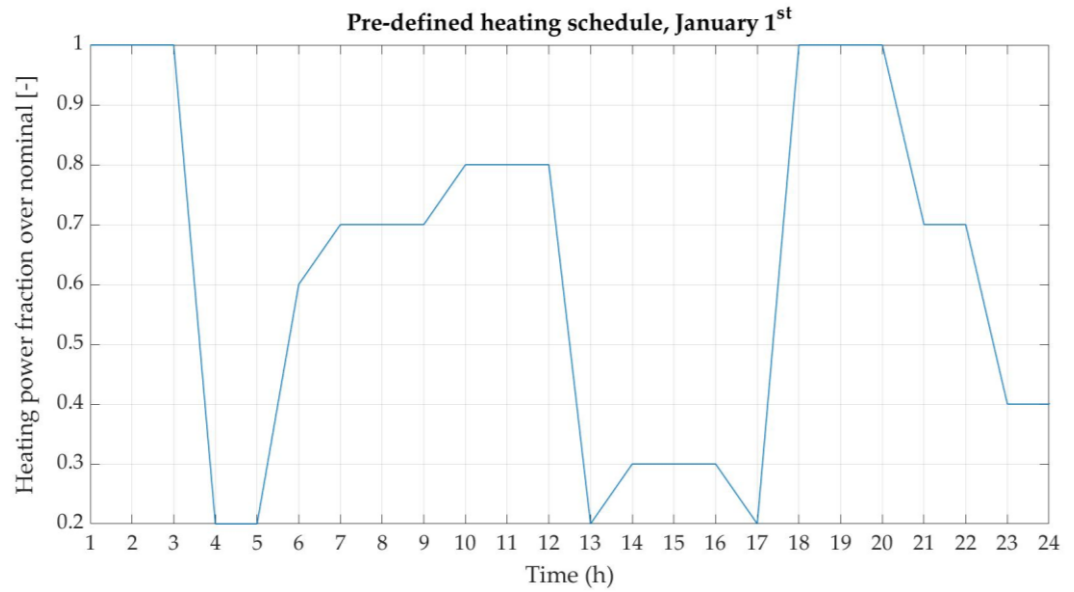


Figure 4.8 – Pre-defined heating power schedule for January 1st.

Source: Author's elaboration.

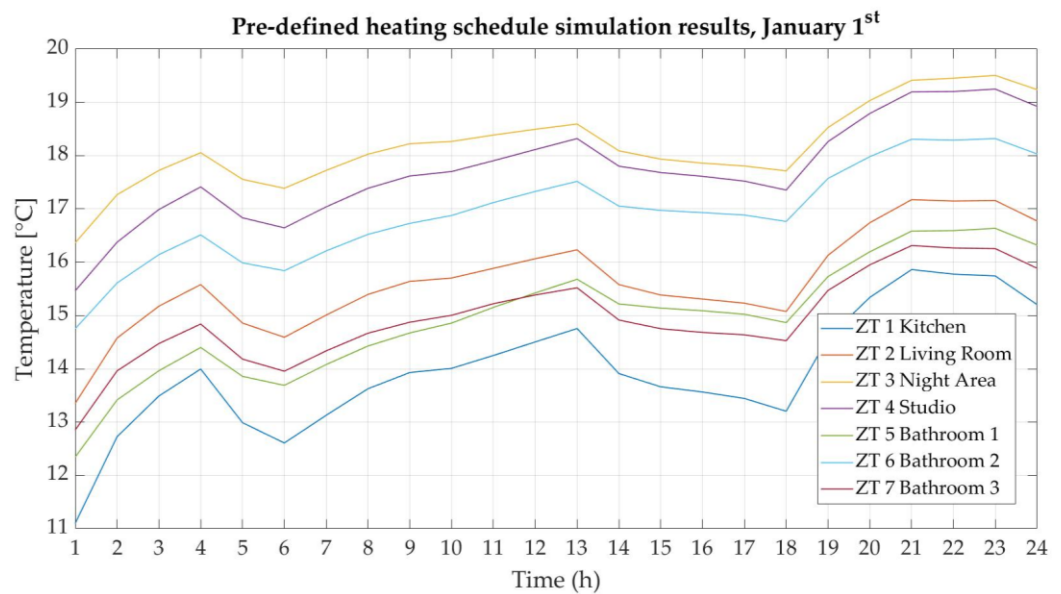


Figure 4.9 – Indoor air temperature results from EnergyPlus with the pre-defined heating power schedule.

Source: Author's elaboration.

A first evidence is that when steep changes in the heating power schedule from one time step to the subsequent are assumed, a softer variation in the EP Zone Mean Air

Temperature output is recorded because of the thermal inertia of the building. Even if the general trend for the indoor temperature is the same, each zone responds to the heating input in a unique way depending on the orientation of its external walls, the relative weight of the opaque and the transparent envelope, and the effect of the weather parameters (first and foremost the external temperature).

The pre-defined heating schedule U , multiplied by the value of the nominal power, and the output T_{indoor} are used to fit the thermal balance equation of each zone that will be later used in the optimization core of the MPC controller. Assuming that the outdoor temperature $T_{external}$ is the main disturbance on the system, except for the power delivery q :

$$k_1 \cdot \frac{dT_{indoor}}{dt} = k_2 \cdot (T_{indoor} - T_{external}) + k_3 \cdot q \quad (4.9)$$

where

- q [W] is the heating power delivered by the fuel cell to the thermal zone.
- k_1, k_2, k_3 are the fitting coefficients of the model.

and by discretizing the time derivative with a forward Euler scheme

$$k_1 \cdot \frac{T_{indoor}^{n+1} - T_{indoor}^n}{\Delta t} = k_2 \cdot (T_{indoor}^n - T_{external}^n) + k_3 \cdot q^n \quad (4.10)$$

Δt must be equal to the co-simulation sample time t_s as the temperature data available from the EP simulation are computed at this rate.

The thermal balance on the zone can be rearranged so that T_{indoor} at the future time step $n+1$ is a linear combination of its current value, the thermal power injection and the

external temperature.

$$T_{indoor}^{n+1} = \left(1 + \frac{k_2 \Delta t}{k_1}\right) T_{indoor}^n + \left(\frac{k_3 \Delta t}{k_1}\right) q^n + \left(-\frac{k_2 \Delta t}{k_1}\right) T_{external}^n \quad (4.11)$$

and by substituting

$$\begin{aligned} T_{indoor} &\rightarrow x \\ \left(1 + \frac{k_2 \Delta t}{k_1}\right) &\rightarrow A \\ \left(\frac{k_3 \Delta t}{k_1}\right) &\rightarrow B \\ \left(-\frac{k_2 \Delta t}{k_1}\right) &\rightarrow C \end{aligned}$$

the simplified model for the building indoor air temperature response is obtained.

$$x^{n+1} = A \cdot x^n + B \cdot q^n + C \cdot T_{external}^n \quad (4.12)$$

The values of the A , B and C coefficients are obtained in MATLAB through a linear regression on the data.

Table 4.5 - Linear regression coefficients for each heated thermal zone.

	A	B	C
ZT 1 Kitchen	6.52 e-01	1.61 e-04	3.60 e-01
ZT 2 Living Room	7.39 e-01	2.92 e-04	2.71 e-01
ZT 3 Night Area	8.46 e-01	2.04 e-04	1.61 e-01
ZT 4 Studio	7.72 e-01	2.49 e-04	2.39 e-01
ZT 5 Bathroom 1	7.17 e-01	6.28 e-04	2.94 e-01
ZT 6 Bathroom 2	7.54 e-01	9.83 e-04	2.58 e-01
ZT 7 Bathroom 3	7.47 e-01	6.49 e-04	2.63 e-01

Source: Author's elaboration.

The relative error in the temperature output introduced by approximating the EP thermal zone model with the simplified one is reported in Figure 4.10. Both the numerator and the denominator of the error expression are computed as Euclidean norms of the vectors spanning throughout the 24 hours of the simulation. Figure 4.11 shows instead how well the linear model approximates the temperature computed by EP over the entire simulation period.

$$Error = \frac{\sqrt{\sum_{k=1}^{24} (T_{linear,k} - T_{EP,k})^2}}{\sqrt{\sum_{k=1}^{24} (T_{EP,k})^2}} \quad (4.13)$$

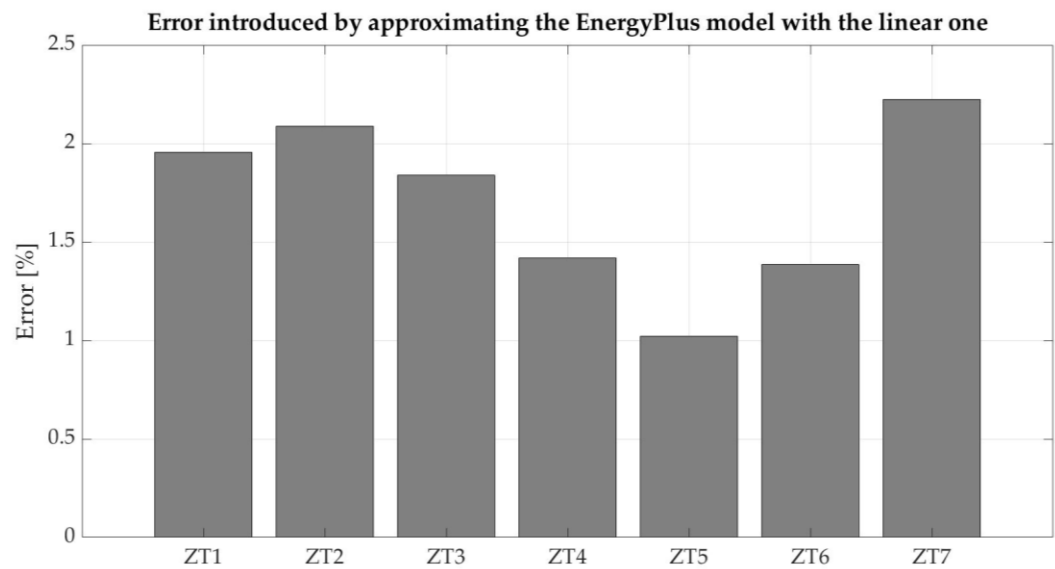


Figure 4.10 – Temperature deviation of the linear model from the EnergyPlus simulation in percentage over the latter.
Source: Author's elaboration.

The deviation of the linear model response from the EnergyPlus simulation results is calibrated in percentage over the EP output. The error introduced when such approximation is introduced falls between 1 % and 2.5 % for the seven thermal zones of the building.

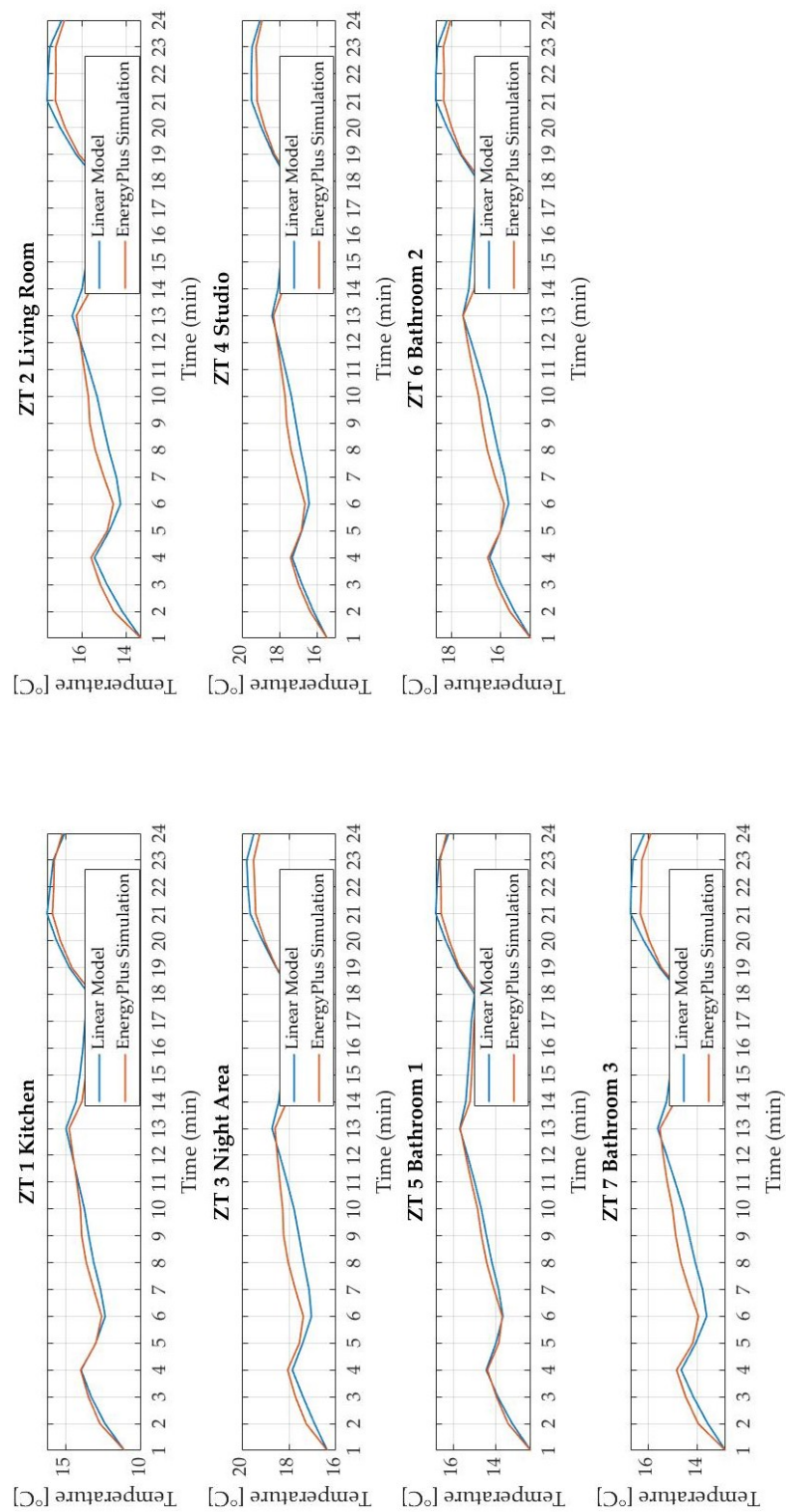


Figure 4.11 – Indoor temperature linear fitting with the pre-defined schedule.

Source: Author’s elaboration.

4.5.4. MPC implementation with the control loop closure in MATLAB

The easiest way to implement the controller is closing the algorithm loop in MATLAB with the linear model developed in Section 4.5.3, giving up on the communication with EP. The response from the closure model will in this case coincide with the prediction from the controller as the plant to which the MPC is sending the input sequence $u(t) = u_{t|t}^*$ is exactly the same linear model over which the optimization is performed.

YALMIP is a MATLAB Toolbox used to solve optimization problems when control strategies are being implemented. It was first developed to work on semidefinite programming (SDP) and linear matrix inequalities but nowadays it supports a variegated set of optimization techniques, relying both on free and commercial solvers. YALMIP can in principle automatically detect the kind of optimization problem defined by the user and set the most appropriate way to solve it accordingly [23].

Table 4.6 – Definition of the MPC controller loop variables.

	Definition	Role	Unit of measurement
$q_{n,j}$	Thermal power demand of the j^{th} thermal zone at time step n .	Output from the MPC Input sequence to the building model	W
$u_{n,j}$	Thermal power demand of the j^{th} thermal zone at time step n normalized over its nominal value.	Normalized output from the MPC Normalized input sequence to the building model	[-]
$x_{n,j}$	Indoor air temperature of the j^{th} heated thermal zone at time step n from the building linear model.	Plant state Output from the building model	K

Source: Author's elaboration.

Figure 4.12 shows the MPC control loop to adopt for the management of the CorTau House indoor temperature. The Building Model item required for the loop closure can be in this case either the thermal zone linear model or the EnergyPlus one. This section is devoted to analyze what would be the controller result with the simplified model closure.

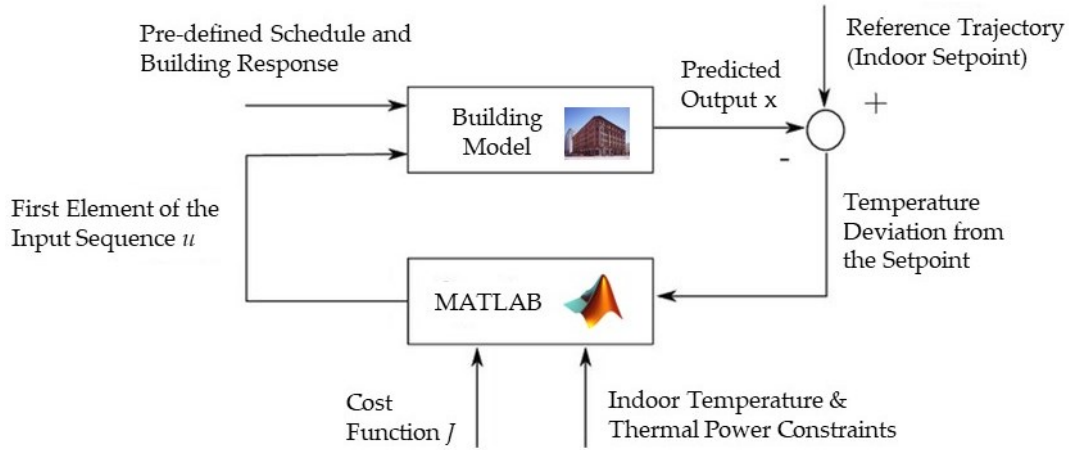


Figure 4.12 – MPC control strategy loop adapted to the CorTau House indoor air temperature management.

Source: Author's elaboration.

Model Predictive Control requires the design parameters to be set before starting the simulation. One entire week is covered to allow for significant variations of the forcing external temperature on the system, from January 2nd to January 8th.

- Sample time $t_s = 1$ hour.
- Control Horizon $N_c = 5$ time steps, $c = 5$ hours.
- Setpoint $T_{setpoint} = 20$ °C, [08:00 – 20:00].
- Setback $T_{setback} = 18$ °C, [00:00 – 07:00] and [21:00 – 24:00].

- Constraints
$$\begin{cases} 0 \leq q_{n,j} \leq q_{nominal} \\ x_{n,j} \leq T_{setpoint} \end{cases}$$

For the indoor temperature output of the controller the only imposed boundary is the 20 °C setpoint as an upper limit since no thermal gains to the system are present except for the decision variable $q_{n,j}$.

The initial condition for the indoor air temperature must be provided along with the values of the MPC design parameters. Two different scenarios can be investigated at this point: the first would be imposing an initial condition equal to the 18 °C setback temperature so that the controller is expected to provide the amount of heat required by each zone to keep the T_{indoor} at the reference levels throughout the day, while the second alternative would be taking as initial condition the indoor air temperature as computed by EnergyPlus in case the HVAC equipment is OFF. For this second option a transient evolution for T_{indoor} is expected towards the setpoint. These stand for the best and worst scenarios respectively as far as the initial indoor temperature is concerned. The starting T_{indoor} in real operation would be somehow in between the two.

The thermal power q is defined in MATLAB as a symbolic decision variable through the `sdpvar` function. This will be a 1×7 array whose columns are assigned to a thermal zone each.

```
>> q = sdpvar(1,7)
```

The MPC output temperature is also defined similarly to the decision variable but as a $N_c \times 7$ array in which each row corresponds to a time step in the control horizon c .

```
>> x = sdpvar(Nc,7)
```

For this set of simulations the initial condition for the indoor temperature is set to the night setback of 18 °C. The value is assigned to all the entries in the first row of the output matrix x .

For each thermal zone, the expression for the indoor temperature at the next time step $x_{n+1,j}$ comes from the simplified linear model. The objective function J to minimize over c can take into account both the deviation of T_{indoor} from the setpoint but also the rate of variation of the power delivery to the zone. As just one objective function is formulated, the two entries need to be dimensionless and ideally normalized. The value assigned to a weighting factor λ in the range $[0;1]$ sets the relative importance of the two requirements included in the objective function J .

$$J = \sum_{l=k}^{k+N_c} (1 - \lambda) \cdot \frac{(x_l - T_{setpoint})^2}{T_{setpoint}^2} + \sum_{l=k}^{k+N_c} \lambda \cdot \frac{(q_l - q_{l-1})^2}{q_{nominal}^2} \quad (4.14)$$

In the definition of the objective function, the temperature entries are expressed in Celsius Degree rather than in Kelvin, otherwise the normalization of the temperature difference over the setpoint would stick close to zero in most cases and such term would almost disappear in the optimization if λ is not sufficiently low. YALMIP automatically sets the optimization solver to the quadratic programming `quadprog` function, but the solution was not converging throughout the entire simulation period. For this reason it was substituted by the highly performing SeDuMi solver developed by Jos F. Sturm. SeDuMi stands for Self-Dual-Minimization, and it is a MATLAB/GNU Octave package developed to solve convex optimization problems which involve linear equations and inequalities but also second-order cone constraints and semidefinite constraints, thus linear matrix inequalities. Such option seems reasonable as the optimization is in this case being performed over a second order objective function and the simplified model for T_{indoor} is linear. The convergence of the optimization problem will be ensured for all the thermal zones at each time step setting a maximum number of iterations of 1000 in the SeDuMi options.

```
>> options = sdpsettings('solver','sedumi');  
>> options.sedumi.maxiter = 1000;
```

```

>> % Model Predictive Control implementation
for k = 1:Np           % Prediction Horizon - One week
    for j = 1:7         % Cycle to go through all the thermal zones
        constraints = [];
        objective = 0;
        for m = 1:Nc    % Control Horizon - 5 timesteps
            x(m+1,j) = A(j)*x(m,j) + B(j)*q(m,j) + C(j)*OutdoorT(k+m-1);
            if m == 1
                objective = objective + (1-lambda)*((x(m+1,j)-Tsetpoint)^2/20^2) + ...
                    (lambda)*((q(m,j))^2)./(nominal(j))^2;
            else
                objective = objective + (1-lambda)*((x(m+1,j)-Tsetpoint)^2/20^2) + ...
                    (lambda)*((q(m,j)-q(m-1,j))^2)./(nominal(j))^2;
            end
            constraints = [constraints, 0 <= q(m,j) <= nominal(j), x(m+1,j) <= Tsetpoint];
        end
        optimize(constraints,objective,options);
        q_mpc(k,j) = value(q(1,j));
        u_mpc(k,j) = q_mpc(k,j)/nominal(j);
        T_mpc(k,j) = value(x(2,j));
        x(1,j) = x(2,j);
    end
end

```

Figure 4.13 – Controller development with YALMIP toolbox closing the loop in MATLAB.

Source: Author's elaboration.

Figure 4.13 shows the core of the control algorithm with the loop closure in MATLAB. In this case the model included in the optimization and the one responding to the controller output are exactly coincident. For each time step the objective function is built through the entire N_c independently for each thermal zone. Then the minimization of the function is performed respecting the constraints on the thermal power. At the very end, the current state of the building is updated by one time step and the subsequent states in the set of control actions resulting from the optimization are discarded.

The value of λ affects the result of the optimization by weighting the two counterbalancing requirements included into the objective function.

- CASE 1 : $\lambda = 0$

If the weighting factor λ is set to 0, the controller will only focus on the minimization of the indoor temperature deviation from the 18 °C and 20 °C reference levels, and the decision variable q is kept in-between the constraints of zero thermal power and the maximum nominal one associated to each thermal zone.

$$J = \sum_{l=k}^{k+N_c} \frac{(x_l - T_{setpoint})^2}{T_{setpoint}^2} \quad (4.15)$$

The results of the simulation both in terms of heating demand and indoor air temperature response are reported in Figures 4.14 and Figures 4.15 respectively. The results on the latter show that the controller can keep the indoor temperature at 18 °C and 20 °C in each thermal zone according to the schedule, with negligible deviations from the reference ascribed to the numerical technique employed in the J minimum search. The controller ensures that the temperature level is perfectly maintained as the only requirement included in J is to minimize the deviation of T_{indoor} from the setpoint and, again, the simplified model and the plant are in this case exactly the same indoor temperature expression. A perfect response of the system is obviously expected.

SeDuMi is always able to find a minimum in the variables domain as the problem resulted to be convex throughout the entire simulation time, respecting the constraints on both the maximum thermal power delivery and the temperature.

The heating power trends follow almost the same evolution throughout the week as the only forcing to the various models is the external temperature. However, the naturally included in the coefficients of the zones' linear models.

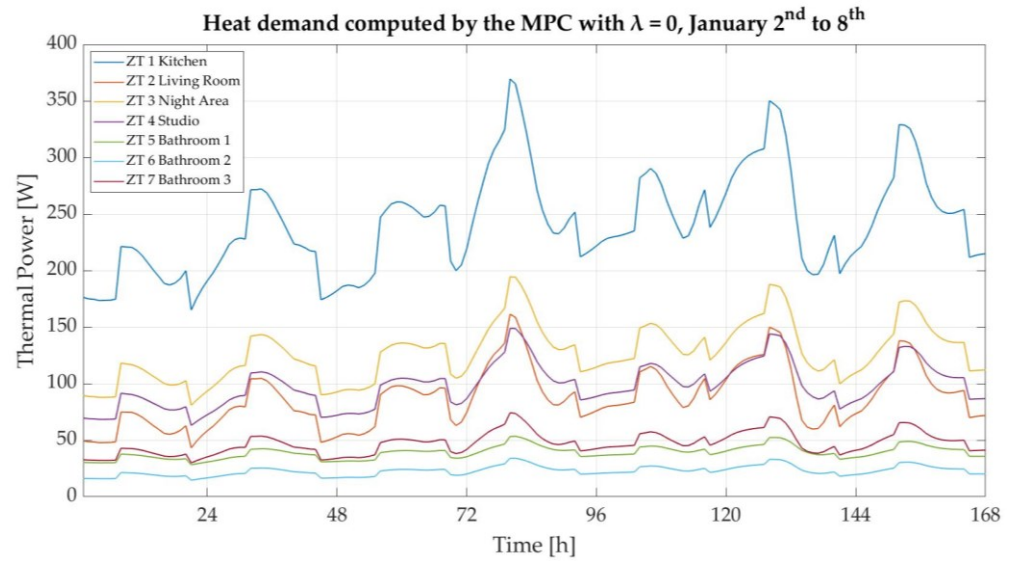


Figure 4.14 – Heating demand computed by the MPC with $\lambda = 0$.

Source: Author's elaboration.

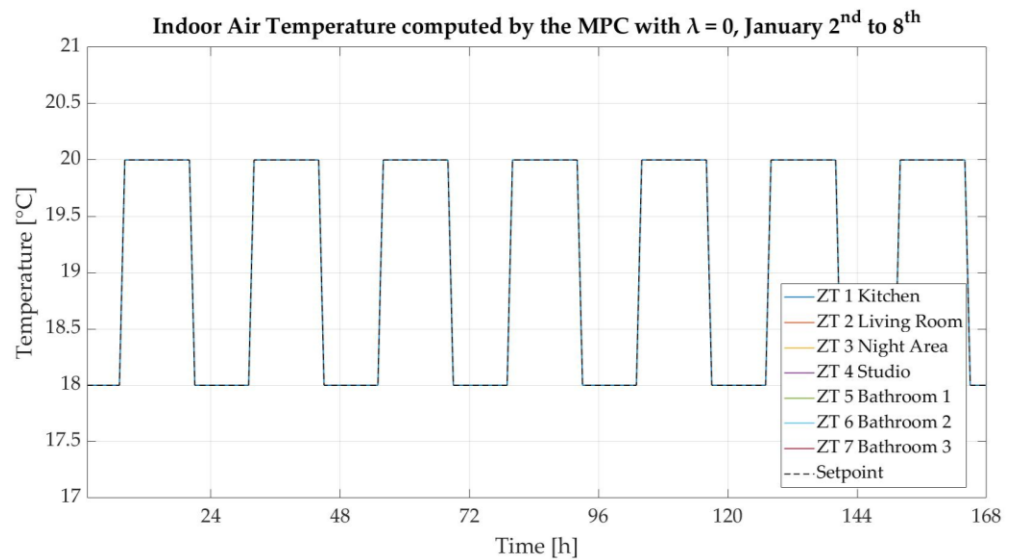


Figure 4.15 – Indoor temperature response of the building linear model with $\lambda = 0$.

Source: Author's elaboration.

The demand coming from the ZT1 Kitchen almost doubles the one from the ZT3 Night Area and is reasonably expected to have a major impact on the total thermal request from the building when the EP co-simulation will be implemented.

- CASE 2 : $\lambda = 1$

When λ is set to 1, the solver is minimizing the heating demand variation at each time step as the requirement on the indoor air temperature is erased. Whenever the term related to q is included in the objective function, to say $\lambda > 0$, the minimization over the heat rate will actually be a minimization over the decision variable q itself, as its initial value is naturally imposed to be null. This is better formulated in Eq. (4.16).

$$J = \begin{cases} \sum_{l=k}^{k+N_c} \lambda \cdot \frac{(q_l)^2}{q_{nominal}^2} & \text{if } k = 1 \\ \sum_{l=k}^{k+N_c} \lambda \cdot \frac{(q_l - q_{l-1})^2}{q_{nominal}^2} & \text{if } k > 1 \end{cases} \quad (4.16)$$

As shown in the resulting trends displayed in Figures 4.16 and 4.17, the MPC computes an optimal set of heating rate inputs throughout the prediction horizon that is almost always null due to the initial minimization of the thermal demand deviation from 0. This consequently leads to the indoor air temperature to decrease in all the CorTau House thermal zones similarly to what happens in the free-running operations condition proposed in Section 4.5.2. The evolution of T_{indoor} resembles the $T_{external}$ one from the EPW dataset for the week January 2nd to January 8th, shown in Figure 4.28 of Section 4.5.5.

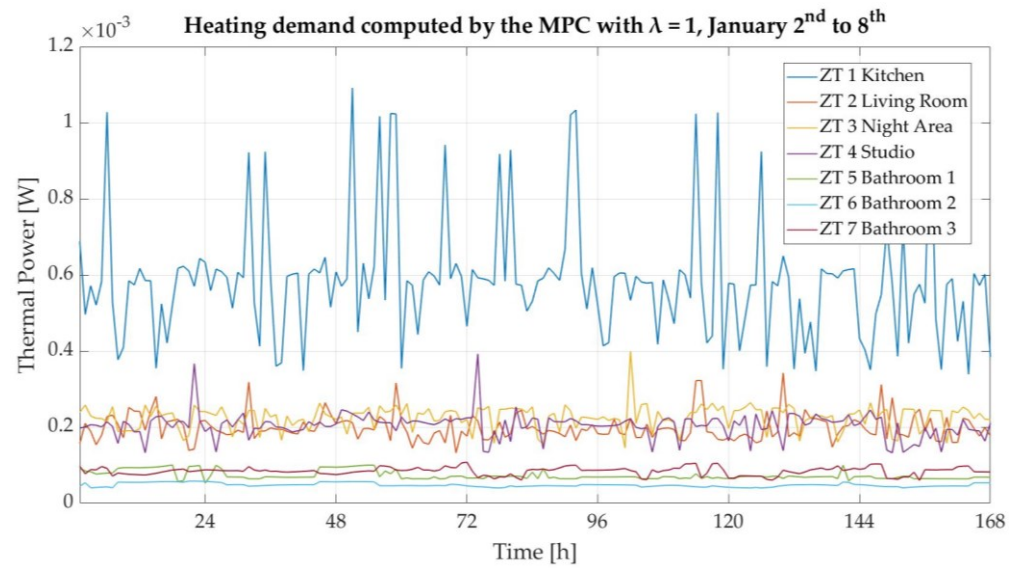


Figure 4.16 – Heating demand computed by the MPC with $\lambda = 1$.

Source: Author's elaboration.

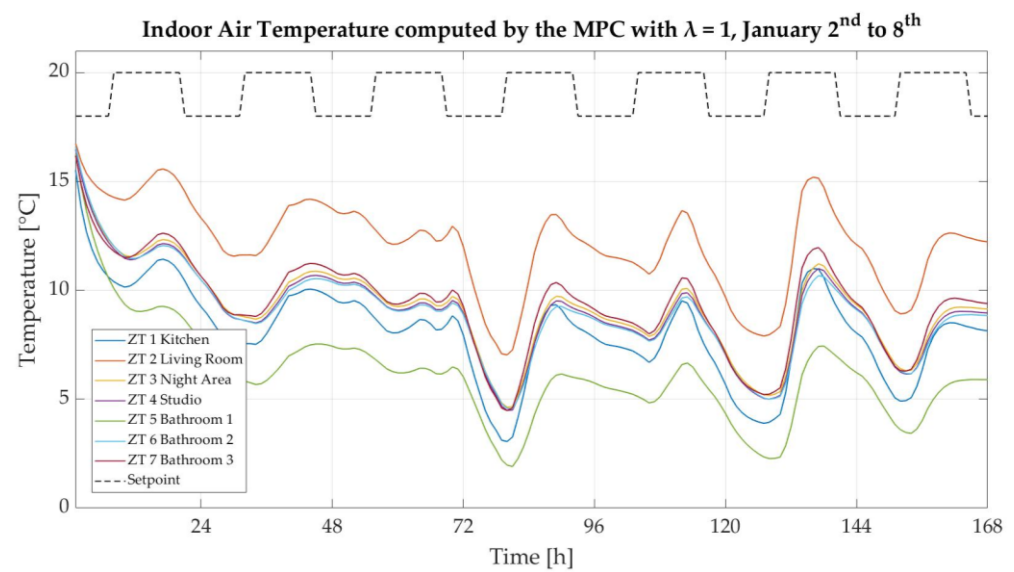


Figure 4.17 – Indoor temperature response of the building linear model with $\lambda = 1$.

Source: Author's elaboration.

- CASE 3 : $\lambda \in [0;1]$

A set of simulations is carried out here to evaluate how the variation of the weighting factor λ in the $[0;1]$ interval affects the operation of the controller. The relevance of such investigation comes from the fact that this requirement could be likely included in the design of the controller in real operation to avoid extremely sharp indoor temperature variation that would affect the occupants' comfort.

From the parametrical analysis on λ only the simulation results for ZT1 Kitchen are displayed and discussed here as the same considerations can be easily extended to the other thermal zones. For the sake of brevity, the simulation period is in this case reduced to two days, from January 2nd to January 3rd. No relevant information would be added by keeping the seven-days long timeframe as in the previous simulation.

Figure 4.18 shows the trend of the hourly heating power demand computed by the MPC varying λ in $[0;1]$ with a 0.1 step. As λ increases from 0, the power variation between two subsequent time steps slows down, apart from the first simulation hours through which the temperature stabilizes. This is quite evident in the demand evolution experienced by the zone in the interval between January 2nd at 21:00 and January 3rd at 07:00. The power variation in such interval for $\lambda = 0$ gets to almost 70 W, while for $\lambda = 0.9$ this reduces to around 30 W. Focusing now on Figure 4.19, the temperature setpoint is not exactly met for any $\lambda > 0$ as the objective function minimization includes now the two conflicting requirements. Indeed, the temperature response stabilizes to a level below the 18°C or 20°C references as the value of λ increases. The idea is then to look for a value of the weighting factor which guarantees an acceptable temperature level during the entire simulation window, for instance in accordance with the tolerance of ± 2 °C specified in the Presidential Decree No 412/1993 from Section 2.2. The indoor temperature keeps inside such band throughout the whole prediction horizon when $\lambda \in [0,0.6]$.

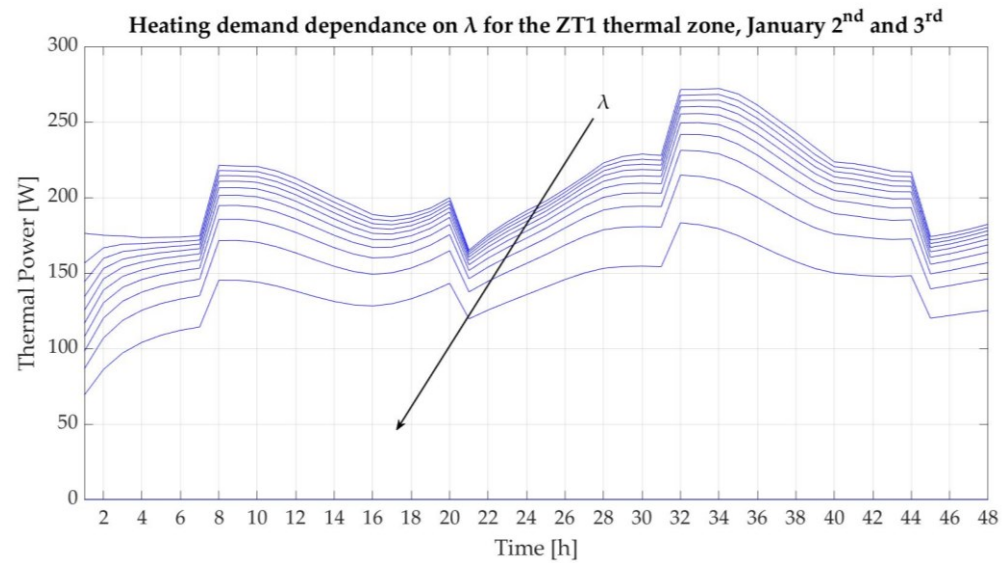


Figure 4.18 – Heat demand of ZT1 Kitchen depending on λ .

Source: Author's elaboration.

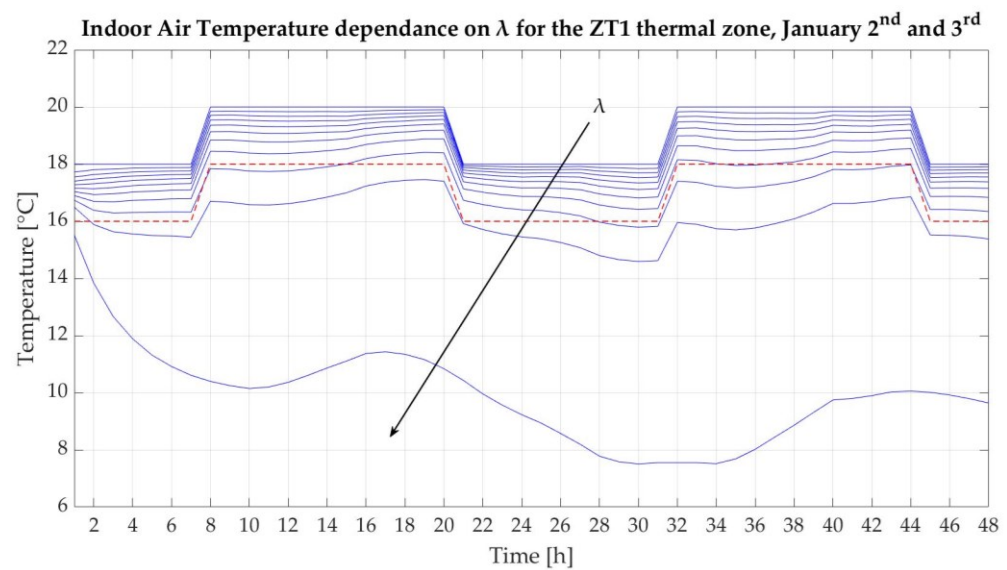


Figure 4.19 – Indoor temperature response of ZT1 Kitchen depending on λ .

Source: Author's elaboration.

The last simulation for this section is run for $\lambda = 0.3$, so that the greatest relative weight in the J minimization is however given to the requirement on the indoor air temperature. The original weekly simulation horizon is kept to check what the the input sequence would look like with an intermediate value of λ and whether the ± 2 °C tolerance band on the temperature set by the regulation is respected.

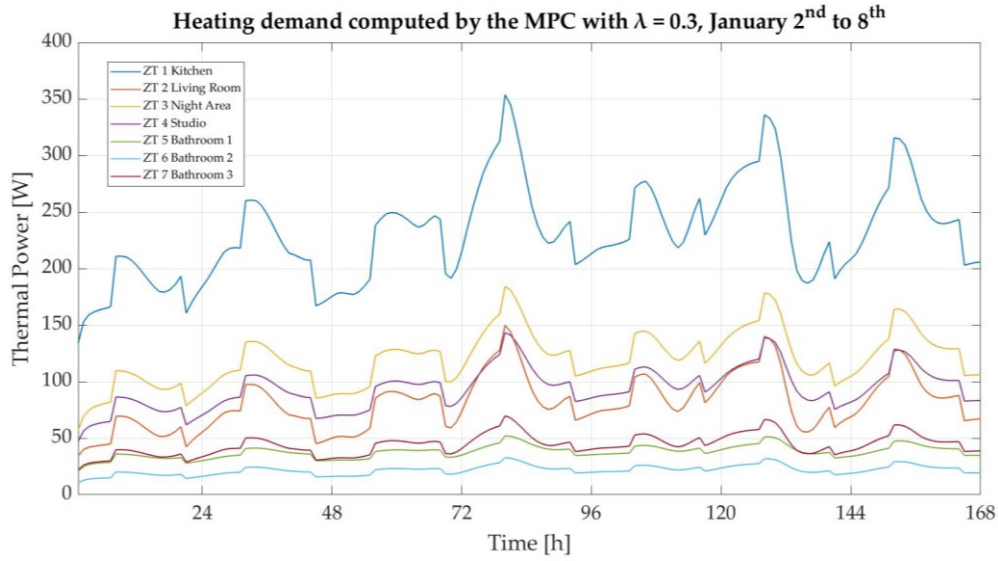


Figure 4.20 – Heating demand computed by the MPC with $\lambda = 0.3$.

Source: Author's elaboration.

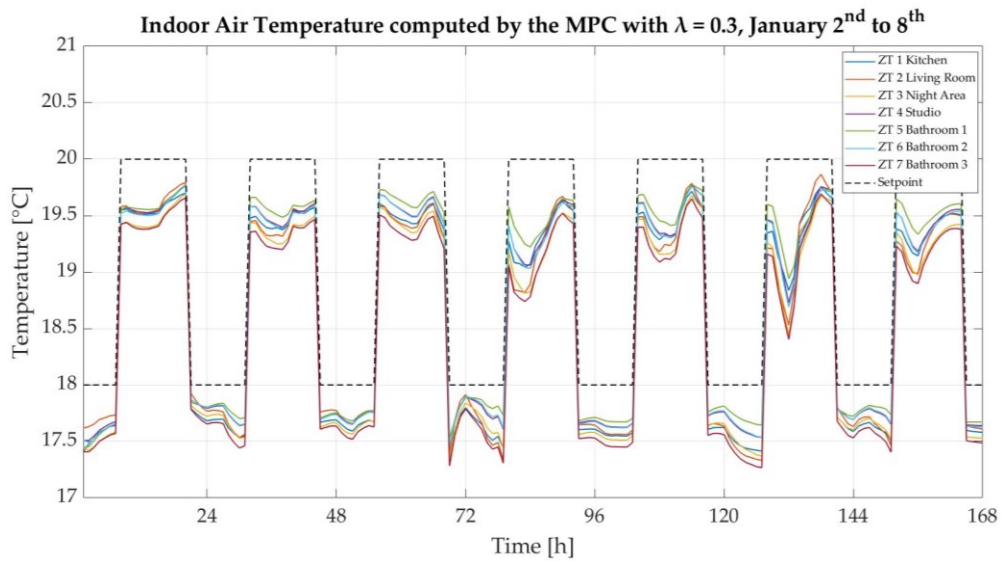


Figure 4.21 – Indoor temperature response of the building linear model with $\lambda = 0.3$.

Source: Author's elaboration.

Figures 4.20 and 4.21 show as usual the results of the simulation in terms of both thermal power and indoor temperature response. A first evidence is that T_{indoor} is always kept inside the 2 °C tolerance range mentioned above. All the zones however experience an important temperature drop on January 7th due to particularly unfavourable weather conditions in conjunction with the relaxation on

meeting the setpoint at the controller side. Demand peaks are observed when the reference is switched from 18 °C to 20 °C, with the absolute maximum on June 5th as a dramatic drop in $T_{external}$ is recorded.

In the next section a similar analysis will be carried out setting the communication interface between MATLAB and EnergyPlus as in Section 4.5.3. In this case, however, the heating schedule will not be set by the designer as it will be the result of the controller operation.

4.5.5. MPC implementation with the control loop closure in EnergyPlus

Setting a MPC control strategy to the CorTau House gathers meaning when a proper co-simulation between MATLAB and EnergyPlus is implemented. The IDF of the house includes a wider number of features with respect to the simplified linear model of the thermal zones, and the EP response is therefore expected to better mimic what the actual behavior of the building would be. In this case the objective function J still requires the linear model in the temperature term, with the major difference being that the first element of U from the minimization over N_c is sent to EnergyPlus rather than to the zone linear model itself. A discrepancy between the MPC computation and the EP output is naturally expected. Its magnitude would decrease as the linear model resembles more and more the whole EP thermal modelling background (which obviously cannot be exactly replicated as many non-linear and complex equations are likely to be included in the EP code).

However, the goal of the controller is to provide the input sequence through a simplified model of the real plant, and the usefulness of such approach should be questioned if the model gets too complex. The main features that are not included in the linear models but actually appear in the IDF file are:

- The effect of the solar radiation as an additional internal heat source to the thermal zones through both the opaque and transparent surfaces. Such approximation is reasonable in climatic zone E in winter.
- The thermal interaction among the zones through the internal partitions.

- The effect of all the other meteorological parameters, such as wind speed and external air humidity.
- Dynamic effects due to the building thermal capacitance and inertia.

In other words, closing the control loop in EP co-simulation gives a measure of how well the linear models developed for each thermal zone approximate the real spaces when the heating schedule is not the one used to build the thermal model itself, as instead investigated at the end of Section 4.5.3.

The MPC design parameters list follows.

- Sample time $t_s = 1$ hour.
- Control Horizon $N_c = 5$ time steps, $c = 5$ hours.
- Setpoint $T_{setpoint} = 20$ °C, [08:00 – 20:00].
- Setback $T_{setback} = 18$ °C, [00:00 – 07:00] and [21:00 – 24:00].

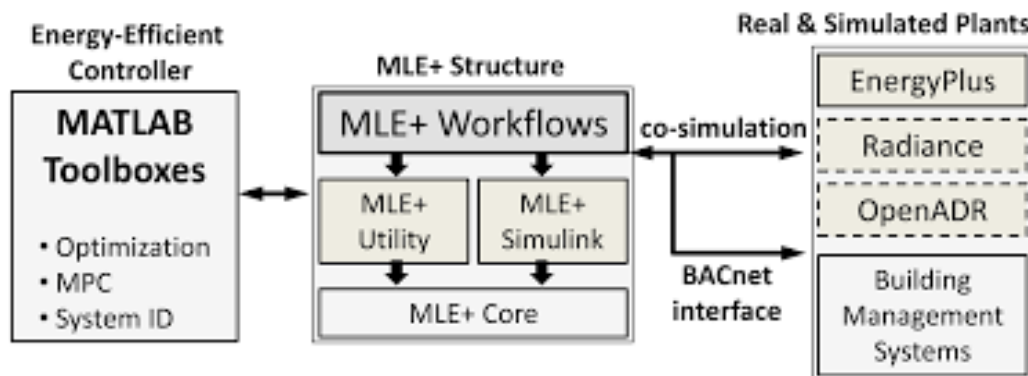


Figure 4.22 – Co-simulation workflow between MATLAB Toolboxes and EnergyPlus through the MLE+ interface.

Source: Bernal, Willy & Behl, Madhur & Nghiem, Truong & Mangharam, Rahul. (2015). Campus-Wide Integrated Building Energy Simulation.

Figure 4.23 shows the controller algorithm developed with the YALMIP and MLE+ toolboxes aid since the EP and MATLAB co-simulation is implemented in this section.

```

while t <= endTime
    for j = 1:7 %Cycle to go through all the thermal zones
        constraints = [];
        objective = 0;
        for m = 1:Nc % Control Horizon - 5 timesteps
            X(m+1,j) = A(j)*X(m,j) + B(j)*Q(m,j) + C(j)*TOUTDOOR(k+m-1);
            if m == 1
                objective = objective + (1-lambda)*((X(m+1,j)-TSETPOINT)^2/20^2) + ...
                    (lambda)*((Q(m,j))^2)./(nominal(j))^2;
            else
                objective = objective + (1-lambda)*((X(m+1,j)-TSETPOINT)^2/20^2) + ...
                    (lambda)*((Q(m,j)-Q(m-1,j))^2)./(nominal(j))^2;
            end
            constraints = [constraints, 0 <= Q(m,j) <= nominal(j), X(m+1,j) <= TSETPOINT+2];
        end
        optimize(constraints,objective,options);
        qMPC(k,j) = value(Q(1,j));
        uMPC(k,j) = qMPC(k,j)/nominal(j);
        T_MPC(k,j) = value(X(2,j));
        X(1,j) = X(2,j);
    end
    % Send inputs to EnergyPlus
    ep.write(uMPC(k,:),t);
    % Get outputs from EnergyPlus
    [TT, t] = ep.read;
    T_EPLUS(k,:) = TT(2:end) + 273.15; % [K]
    X(1,:) = TT(2:end) + 273.15; % [K]
end

```

Figure 4.23 – Controller development with YALMIP and MLE+ toolboxes closing the loop in EnergyPlus.

Source: Author's elaboration.

- CASE 1 : $\lambda = 0$

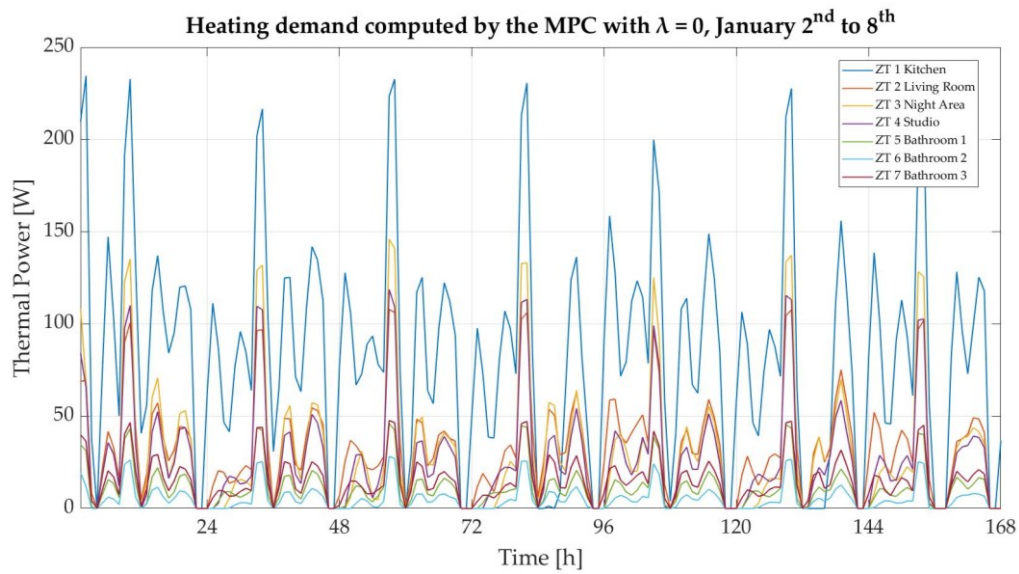


Figure 4.24 – Heating demand computed by the MPC from the MATLAB and EnergyPlus co-simulation with $\lambda = 0$.

Source: Author's elaboration.

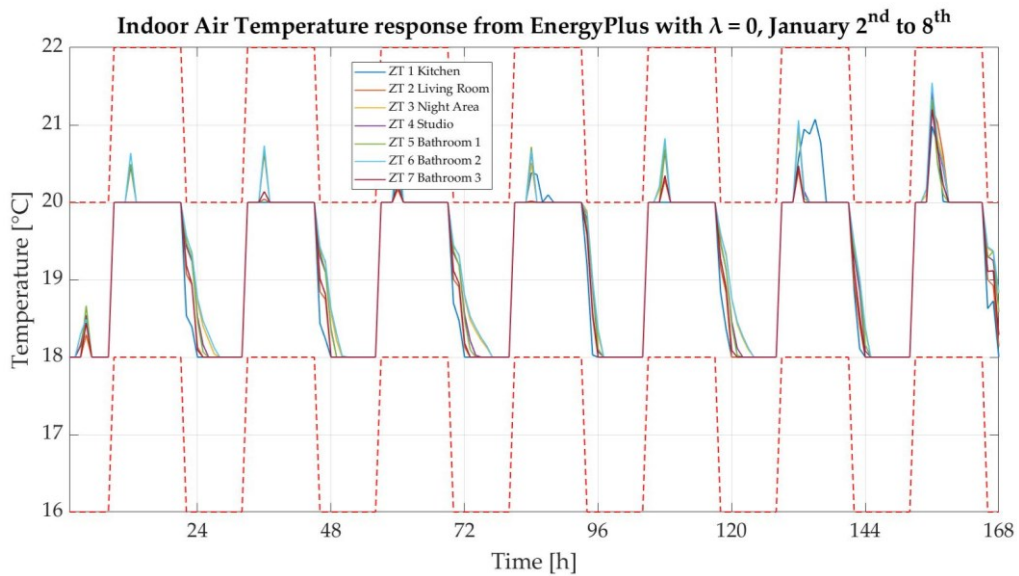


Figure 4.25 – Indoor air temperature response from the MATLAB and EnergyPlus co-simulation with $\lambda = 0$.

Source: Author's elaboration.

The evolution of the indoor temperature in Figure 4.25 confirms the goodness of the controller design and operation, as the setpoint and setback levels are met for almost the entire prediction horizon. As expected, some differences with respect to the control loop closure in MATLAB from Figure 4.15 can be however observed. The indoor air temperature moves away from the 20 °C setpoint most likely because of the solar radiation. The heating demand computed by the MPC is in fact pushed to zero on January 7th but the indoor temperature in ZT 1 Kitchen rises to slightly above 21 °C due to the solar gains through both the opaque envelope and the fenestration. The analysis on the simulation running in extreme operation conditions for $\lambda=1$ upholds this reasoning. When the reference level switches from 20 °C to 18 °C at 21:00, the T_{indoor} drop is not as instantaneous. The heating demand is actually pushed to zero here, but, as no thermal power subtraction from the spaces is designed at the controller side, some time is required to let T_{indoor} lower to the setback temperature reference. The time required to reach 18 °C depends on the features of each confined zone and the outdoor conditions, with the ZT1 Kitchen and ZT6 Bathroom 2 showing the fastest and the slowest response to the reference variation respectively. This, again, confirms the poor insulation capability of ZT1 if compared to the other thermal zones.

- CASE 2 : $\lambda = 1$

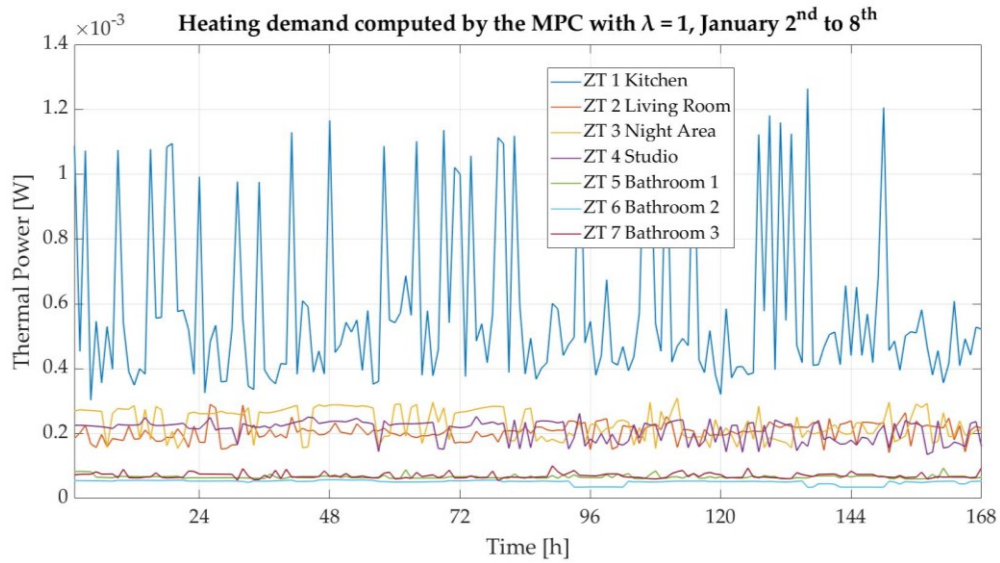


Figure 4.26 – Heating demand computed by the MPC from the MATLAB and EnergyPlus co-simulation with $\lambda = 1$.

Source: Author's elaboration.

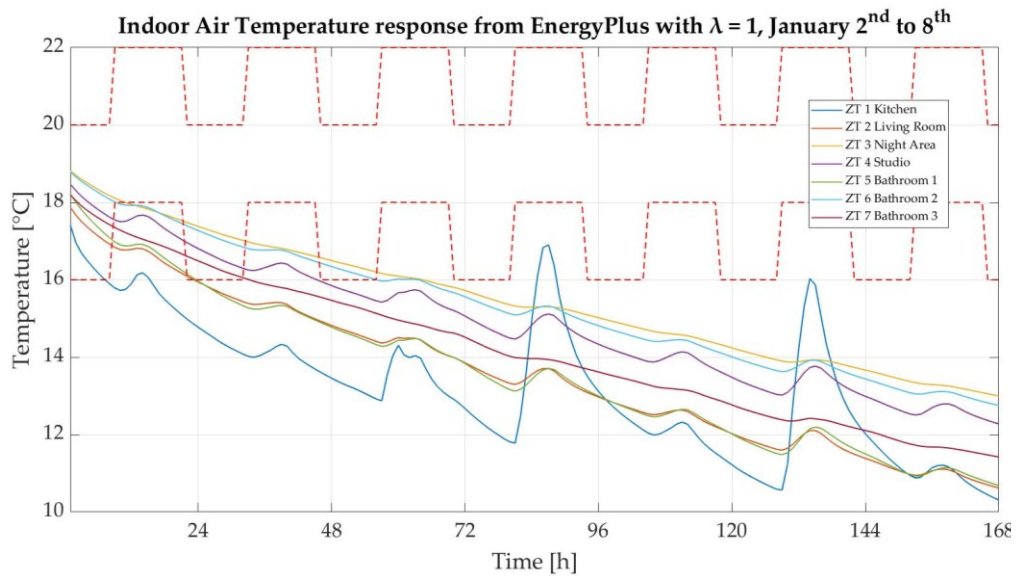


Figure 4.27 – Indoor air temperature response from the MATLAB and EnergyPlus co-simulation with $\lambda = 1$.

Source: Author's elaboration.

The influence on T_{indoor} by both the outdoor temperature and the solar radiation according to the dataset from the Turin EPW file is quite evident when $\lambda = 1$, since

this value of the weighting factor in J directly takes the EP simulation to free-running operation conditions as already discussed in Section 4.5.4. Similarly to what was observed for January 1st, the ZT1 Kitchen thermal zone experiences the highest indoor air temperature peaks during daylight hours as a consequence of the weather conditions. Figure 4.27 displays both the evolution of the outdoor and the kitchen indoor temperatures (the blue solid and dotted lines respectively) and the total irradiance in W/m^2 in Turin from January 2nd to January 8th, as the sum of the direct I_{beam} , diffuse I_{diff} and reflected I_{refl} radiation components over the horizontal plane. The analysis of the cross effect of one weather parameter on the other is quite complex and out of the scope of this study but their influence on the indoor temperature seems straightforward. The low outdoor temperature is the driver for the almost linear drop of the indoor one at night.

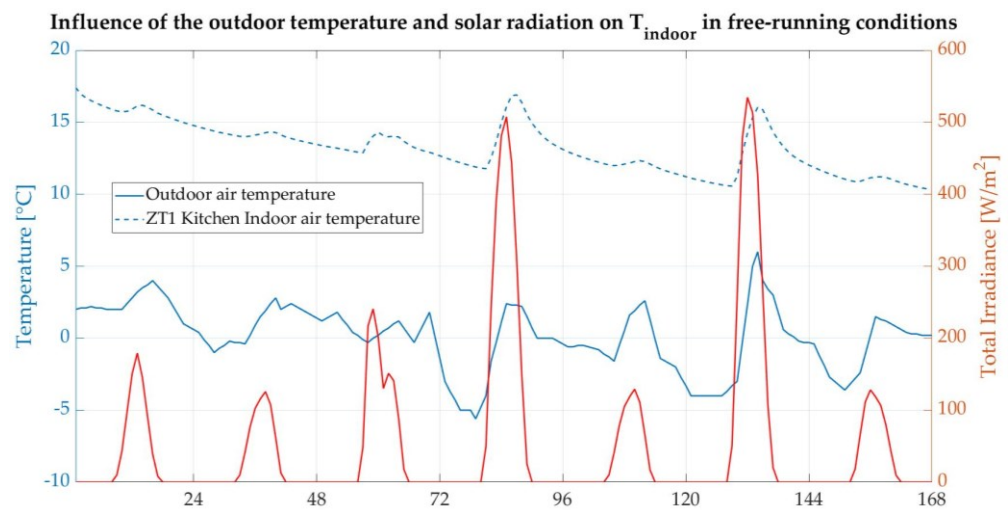


Figure 4.28 – Effect of both the external temperature and solar radiation on ZT1 Kitchen indoor air temperature in free-running operation condition.

Source: Author's elaboration.

The indoor temperature peaks observed in ZT1 Kitchen follow the shape of the total irradiance ones, with a evident proof laying in the two-peaks irradiance and temperature response on January 4th. The indoor temperature local maxima are always delayed with respect to the irradiance ones by two hours.

- CASE 3 : $\lambda \in [0; 1]$

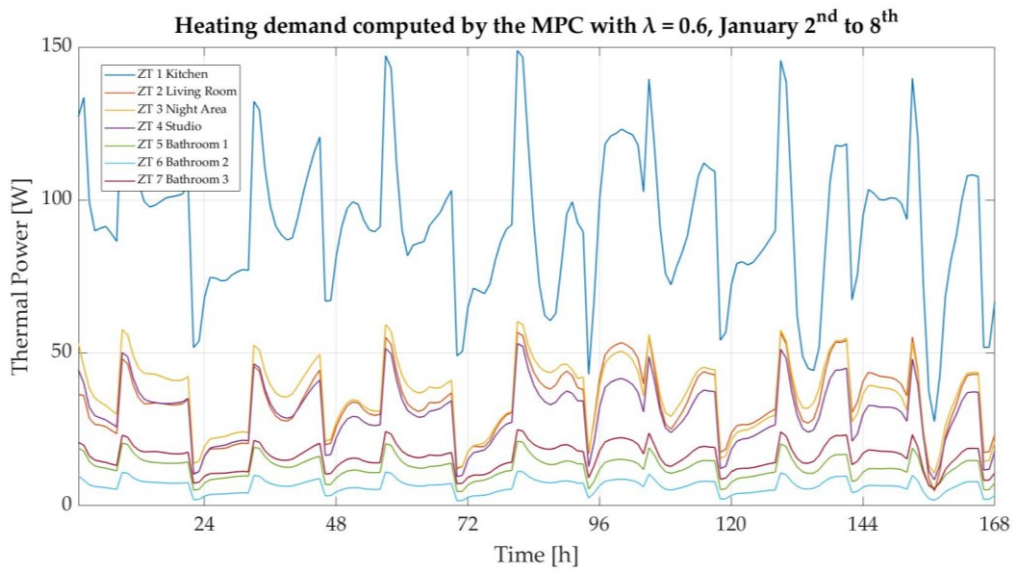


Figure 4.29 – Heating demand computed by the MPC from the MATLAB and EnergyPlus co-simulation with $\lambda = 0.6$.

Source: Author's elaboration.

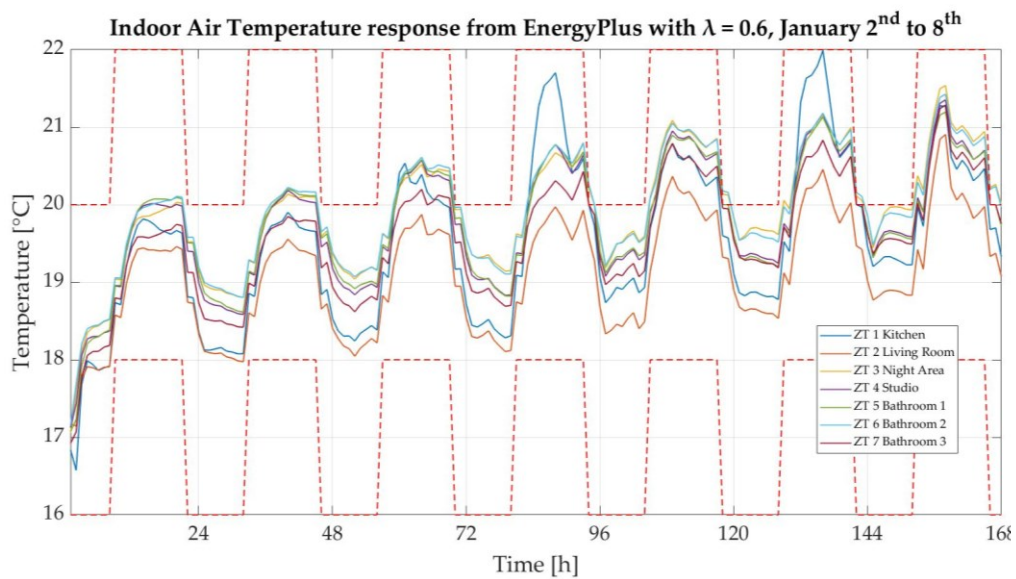


Figure 4.30 – Indoor air temperature response from the MATLAB and EnergyPlus co-simulation with $\lambda = 0.6$.

Source: Author's elaboration.

The evolution of the indoor air temperature as resulting from the co-simulation

between the two softwares allows some interesting considerations. First of all, the value chosen for the weighting factor is $\lambda = 0.6$, sensibly higher than the one selected in the control loop closure with MATLAB. In this way the effect of the building features that are not included in the simplified model is however kept under control. The thermal power demand computed by the controller is in fact reduced due to such increased value of λ . The thermal gains from the EP model features that are not included in the linearization account for the λ increase so that the indoor temperature never gets out of the tolerance band, as observed in Figure 4.30. As the simulation runs through the week, however, a general increase in the temperature trend is observed mainly due to two reasons, the first being that the thermal models of the zone are tuned on the outdoor temperature variation observed on January 1st and, as a consequence, a different evolution of this quantity in the successive days may inficiate the accuracy of the model. As reported in Figure 4.30, the building is subject to a high variability of the external temperature from day to night hours. The second reason could be related to the absence of thermal capacity terms in the simplified models of the zones. A possible improvement at least to the first algorithm weakness could be updating the A , B and C fitting coefficients after a shorter period, three days for instance.

On the other side, the effect of the solar radiation plays a major role especially on the ZT1 Kitchen thermal zone, exposed towards the south direction and not properly shadowed for the winter season, as already mentioned in Section 4.5.2. Peaks in the air temperature can be attributed to the effect of the solar radiation as already mentioned in the free-running operation conditions paragraph above.

The heating demand is then divided by each thermal zone surface and displayed in Figure 4.31. The high request from ZT1 Kitchen appears to be also due to the room size as the zone heating load per square meter reaches intermediate values. The interesting observation, indeed is that the smallest thermal zones, namely the three bathrooms, are actually those requiring on average most of the thermal demand per square meter. This is also due to the fact that the gains from the occupants metabolic rate is set to 0 in these zones, as mentioned in Section 2.3.2.

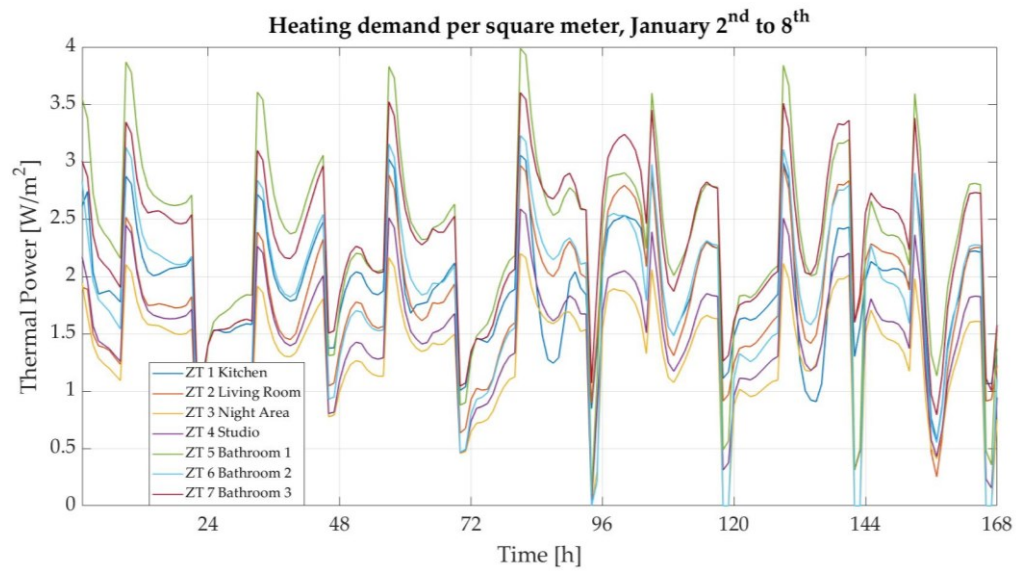


Figure 4.31 – Heating demand computed by the MPC from the MATLAB and EnergyPlus co-simulation with $\lambda = 0.6$ normalized over the floor area.

Source: Author's elaboration.

5. Technical and economic considerations

Once the evolution of the thermal demand is obtained from the MPC, the results are used to effectively control the PEMFC stack operation, as the device would be in charge of the heating load fulfillment. In this sense, the first step would be retrieving the expression of the polarization curve of the NEDSTACK FCS 7-XXL fuel cells' stack from Section 3.2 and writing both the electrical and thermal power expressions as a function of the voltage at the stack terminals.

$$\begin{aligned}
 V_{stack} &= V_{theoretical} - \Delta V_{act} - \Delta V_{ohmic} = \\
 &= V_{theoretical} - \frac{RT}{\alpha_c F n} \ln \left(\frac{j}{j_0} \right) \Big|_c - j \cdot R_{ohmic} = \\
 &= V_{theoretical} - (a + b \cdot \ln(j)) - j \cdot R_{ohmic} = \\
 &= 47 - (7.157 + 0.5747 \cdot \ln(j)) - j \cdot 8.639 \text{ V}
 \end{aligned} \tag{4.17}$$

$$\begin{aligned}
 P_{thermal} &= (\Delta V_{act} + \Delta V_{ohmic}) \cdot I_{stack} = \\
 &= \left(\frac{RT}{\alpha_c F n} \ln \left(\frac{j}{j_0} \right) \Big|_c + j \cdot R_{ohmic} \right) \cdot j \cdot A_{cross} = \\
 &= (a + b \cdot \ln(j) + j \cdot R_{ohmic}) \cdot j \cdot A_{cross} = \\
 &= (7.157 + 0.5747 \cdot \ln(j) + j \cdot 8.639) \cdot j \cdot 0.2 \text{ W}
 \end{aligned} \tag{4.18}$$

$$\begin{aligned}
P_{electrical} &= P_{theoretical} - P_{thermal} = \\
&= (V_{theoretical} - \Delta V_{act} - \Delta V_{ohmic}) \cdot I_{stack} = \\
&= (V_{theoretical} - (a + b \cdot \ln(j)) - j \cdot R_{ohmic}) \cdot j \cdot A_{cross} = \\
&= (47 - (7.157 + 0.5747 \cdot \ln(j)) - j \cdot 8.639) \cdot j \cdot 0.2 \text{ W}
\end{aligned}
\tag{4.19}$$

The amount of hydrogen required by the fuel cells' stack to meet the thermal demand from the building as a result of the MPC controller operation can be estimated as in (4.17) knowing the voltage and the electrical power demanded at the stack side, or directly its current density [24].

$$\begin{aligned}
H_2 \text{ usage} &= \frac{I \cdot n}{2 \cdot F} \text{ moles } s^{-1} = \\
&= \frac{P_e}{2 \cdot V_c \cdot F} \text{ moles } s^{-1} = \\
&= \frac{2.02 \cdot 10^{-3} \cdot P_e}{2 \cdot V_c \cdot F} \text{ kg } s^{-1} = \\
&= 1.05 \cdot 10^{-8} \cdot \frac{P_e}{V_c} \text{ kg } s^{-1} = 1.05 \cdot 10^{-8} \cdot j \cdot A_{cross} \text{ kg } s^{-1} = \\
&= 1.05 \cdot 10^{-8} \cdot j \cdot 0.2 \text{ kg } s^{-1}
\end{aligned}
\tag{4.20}$$

Knowing on one side the expression of the thermal power produced by the stack as a function of the current density (4.18) and the building heating demand computed by

the MPC throughout the week on the other, the MATLAB equation solver `solve()` provides the evolution of the stack current density to meet the load. Then the total H_2 consumption on hourly basis is evaluated with (4.20) and shown in Figure 4.32.

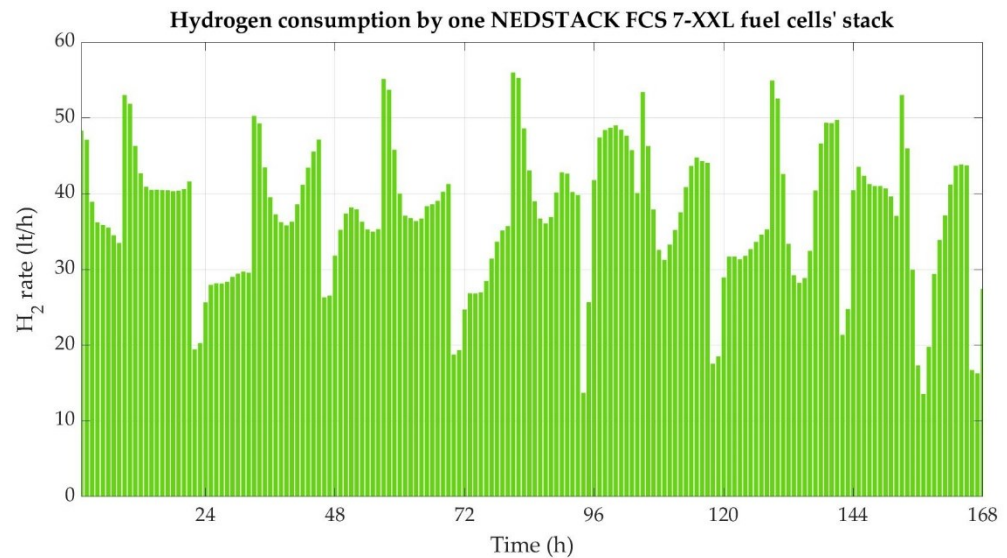


Figure 4.32 – Total hydrogen consumption by one NEDSTACK FCS 7-XXL fuel cells' stack according to the heating request computed by the MPC.

Source: Author's elaboration

The minimum allowable H_2 flow through the stack according to the producer equals 30 NI/min and the results obtained from the simulation are quite below this threshold. The stack size should therefore be reduced accordingly. This to confirm the high CorTau House performance as a nZEB, at least from the thermal demand side. Nedstack, as the FCS 7-XXL developer, provides for the possibility to configure the stack in a flexible way to satisfy the customer requirements on the power needs. However, no data on the stack voltage, current and power production are available at the moment as such adapted stacks are tuned case by case. Downsizing the cells' stack would mean in this case that on one side the hydrogen flow is kept within the range (to be, however, checked once the datasheet for such stack is available), but also a reduced deviation of the power generation from the actual electrical demand from the house is expected. Figure 4.33 shows, indeed, the evolution of both the electrical power generation from the PEMFC stack and the building demand throughout the week from

January 2nd to January 8th, with a slight difference between weekdays and weekends on the latter as discussed in Section 2.3.2.

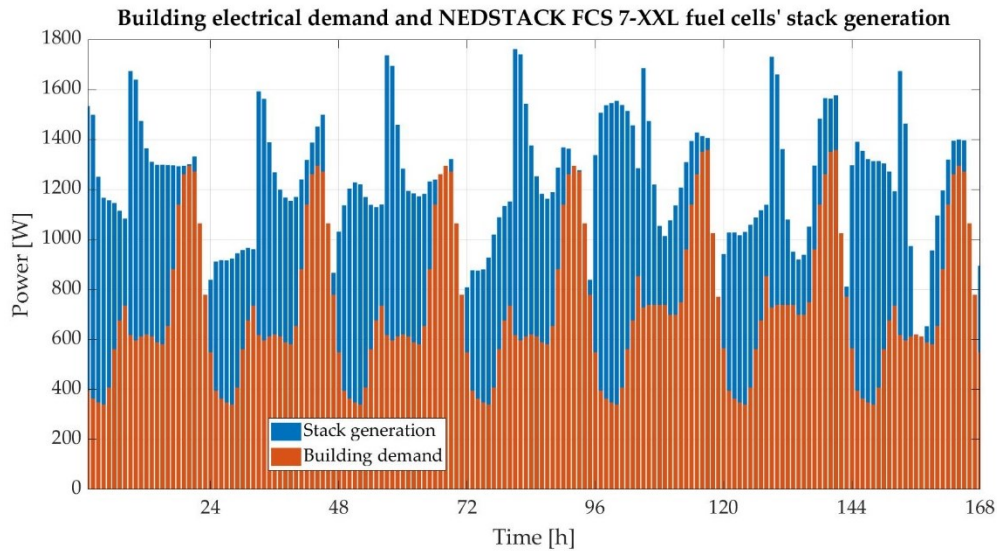


Figure 4.33 – Comparison between the building hourly electrical demand and the generation by one NEDSTACK FCS 7-XXL fuel cells' stack resulting from the heating schedule.

Source: Author's elaboration.

In Figure 4.34 the stack working points are positioned along the polarization and the electrical power curves in accordance with the MPC schedule result. Operation at low current density could inficiate the durability of the PEM fuel cells in the stack. In particular, increased cell voltage, for instance above 0.8 V/cell, means higher energy availability for degradation mechanisms. In addition, the fact that the FCS 7-XXL stack design is optimized for higher power levels and is in this case working with reduced gas flows could result in water management and flooding issues [64].

The points positions along the polarization curve, reported in this case for a single cell of the stack, is always above the 0.8 V voltage level, confirming that downsizing the stack is a priority for it to work correctly with no major damages.

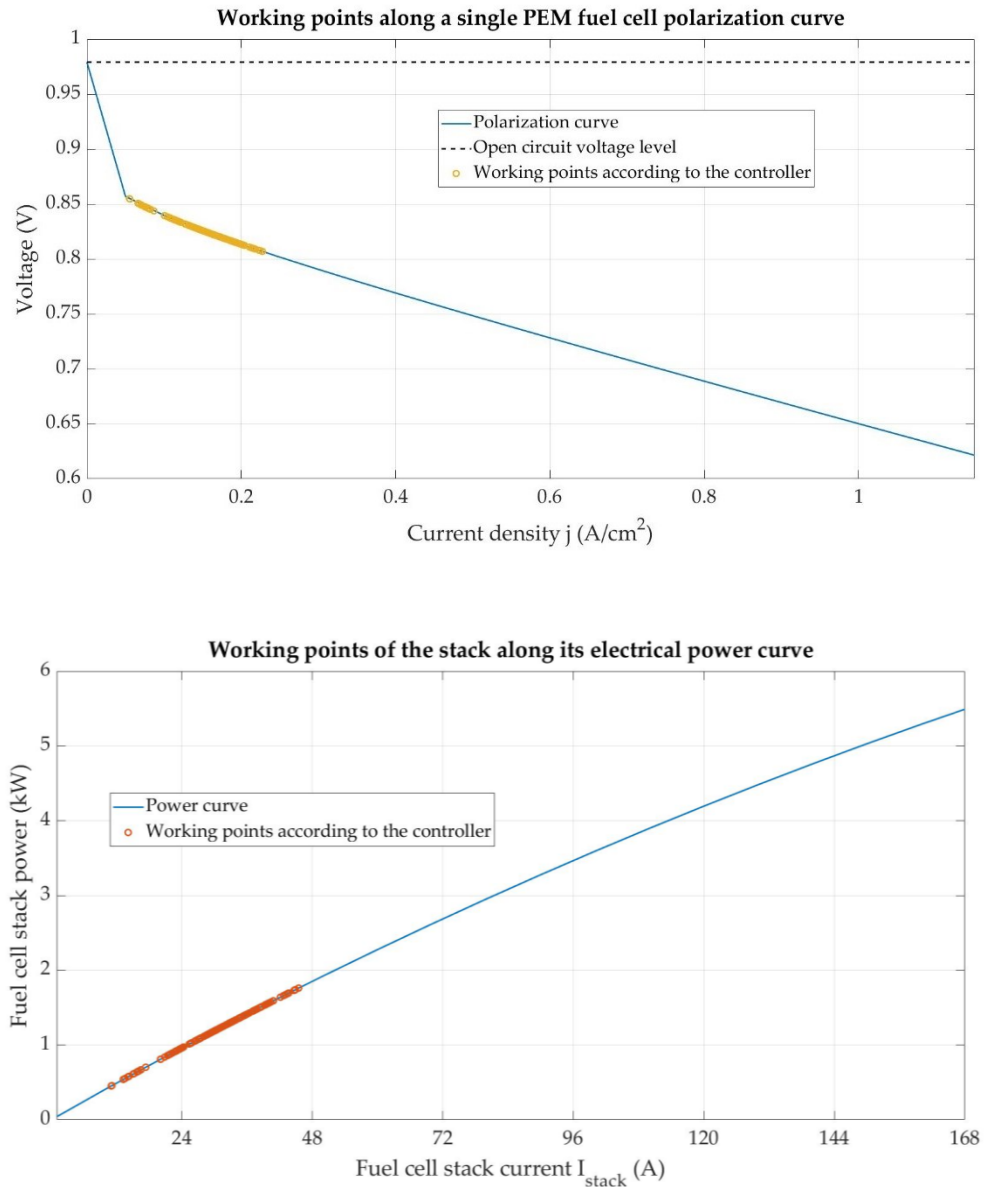


Figure 4.34 – Position of the stack working points over the polarization and electrical power curve according to the MPC operation.

Source: Author's elaboration.

Some basic economic consideration can be ultimately carried out at this point once the evolution of the hydrogen consumption is acquired. The Levelized Cost of Hydrogen (LCOH) is a variable that quantifies the cost related to the production of 1 kg of Hydrogen via water electrolysis. The Fuel Cells and Hydrogen Observatory (FCHO) provides the value of this parameter for each EU country as of March 2022 in two different scenarios, the first in which H₂ is produced via electrolysis powered with

electricity coming from the national power grid, while in the second the electrolysis is powered by on-site photovoltaic generation. The values of the *LCOH* in EU Member States are reported in Figures 5.1 and 5.2 for the two scenarios.

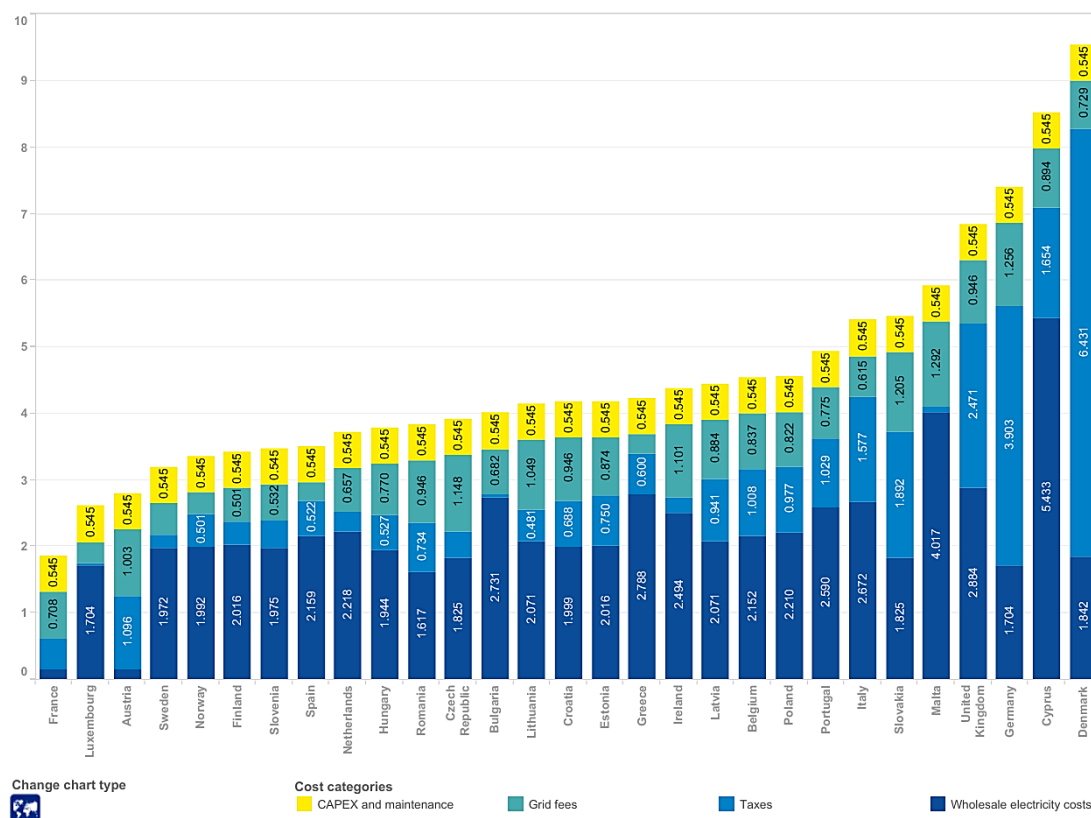


Figure 5.1 – Production costs of hydrogen (€/kg) produced via water electrolysis powered with electricity sourced from the national power grid in EU as of March 2022.

Source: Fuel Cells and Hydrogen Observatory (FCHO).

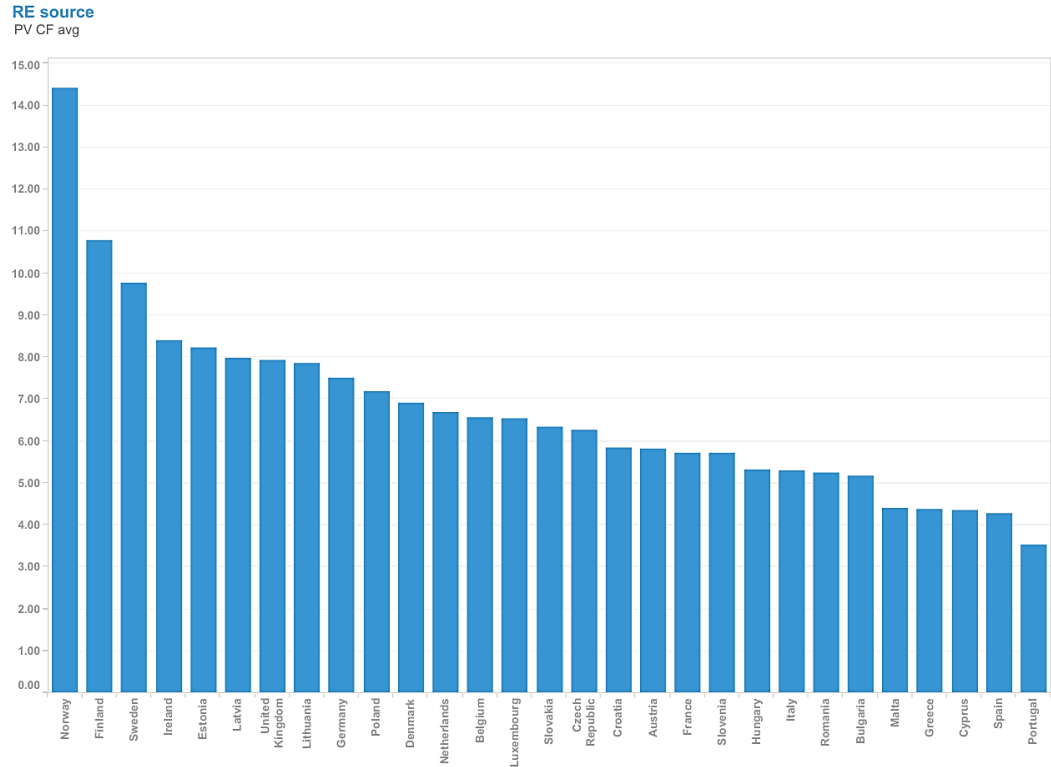


Figure 5.2 – Production costs of renewable hydrogen (€/kg) from PV directly connected to the electrolyser (without grid connection) in EU as of March 2022.

Source: Fuel Cells and Hydrogen Observatory (FCHO).

The *LCOH* indicator is evaluated in the FCHO analysis as:

$$LCOH = \frac{I_0 + \sum_{t=1}^n \frac{I_t + E_t + M_t}{(1+r)^t}}{\sum_{t=1}^n \frac{H_t}{(1+r)^t}} \quad (5.1)$$

where

- I_0 is the investment expenditure at year 0.
- I_t is the investment expenditure at year t (stack replacement costs).

- E_t is the electricity consumed at year t including generation costs (wholesale price or RES LCOE + capacity factor), grid costs and taxes when applicable, and electrolyser stack degradation.
- M_t includes other operational expenditures at year t .
- H_t is the hydrogen production at year t .
- r is the discount rate.
- n is the system lifetime.

The assumptions on the Alkaline Electrolyser (AE) system costs made for the *LCOH* evaluation are listed in Table 5.1.

Table 5.1 – Electrolysis system cost assuming a multi-MW AE system.

CAPEX	600	€/kW
CAPEX: Economic lifetime	30	Years
OPEX: stack durability	80000	h
OPEX: stack replacement costs	20	% CAPEX
OPEX: Energy consumption	50	kWh/kg
OPEX: Stack degradation	0.0012	Per 1000 hrs
OPEX: Other OPEX	4	% CAPEX

Source: Fuel Cells and Hydrogen Observatory (FCHO).

As far as Italy is concerned, the *LCOH* equals 5.409 €/kg and 5.30 €/kg in the first and second scenarios respectively, meaning that no significative difference in the hydrogen production cost is observed. When compared to the other EU States data, the H₂ production cost in Italy with the national grid is among the highest, while the opposite is observed with on-site PV, mainly due to the high availability of the solar resource in the country.

The generation from the roof PV panels throughout the 2nd to 8th of January week is reported in Figure 5.3.

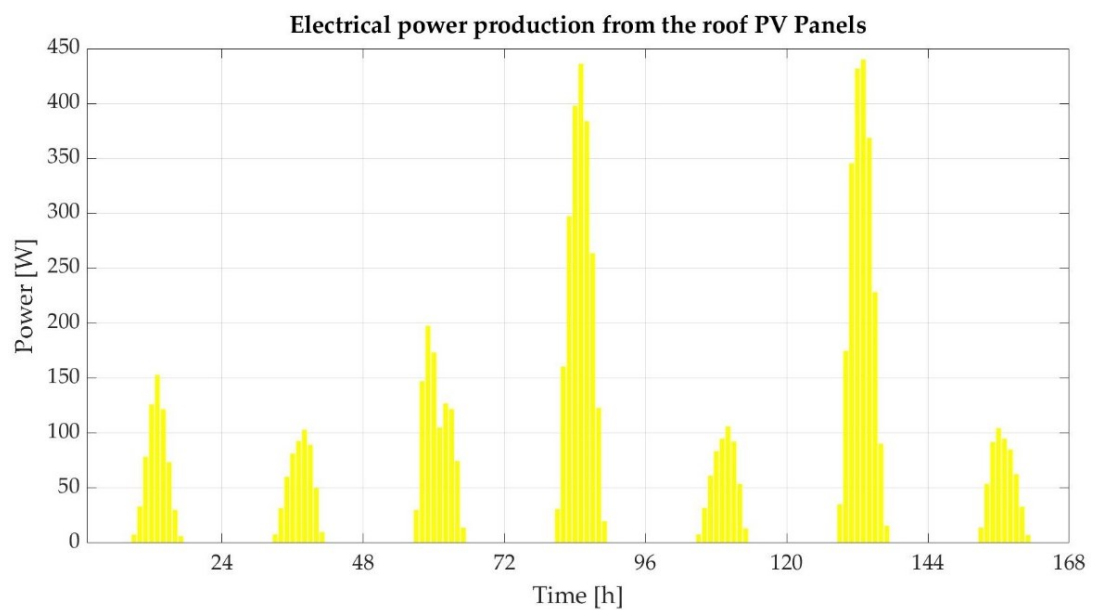


Figure 5.3 – PV power production from the CorTau House roof panels.

Source: Author's elaboration.

With the data provided in Table 5.1, the evolution of the energy consumption at the electrolyser can be obtained, along with the cost related to its production in the first scenario with the electrolyser running on the national grid supply.

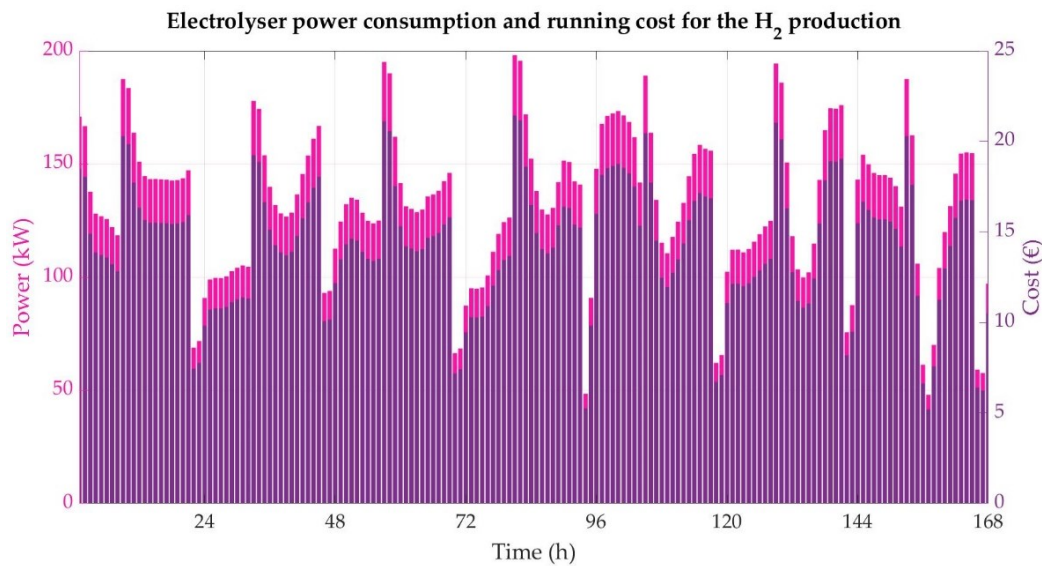


Figure 5.4 – Electrolyser energy consumption and running cost to meet the H₂ demand from the FC stack.

Source: Author's elaboration.

The PV power production is compared to both the electrolyser request to produce green hydrogen on site and the electrical demand from the building light system and appliances. The main evidence is that the first is not sufficient to satisfy the power demand for the H₂ production, at least in the 2nd to 8th of January week and for the NEDSTACK FCS 7-XXL stack. Two alternatives are therefore in principle possible if no storage solutions are investigated:

1. Ensuring that the electrolyser works connected to the national grid. This, however, could be conflicting with the definition of nZEB as most of the energy consumed by the house is not produced on site and fossil fuels accounted for 79% of the total primary energy supply in Italy as of 2021.
2. The hydrogen is not produced at the house location, but the H₂ infrastructure for transport, points of production and stations is still not developed in Italy. In addition the hydrogen consumed by the FC stack is not guaranteed to be in this case renewable again due to the high share of fossil fuels in the Italian power mix.

The high cost related to the hydrogen production independently from the scenario still makes this solution unfeasible, at least until increased H₂ infrastructure both at the production and transport levels will lower the values found for the LCOH.

Conclusions and further research

The aim of this study was developing and verifying the operation of a Model Predictive Control strategy for the indoor air temperature of a single-family house in the heating season. The chosen case-study is the CorTau House, an existing nearly Zero-Energy Building located in Livorno Ferraris (VC) and characterized by a very high thermal performance.

The controller is intended to operate for an entire week from January 2nd to January 8th, and the objective function to minimize includes seven simplified linear models of the house thermal zones. Such models and the MPC design parameters were set through three preliminary simulations in EnergyPlus: normal operation conditions, free-running operation conditions and a pre-defined heating schedule for the linear models coefficients fitting.

The analysis led to reasonable results for the evolution of both the indoor air temperature and the heating power in each zone throughout the entire simulation period both when the MPC loop is closed in MATLAB and, most important, when the co-simulation interface with EnergyPlus is implemented. The quite low level of thermal demand from the house confirms the good performance of the building as a nZEB. With a value of the weighting factor $\lambda = 0$, T_{indoor} is kept as close as possible to the reference. An acceptable compromise between reaching the setpoint and reducing the variation rate of thermal power supply is found for $\lambda = 0.6$ in co-simulation. At this point, the methodology could be validated by providing the found heating schedule to the real building or, alternatively, directly implementing the MPC technique and comparing the results with the EnergyPlus and MATLAB co-simulation ones.

Future developments on this topic could first be including an additional requirement in the definition of the objective function J , for instance to meet the electrical demand from the building specified in the IDF file of the CorTau House. In this case, however, EnergyPlus might not be the best dynamic simulation software as both thermal and electrical power schedules should be sent from MATLAB. As the fuel cell stack would in this case also directly take care of the variable power load schedule introduced in the CorTau House IDF model at each time step, the `OtherEquipment` object would not be sufficient anymore for the data exchange. For this reason, both the stack and the building could be modelled in TRNSYS, as a co-simulation interface with MATLAB is again available. A MIMO (Multi-Input Multi-Output) problem would be solved in this case. As the thermal and electrical power produced by the stack are strictly related through the expression of the polarization curve, finding the optimal input

sequence can get quite complex and again some compromise in the solution must be accepted. Unfortunately a user licence is required as the demo version of TRNSYS is not sufficient for this scope.

On the other side, it is worth pointing out that the simplified thermal models of the building zones could be further improved by introducing, for instance, the effect of the solar gains through both the opaque envelope and the fenestration or even the thermal exchange through the internal partitions. The expected increased accuracy in the face of such higher level of complexity in both the thermal zones modelling and the objective function minimization should be however proven.

Acknowledgments

I would like to express my gratitude to my supervisors Stefano Paolo Corgnati, Andrea Lanzini, Cristina Becchio and Daniele Salvatore Schiera for the constant support shown during this journey and for all the advices they gave me to develop this work.

Many thanks to my family and to all the friends I met in Andria, Turin and Barcelona for accompanying me and for always standing by my side. I feel blessed and grateful.

References

- [1] International Energy Agency. (n.d.). Energy Efficiency: Buildings. [online] Available at: <https://www.iea.org/topics/energyefficiency/buildings/>
- [2] Roadmap on carcinogens. (n.d.). Hardwood Dust [online] Available at: <https://roadmaponcarcinogens.eu/hardwooddust/>
- [3] IEA (2021), World Energy Balances: Overview, IEA, Paris [online] Available at: <https://www.iea.org/reports/world-energy-balances-overview>
- [4] Directive (EU) 2018/844 of the European Parliament and of the Council of 30 May 2018 amending Directive 2010/31/EU on the energy performance of buildings and Directive 2012/27/EU on energy efficiency
- [5] EnergyPlus Version 9.6. US Department of Energy
- [6] David Kehmeier, Intermedius Design Integration, LLC. *Intermediate Data Format. Mechanical Data Exchange Specification for the Design and Analysis of. Printed Wiring Assemblies. Version 3.0. October 31, 1996.*
- [7] Directive (EU) 2018/844 of the European Parliament and of the Council of 30 May 2018 amending Directive 2010/31/EU on the energy performance of buildings and Directive 2012/27/EU on energy efficiency
- [8] Grove, W. R. (1838). "On a new voltaic combination". *The London and Edinburgh Philosophical Magazine and Journal of Science. 3rd series.* **13** (84): 430–431.
- [9] Frano Barbir, PEM Fuel Cells, Theory and Practice, 2005, Elsevier
- [10] Schalenbach, Maximilian; Hoefner, Tobias; Paciok, Paul; Carmo, Marcelo; Lueke, Wiebke; Stolten, Detlef (2015-10-28). "Gas Permeation through Nafion. Part 1: Measurements". *The Journal of Physical Chemistry C.* **119** (45): 25145–25155. [doi:10.1021/acs.jpcc.5b04155](https://doi.org/10.1021/acs.jpcc.5b04155).
- [11] Nakhiah Goulbourne. "Research Topics for Materials and Processes for PEM Fuel Cells REU for 2008". *Virginia Tech*. Archived from [the original](#) on 27 February 2009. Retrieved 18 July 2008.
- [12] Yoshitsugu Sone, Per Ekdunge and Daniel Simonsson, *Proton Conductivity of Nafion 117 as Measured by a Four-Electrode AC Impedance Method*, 1996 ECS – The Electrochemical Society, Journal of The Electrochemical Society, Volume 143, Number 4
- [13] E. Proietti, F. Jaouen, M. Lefevre, N. Larouche, J. Tian, J. Herranz, and J.-P. Dodelet. 2011 Iron-based cathode catalyst with enhanced power density in polymer electrolyte membrane fuel cells" *Nature Communications* 2(1)
- [14] Welaya, Yousri & Elgohary, Mohamed & Ammar, Nader. (2011). A comparison between fuel cells and other alternatives for marine electric power generation. *International Journal of Naval Architecture and Ocean Engineering.* 3. 141-149. [10.3744/JNAOE.2011.3.2.141](https://doi.org/10.3744/JNAOE.2011.3.2.141).

-
- [15] Louzazni, M.; Al-Dahidi, S.; Mussetta, M. Fuel Cell Characteristic Curve Approximation Using the Bézier Curve Technique. *Sustainability* **2020**, *12*, 8127.
- [16] Kandidayeni, M.; Macias, A.; Khalatbarisoltani-Boulon, A.L.; Kelouwani, S. Benchmark of proton exchange membrane fuel cell parameters extraction with metaheuristic optimization algorithms. *Energy* **2019**, *183*, 912–925.
- [17] Carlos E. García, David M. Prett, Manfred Morari, Model predictive control: Theory and practice—A survey, *Automatica*, Volume 25, Issue 3, 1989, Pages 335–348, ISSN 0005-1098
- [18] Pendleton, Scott & Andersen, Hans & Du, Xinxin & Shen, Xiaotong & Meghjani, Malika & Eng, You & Rus, Daniela & Jr, Marcelo. (2017). Perception, Planning, Control, and Coordination for Autonomous Vehicles. *Machines*. 5. 6. 10.3390/machines5010006.
- [19] MATLAB. (R2021b). Natick, Massachusetts: The MathWorks Inc.; 2022.
- [20] Negenborn, R.R. & De Schutter, Bart & Wiering, Marco & Hellendoorn, J.. (2022). Experience-based model predictive control using reinforcement learning.
- [21] Building Controls Virtual Test Bed User Manual Version 1.6.0, Simulation Research Group Building Technology and Urban Systems Department Environmental Energy Technologies Division Lawrence Berkeley National Laboratory Berkeley, CA 94720, April 20, 2016.
- [22] MLE+: A MATLAB-ENERGYPLUS CO-SIMULATION INTERFACE Truong X. Nghiem Automatic Control Laboratory Ecole Polytechnique Fed' erale de Lausanne (EPFL), Switzerland
- [23] Johan Löfberg, A toolbox for modeling and optimization in MATLAB, October 2004
- [24] JE, Larminie & Dicks, Andrew. (2013). Fuel Cell System Explained. 10.1002/9781118878330.
- [25] Eurostat Database, 2022.
- [26] Ministry of Ecological transition, “Piano nazionale di contenimento dei consumi di gas naturale”, September 2022.
- [27] Decreto del Presidente della Repubblica 26 agosto 1993, n. 412. Regolamento recante norme per la progettazione, l'installazione, l'esercizio e la manutenzione degli impianti termici degli edifici ai fini del contenimento dei consumi di energia, in attuazione dell'art. 4, comma 4, della legge 9 gennaio 1991, n. 10.
- [28] Bernal, Willy & Behl, Madhur & Nghiem, Truong & Mangharam, Rahul. (2015). Campus-Wide Integrated Building Energy Simulation.
- [29] Directive 2002/91/EC of the European Parliament and of the Council of 16 December 2002 on the energy performance of buildings. Official Journal of the European Union L 001 , 04/01/2003 P. 0065 - 0071
- [30] Directive (EU) 2018/844 of the European Parliament and of the Council of 30 May 2018 amending Directive 2010/31/EU on the energy performance of buildings and Directive 2012/27/EU on energy efficiency. Official Journal of the European Union L 156/75.

[31] Directive 2010/31/EU of the European Parliament and of the Council of 19 May 2010 on the energy performance of buildings (recast). Official Journal of the European Union L 153/13.

[32] European Commission, 2021, Proposal of revision of the Directive of the European Parliament and of the Council on the energy performance of buildings (recast), COM(2021) 802 final. Available at <https://ec.europa.eu/energy/sites/default/files/proposal-recast-energy-performance-buildings-directive.pdf>

[33] European Commission, 2022 a, Communication from the Commission to the European Parliament, the Council, the European Economic and Social Committee and the Committee of the Regions. EU 'Save Energy', COM(2022) 240 final. available at <https://eur-lex.europa.eu/legal-content/EN/TXT/PDF/?uri=CELEX:52022DC0240&from=EN>

[34] European Commission, 2022b, REPowerEU Plan. COM(2022) 230 final. available at <https://eur-lex.europa.eu/legal-content/EN/TXT/?uri=COM%3A2022%3A230%3AFIN&qid=1653033742483>

[35] European Commission, 2020, A Renovation Wave for Europe - greening our buildings, creating jobs, improving, COM(2020) 662 final, available at: <https://eur-lex.europa.eu/legal-content/EN/TXT/?qid=1603122220757&uri=CELEX:52020DC0662>.

[36] European Commission, 2019, Communication from the Commission to the European Parliament, the European Council, the Council, the European Economic and Social Committee and the Committee of the Regions, the European Green Deal, COM(2019) 640, 11.12.2019, <https://eur-lex.europa.eu/legal-content/EN/TXT/?uri=COM%3A2019%3A640%3AFIN>

[37] European Committee for Standardization, 2019, Energy performance of buildings – Ventilation for buildings. Part 1: Indoor environmental input parameters for design and assessment of energy performance of buildings addressing indoor air quality, thermal environment, lighting, and acoustics (EN 16798-1).

[38] Paris Agreement to the United Nations Framework Convention on Climate Change, Dec. 12, 2015, T.I.A.S. No. 16-1104.

[39] EPBD implementation in Italy S t a t u s i n D e c e m b e r 2 0 1 6 AUTHORS Ezilda Costanzo, Anna Martino, Gian Mario Varalda, Marcello Antinucci, Alessandro Federici

[40] Yao, Jian. (2014). An investigation into the impact of movable solar shades on energy, indoor thermal and visual comfort improvements. Building and Environment. 71. 24–32.

[41] IEA 021a. All rights reserved. Adapted from “Tracking Clean Energy Progress”.

[42] IEA 2021c, Net Zero by 2050: A Roadmap for the Global Energy Sector.

[43] Littelfuse®.

[44] Example of an Energy Performance Certificate. Government of the United Kingdom. 2012

[45] Directive 2002/91/EC of the European Parliament and of the Council of 16 December 2002 on the energy performance of buildings, Official Journal L 001 , 04/01/2003 P. 0065 – 0071

-
- [46] S. Hobart, M. Schantz, The Time for a Net-Zero Building Boom is Now, UrbanLand, March 26, 2021
- [47] Riqualificazione energetica degli edifici pubblici esistenti: direzione nZEB, V. Corrado, I. Ballarini, G. De Luca, E. Primo, D. Iatauro, ENEA, Report RdS/PAR2016/252.
- [48] Decreto interministeriale 26 giugno 2015 - Applicazione delle metodologie di calcolo delle prestazioni energetiche e definizione delle prescrizioni e dei requisiti minimi degli edifici.
- [49] Energy & Strategy Group. (July 26, 2017). Number of nearly zero energy buildings (nZEB)* as of May 2017, by type of certification [Graph]. In Statista.
- [50] ASHRAE Handbook Fundamentals, 2005.
- [51] The Engineering Toolbox.
- [52] S.P. Corgnati, C. Guala, M. Luciano, 'The challenge of designing and building nZEBs: a single-family house in Italy', REHVA Journal – November 2014
- [53] UNI 10339
- [54] ASHRAE 90.1 Standard.
- [55] David Simula. Qualità dell'aria e comfort termico in un edificio NZEB: analisi CFD di possibili strategie di ventilazione = Indoor Air Quality and thermal comfort in a NZEB building: CFD analysis of possible ventilation strategies. Tesi di laurea. 2019.
- [56] Piatkowski, Piotr, Iwona Michalska-Pozoga, and Marcin Szczepanek. 2022. "Fuel Cells in Road Vehicles" *Energies* 15, no. 22: 8606. <https://doi.org/10.3390/en15228606>.
- [57] Andrey, Yaroslavtsev & Dobrovolsky, Yurii & Shaglaeva, N & Frolova, L & Gerasimova, Ekaterina & Sanginov, E.. (2012). Nanostructured materials for low-temperature fuel cells. *Russian Chemical Reviews*. 81. 191. 10.1070/RC2012v081n03ABEH004290.
- [58] Andersen, Shuang & Chen, Qian & Joegensen, Fleming & Stein, Paul & Skou, Eivind. (2007). F-19 NMR studies of Nafion (TM) ionomer adsorption on PEMFC catalysts and supporting carbons. *Solid State Ionics*. 178. 1568-1575. 10.1016/j.ssi.2007.10.007.
- [59] PRODUCT DATA SHEET FCS 7-XXL Gen 2.9. Revision 01, 05-07-2022. Nedstack PEM FUEL CELLS.
- [60] Jung, Jee-Hoon & Ahmed, Shehab. (2010). Dynamic Model of PEM Fuel Cell Using Real-time Simulation Techniques. *Journal of Power Electronics*. 10. 10.6113/JPE.2010.10.6.739.
- [61] EnergyPlus Documentation.
- [62] Borkovski, Stefan & Erkechova, Maja. (2020). Control approaches of pem fuel cells: a review. 5. 126.
- [63] U.S. Department of Energy.

[64] S. Knights, Polymer Electrolyte Membrane and Direct Methanol Fuel Cell Technology: Fundamentals and Performance of Low Temperature Fuel Cells, 2012.

[65] Fuel Cells and Hydrogen Observatory (FCHO).

[66] Jiang, S.P., Li, Q. (2022). Fuel Cell Thermodynamics. In: Introduction to Fuel Cells. Springer, Singapore. https://doi.org/10.1007/978-981-10-7626-8_2.

Appendix A

Stratigraphy specification

Table A.1 – Adjacent building wall stratigraphy

Material	Thickness (m)	Conductivity (W/mK)	Density (kg/m ³)	Specific Heat (J/kgK)
EW – LAT 10	0.1	0.25	600	840
EW – ISOL.	0.2	0.037	150	1030
EW – LAT.	0.25	0.25	600	840

Table A.2 – Fake adjacent building partition stratigraphy

Material	Thickness (m)	Conductivity (W/mK)	Density (kg/m ³)	Specific Heat (J/kgK)
SOL - ARIA	0.63	0.026	1.225	1030

Table A.3 – External wall stratigraphy

Material	Thickness (m)	Conductivity (W/mK)	Density (kg/m ³)	Specific Heat (J/kgK)
EW – RIV. EST.	0.004	45	7680	840
EW – ISOL.	0.2	0.037	150	1030
EW – LAT.	0.25	0.25	600	840
EW – CART.	0.03	0.16	950	109
EW – INT.	0.02	0.7	1400	1010

Table A.4 – Ceiling stratigraphy

Material	Thickness (m)	Conductivity (W/m·K)	Density (kg/m ³)	Specific Heat (J/kg·K)
CEIL - MASS	0.05	0.15	400	1000
CEIL – ISOL.	0.2	0.037	150	1030
CEIL – CLS	0.25	1.13	2000	880
CEIL – CART.	0.03	0.16	950	109

Table A.5 – Gravel floor stratigraphy

Material	Thickness (m)	Conductivity (W/m·K)	Density (kg/m ³)	Specific Heat (J/kg·K)
CEIL – GHIAIA	0.25	0.36	1840	840
CEIL - MAG	0.15	1.7	2200	920
CEIL - CLS	0.15	1.13	2000	880
CEIL – ISOL.	0.12	0.037	150	1030
CEIL – MASS + PANN	0.05	0.15	400	1000
CEIL – MASS + PANN	0.05	0.15	400	1000
CEIL – PAV	0.01	0.06	200	840

Table A.6 – Crawl space stratigraphy

Material	Thickness (m)	Conductivity (W/m·K)	Density (kg/m ³)	Specific Heat (J/kg·K)	Thermal Resistance (m ² ·K/W)
CEIL - CLS	0.15	1.13	2000	880	/

CEIL – AIR	/	/	/	/	0.18
CEIL - CLS	0.15	1.13	2000	880	/
CEIL – ISOL.	0.12	0.037	150	1030	/
CEIL – MASS + PANN	0.05	0.15	400	1000	/
CEIL – MASS + PANN	0.05	0.15	400	1000	/
CEIL – PAV	0.01	0.06	200	840	/

Table A.7 – Pier stratigraphy

Material	Thickness (m)	Conductivity (W/m·K)	Density (kg/m ³)	Specific Heat (J/kg·K)
PIER – CART.	0.03	0.16	950	109
PIER – ISOL.	0.08	0.037	150	1030
PIER – CART.	0.03	0.16	950	109

Table A.8 – Internal partition stratigraphy

Material	Thickness (m)	Conductivity (W/m·K)	Density (kg/m ³)	Specific Heat (J/kg·K)
INT – CART.	0.03	0.16	950	109
INT – ISOL.	0.08	0.037	150	1030
INT – CART.	0.03	0.16	950	109

Table A.9 – Low Emissivity Glass specifications

	LoE CLEAR 4MM Rev
Thickness (m)	0.004
Solar Transmittance at Normal Incidence	0.6
Front Side Solar Reflectance at Normal Incidence	0.22
Back Side Solar Reflectance at Normal Incidence	0.17
Visible Transmittance at Normal Incidence	0.84
Front Side Visible Reflectance at Normal Incidence	0.078
Back Side Visible Reflectance at Normal Incidence	0.055
Infrared Transmittance at Normal Incidence	0
Front Side Infrared Hemispherical Emissivity	0.1
Back Side Infrared Hemispherical Emissivity	0.84
Conductivity (W/m·K)	0.9

	ARGON 15MM
Thickness (m)	0.015

Appendix B

NEDSTACK FCS 7-XXL Datasheet

PRODUCT DATA SHEET FCS 7-XXL Gen 2.9
Revision 01, 05-07-2022



NEDSTACK FCS 7-XXL

Stack specifications and operating conditions

Electrical – Beginning of life	
Rated power ¹	6.8 kWe
Voltage range	29 – 47 V
Current range	0 – 230 A
Mechanical	
Cell count	48 cells
Weight	26 kg
Size (excl. connectors)	351 x 196 x 288 mm
Fuel	
Composition ² (dry)	Hydrogen according to ISO 14687-2 Grade ≥ 2.5
Inlet temperature	50 – 60 °C
Humidification	50 – 80% RH at coolant inlet temperature
Maximum operating pressure	250 mbarg
Allowable working pressure	450 mbarg
Pressure drop ³	< 60 mbar
Stoichiometry	≥ 1.25
Minimum H ₂ flow	30 Nl/min
Maximum H ₂ consumption	77 Nl/min
Air	
Composition ²	Filtered air
Inlet temperature	55 – 60 °C
Humidification	75 – 85% RH at coolant inlet temperature
Maximum operating pressure	200 mbarg
Allowable working pressure	450 mbarg
Pressure drop ³	< 110 mbar
Stoichiometry	≥ 2.0
Minimum air flow	48 Nl/min
Maximum air flow	366 Nl/min
Cooling	
Coolant	Demineralized water or BASF Glycantin FC G20
Conductivity	< 10 µS/cm
Inlet temperature	60 – 65 °C
Coolant temperature increase	< 5 °C
Maximum operating pressure	450 mbarg
Allowable working pressure	450 mbarg
Pressure drop	< 100 mbar for demi-water / < 250 mbar for Glycantin FC G20
Cooling capacity	< 9 kWth
MEA	
Safety differential pressure anode	50 mbar above cathode pressure
Maximum allowable differential working pressure	300 mbar
CVM unit	
Power supply	18 – 32 VDC
Communication interface	CAN 2.0B, baud rate 500 kbit/s
Emissions	
Water production	< 0.6 L/kWh _{el}
External hydrogen leakage	< 1 mL/min/cell (BoL)
Ambient conditions	
Climate conditions	-20 – 55 °C, 0 – 100% RH
Altitude	< 2000 m above sea level

¹ At reference conditions, see page 2.

² Contact Nedstack for a specification of allowable contaminants.

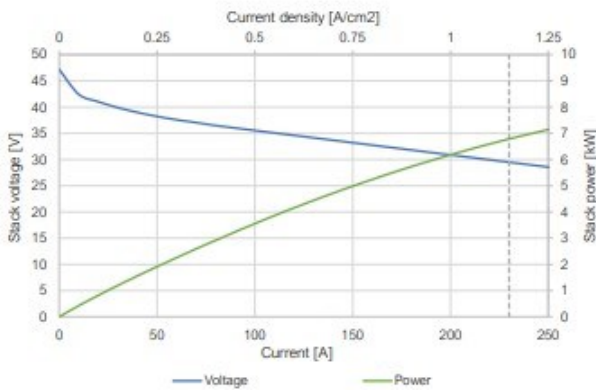
³ At reference stoichiometry, see page 2.

Appearance impression



Stack performance

Beginning-of-life stack performance at reference conditions given below.



Current (A)	0	40	80	120	160	200	230
Stack voltage (V)	47	39	37	35	33	31	30
Stack power (kW)	0.0	1.6	2.9	4.2	5.2	6.2	6.8

Stack temperature	
Coolant inlet temperature	62 °C
Coolant outlet temperature	< 67 °C
Anode	
Inlet humidity	80% RH at 62 °C
Backpressure	100 mbarg
Stoichiometry	1.25
Cathode	
Inlet humidity	80% RH at 62 °C
Backpressure	Ambient
Stoichiometry	2

Appendix C

MPC development in the MATLAB environment

```

%% MPC Development for the CorTau House case study

clear all
close all
clc

nominal = [1117, 474, 513, 467, 176, 104, 190];      %[W]
surface = [48.7, 19.1, 27.4, 20.5, 5.3, 3.5, 6.9, 5];  %[m2]

% ZT 1 Kitchen
% ZT 2 Living Room
% ZT 3 Night Area
% ZT 4 Studio
% ZT 5 Bathroom 1
% ZT 6 Bathroom 2
% ZT 7 Bathroom 3

ZoneNames = ["ZT 1 Kitchen", "ZT 2 Living Room", "ZT 3 Night Area", "ZT 4
Studio", "ZT 5 Bathroom 1", "ZT 6 Bathroom 2", "ZT 7 Bathroom 3"];
ZoneAcr = ["ZT1", "ZT2", "ZT3", "ZT4", "ZT5", "ZT6", "ZT7"];

%% Create mlep instance and configure it

% Instantiate co-simulation tool
ep = mlep;

% Building simulation configuration file
ep.idfFile = 'CorTau_OneWeek_1htimestep';

% Weather file
ep.epwFile = 'ITA_Torino.160590_IWEC';

%% Input/output configuration

% Initialize the co-simulation. This will load the IDF file.
ep.initialize;

% Display inputs/outputs defined in the IDF file.
disp('Input/output configuration. ');
inputTable = ep.inputTable
outputTable = ep.outputTable

%% EnergyPlus simulation with pre-defined heating schedule

% Specify simulation duration
endTime = 60*60*24; %[s]

% Start the co-simulation process and communication.
ep.start

% The simulation loop

```

```
t = 0;
n = 1;

fuel_cell = zeros(1,7);
heat_rate(n,:) = fuel_cell;

while t <= endTime

    if t <= 60*60*1 || t >= 60*60*23
        fuel_cell(:) = 1;
    elseif t > 60*60*3 && t < 60*60*5
        fuel_cell(:) = 0.6;
    elseif t >= 60*60*5 && t <= 60*60*7
        fuel_cell(:) = 0.7;
    elseif t > 60*60*7 && t <= 60*60*10
        fuel_cell(:) = 0.8;
    elseif t >= 60*60*12 && t <= 60*60*14
        fuel_cell(:) = 0.3;
    elseif t >= 60*60*16 && t <= 60*60*18
        fuel_cell(:) = 1;
    elseif t >= 60*60*19 && t <= 60*60*20
        fuel_cell(:) = 0.7;
    elseif t >= 60*60*21 && t < 60*60*23
        fuel_cell(:) = 0.4;
    else
        fuel_cell(:) = 0.2;
    end

    % Prepare inputs (possibly from last outputs)
    u = fuel_cell;    %[heating rate fraction]

    % Get outputs from EnergyPlus
    [y, t] = ep.read;

    % Send inputs to EnergyPlus
    ep.write(u,t);

    heat_rate(n,:) = fuel_cell;
    TemperatureEP(n,:) = y(2:end);
    OutdoorT(n) = y(1);
    time(n) = t;

    n = n+1;

end

% Stop co-simulation process
ep.stop;

%% Plot results - Indoor and outdoor temperature - Heat rate (predefined)

figure(1)
plot(TemperatureEP,'linewidth',1);
xlabel('Time (h)');
ylabel('Temperature [°C]');
title('Pre-defined heating schedule simulation results, January 1^s^t');
grid on
box on
set(gca,'fontsize',20,'FontName','Palatino Linotype');
legend('ZT 1 Kitchen', 'ZT 2 Living Room', 'ZT 3 Night Area', 'ZT 4 Studio', 'ZT 5 Bathroom 1', 'ZT 6 Bathroom 2', 'ZT 7 Bathroom 3', 'location', 'best');
xlim([1 24]);
```

```

xticks([1:1:24]);

figure(2)
plot(heat_rate(:,1),'linewidth',1);
xlabel('Time (h)');
ylabel('Heating power fraction over nominal [-]');
title('Pre-defined heating schedule, January 1s^t');
grid on
box on
set(gca,'fontsize',20,'FontName','Palatino Linotype');
xlim([1 24]);
xticks([1:1:24]);

%% Evaluation of A,B,C parameters for the linear building model

OutdoorT = xlsread('Turin_OutdoorT_1hour timestep.csv','B2:B25'); % One day as
in the pre-defined schedule
TemperatureEP = TemperatureEP(1:length(OutdoorT),:);
heat_rate = heat_rate(1:length(OutdoorT),:);

for j = 1:7 % Pre-defined
heating matrix building
    Heat_pre(:,j) = heat_rate(:,j)*nominal(j); % [W]
end
OutdoorT = OutdoorT + 273.15; % [K]
TemperatureEP = TemperatureEP + 273.15; % [K]

% MODEL ESTIMATION - MULTIVARIABLE LINEAR REGRESSION
%  $C * ((T_{indoor\_n+1} - T_{indoor\_n}) / \Delta t) = k_1 * (T_{indoor\_n} - T_{ext\_n}) + k_2 * u_n$ 
% To find C, k1, k2 we rewrite it as:
%  $T_{indoor\_n+1} = (1 + k_1 * \Delta t / C) * (T_{indoor\_n}) + k_2 * \Delta t / C * (u_n) - k_1 * \Delta t / C * (T_{ext\_n})$ 

for i = 1:7

    X = [TemperatureEP(1:end-1,i) , Heat_pre(1:end-1,i) , OutdoorT(1:end-1)];
    Y = TemperatureEP(2:end,i);

    P = regress(Y,X);

    A(i) = P(1);
    B(i) = P(2);
    C(i) = P(3);

end

%% Comparison between the A,B,C model and the results coming from EnergyPlus

% A,B,C model
Tabc(1,1:7) = TemperatureEP(1,1:7); % Initial temperatures for each thermal
zone from EP
for j = 1:7
    for n = 1:23
        Tabc(n+1,j) = A(j)*Tabc(n,j) + B(j)*Heat_pre(n,j) + C(j)*OutdoorT(n);
    end
end

% EnergyPlus
Tepplus = TemperatureEP - 273.15; % [°C]

```

```

Tabc = Tabc - 273.15;                                % [°C]

% Comparison
figure(3)
for j = 1:7
    subplot(4,2,j)
    plot(Tabc(:,j), 'linewidth',1)
    hold on
    plot(Teplus(:,j), 'linewidth',1)
    xlabel('Time (min)');
    ylabel('Temperature [°C]');
    title(sprintf('ZoneNames(j)'));
    grid on
    box on
    set(gca, 'FontSize',12, 'FontName', 'Palatino Linotype');
    legend('Linear Model', 'EnergyPlus Simulation', 'location', 'best')
    xlim([1 24])
    xticks([1:1:24]);
end

% Error comparison between EP and Linear Model
for j = 1:7
    error(j) = norm(Tabc(:,j)-Teplus(:,j))./norm(Teplus(:,j));    % Relative error
    over the EP results (as it is the "accurate" one)
end

figure(4)
bar((1:7),error*100, 'FaceColor', [.5 .5 .5])
ylabel('Error [%]');
grid on
box on
set(gca, 'FontSize',20, 'FontName', 'Palatino Linotype');
title('Error introduced by approximating the EnergyPlus model with the linear
one');
xticklabels([ZoneAcr]);
xlim([0 8]);

%% MPC implementation WITHOUT the EnergyPlus co-simulation for one week

% Model data
OutdoorT = xlsread('Turin_OutdoorT_1hourimestep.csv', 'B26:B241') + 273.15;
%[K]

% MPC data
Np = 168;                % Control horizon timesteps - One week
Nc = 5;                  % Predictionhorizon timesteps - 5 hours
q = sdpvar(Np,7);        % Decision variable
x = sdpvar(Np,7);        % Output variable
u = sdpvar(Np,7);        % Normalized decision variable
lambda = 0;              % Cost function weight variable in the range [0...1]

options = sdpsettings('solver', 'sedumi');
options.sedumi.maxiter = 1000;

% Initial state
x0(1:7) = 18 + 273.15;
x(1,1:7) = x0;

TsetpointPLOT = 0;

% Model Predictive Control implementation
for k = 1:Np              % Prediction Horizon - one week

```

```

    if k <= 7 || (k >= 21 && k <= 31) || (k >= 45 && k <= 55) || (k >= 69 && k <=
79) || (k >= 93 && k <= 103) || (k >= 117 && k <= 127) || (k >= 141 && k <= 151)
|| (k >= 165 && k <= 168)
        Tsetpoint = 18 + 273.15;
    else
        Tsetpoint = 20 + 273.15;
    end

    for j = 1:7 % Cycle to go through all the thermal zones
        constraints = [];
        objective = 0;

        for m = 1:Nc % Control Horizon - 5 timesteps
            x(m+1,j) = A(j)*x(m,j) + B(j)*q(m,j) + C(j)*OutdoorT(k+m-1);
            if m == 1
                objective = objective + (1-lambda)*((x(m+1,j)-Tsetpoint)^2/20^2)
+ ...
                (lambda)*((q(m,j))^2)/(nominal(j))^2;
            else
                objective = objective + (1-lambda)*((x(m+1,j)-Tsetpoint)^2/20^2)
+ ...
                (lambda)*((q(m,j)-q(m-1,j))^2)/(nominal(j))^2;
            end
            constraints = [constraints, 0 <= q(m,j) <= nominal(j), x(m+1,j)
<= Tsetpoint];
        end

        optimize(constraints,objective,options);

        q_mpc(k,j) = value(q(1,j));
        u_mpc(k,j) = q_mpc(k,j)/nominal(j);
        T_mpc(k,j) = value(x(2,j));

        x(1,j) = x(2,j);
    end

    TsetpointPLOT = [TsetpointPLOT,Tsetpoint];

    k

end

figure(5)
plot([1:1:168],q_mpc,'linewidth',1)
title(['Heating demand computed by the MPC with ? = ',num2str(lambda),' , January
2^n^d to 8^t^h']);
xlabel('Time [h]');
ylabel('Thermal Power [W]');
grid on
box on
set(gca,'fontsize',20,'FontName','Palatino Linotype');
legend('ZT 1 Kitchen', 'ZT 2 Living Room', 'ZT 3 Night Area', 'ZT 4 Studio', 'ZT
5 Bathroom 1', 'ZT 6 Bathroom 2', 'ZT 7 Bathroom 3', 'location', 'best');
xlim([1 168]);
xticks([0:24:168]);

figure(6)
plot([1:1:168],T_mpc-273.15,'linewidth',1)
title(['Indoor Air Temperature computed by the MPC with ? = ',num2str(lambda),' ,
January 2^n^d to 8^t^h']);
xlabel('Time [h]');
ylabel('Temperature [°C]');
grid on

```

```

box on
set(gca,'fontsize',20,'FontName','Palatino Linotype');
hold on
plot([1:1:168],TsetpointPLOT(2:end)-273.15,'--k','linewidth',1);
legend('ZT 1 Kitchen', 'ZT 2 Living Room', 'ZT 3 Night Area', 'ZT 4 Studio', 'ZT
5 Bathroom 1', 'ZT 6 Bathroom 2', 'ZT 7 Bathroom 3', 'Setpoint', 'location',
'best');
xlim([1 168]);
xticks([0:24:168]);
ylim([17 21]);

%% Evaluation of the lambda variation effect on q and Tindoor

% Model data
OutdoorT = xlsread('Turin_OutdoorT_1hour timestep.csv','B26:B241') + 273.15;
%[K]

% MPC data
Np = 48; % Control horizon timesteps - Two days
Nc = 5; % Prediction horizon timesteps - 5 hours
q = sdpvar(Nc,7); % Decision variable
x = sdpvar(Nc,7); % Output variable
u = sdpvar(Nc,7); % Normalized decision variable

L = (0:0.1:1);

for i = 1:length(L)

    lambda = L(i);

    % Initial state
    x0 = 18 + 273.15;
    x(1,1) = x0;

    options = sdpsettings('solver','sedumi');
    options.sedumi.maxiter = 1000;

    % Model Predictive Control implementation
    for k = 1:Np % Prediction Horizon
        if k <= 7 || (k >= 21 && k <= 31) || (k >= 45 && k <= 55) || (k >= 69 &&
k <= 79) || (k >= 93 && k <= 103) || (k >= 117 && k <= 127) || (k >= 141 && k <=
151) || (k >= 165 && k <= 168)
            Tsetpoint = 18 + 273.15;
        else
            Tsetpoint = 20 + 273.15;
        end

        for j = 1 % Only focusing on ZT1 Kitchen

            constraints = [];
            objective = 0;

            for m = 1:Nc % Control Horizon
                x(m+1,j) = A(j)*x(m,j) + B(j)*q(m,j) + C(j)*OutdoorT(k+m-1);
                if m == 1
                    objective = objective + (1-lambda)*((x(m+1,j)-
Tsetpoint)^2/20^2) + ...
                        (lambda)*((q(m,j))^2)/(nominal(j))^2;
                else
                    objective = objective + (1-lambda)*((x(m+1,j)-
Tsetpoint)^2/20^2) + ...
                        (lambda)*((q(m,j)-q(m-1,j))^2)/(nominal(j))^2;
                end
            end
        end
    end
end

```

```

        end
        constraints = [constraints, 0 <= q(m,j) <= nominal(j),
x(m+1,j) <= Tsetpoint];
    end

    optimize(constraints,objective,options);

    q_mpc(k,j) = value(q(1,j));
    u_mpc(k,j) = q_mpc(k,j)/nominal(j);
    T_mpc(k,j) = value(x(2,j));

    x(1,j) = x(2,j);

    end

    k
end

qlambda(:,i) = q_mpc;
Tlambd(:,i) = T_mpc;

end

figure(7)
plot(qlambda,'b')
title('Heating demand dependance on ? for the ZT1 Kitchen thermal zone, January 2^n^d and 3^r^d');
xlabel('Time [h]');
ylabel('Thermal Power [W]');
grid on
box on
set(gca,'fontsize',20,'FontName','Palatino Linotype');
xlim([1 48]);
xticks([0:2:48]);

figure(8)
plot(Tlambd-273.15,'b')
title('Indoor Air Temperature dependance on ? for the ZT1 Kitchen thermal zone, January 2^n^d and 3^r^d');
xlabel('Time [h]');
ylabel('Temperature [°C]');
hold on
plot([1:1:48],TsetpointPLOT(2:49)-273.15-2,'--r','linewidth',1);
grid on
box on
set(gca,'fontsize',20,'FontName','Palatino Linotype');
xlim([1 48]);
xticks([0:2:48]);

%% MPC implementation with the EnergyPlus co-simulation

yalmip('clear');

% Instantiate co-simulation tool
ep = mlep;

% Building simulation configuration file
ep.idfFile = 'CorTau_OneWeek_1htimestep_CoSimulation';

% Weather file
ep.epwFile = 'ITA_Torino.160590_IWEC';

```

```

% Initialize the co-simulation. This will load the IDF file.
ep.initialize;

TemperatureEP = (18+273.15)*ones(7,1);
nominal = [1117, 474, 513, 467, 176, 104, 190];    %[W]

endTime = 60*60*192;    %[s]

% Model data
TOUTDOOR = xlsread('Turin_OutdoorT_1hour timestep.csv','B2:B241') + 273.15;    %[K]

% MPC data
Np = 192;                % Prediction horizon timesteps
Nc = 5;                  % Control horizon timesteps
Q = sdpvar(Np,7);        % Decision variable
X = sdpvar(Np,7);        % Output variable
lambda = 0;              % Cost function weight variable in the range [0...1]

options = sdpsettings('solver','sedumi');
options.sedumi.maxiter = 1000;

% Initial state
X(1,1:7) = TemperatureEP;
T_MPC(1,1:7) = TemperatureEP;

% Start the co-simulation process and communication.
ep.start

% The simulation loop
t = 0;
k = 1;

TsetpointPLOT = 0;
while t <= endTime

    if t >= 60*60*24
        if t <= 60*60*31 || (t >= 60*60*45 && t <= 60*60*55) || (t >= 60*60*69 &&
t <= 60*60*79) || (t >= 60*60*93 && t <= 60*60*103) || (t >= 60*60*117 && t <=
60*60*127) || (t >= 60*60*141 && t <= 60*60*151) || (t >= 60*60*165 && t <=
60*60*175) || (t >= 60*60*189 && t <= 60*60*192)
            TSETPOINT = 18 + 273.15;
        else
            TSETPOINT = 20 + 273.15;
        end

        for j = 1:7                % Cycle to go through all the thermal zones
            constraints = [];
            objective = 0;

            for m = 1:Nc            % Control Horizon - 5 timesteps
                X(m+1,j) = A(j)*X(m,j) + B(j)*Q(m,j) + C(j)*TOUTDOOR(k+m-1);
                if m == 1
                    objective = objective + (1-lambda)*((X(m+1,j)-
TSETPOINT)^2/20^2) + ...
                        (lambda)*((Q(m,j))^2)./(nominal(j))^2;
                else
                    objective = objective + (1-lambda)*((X(m+1,j)-
TSETPOINT)^2/20^2) + ...
                        (lambda)*((Q(m,j)-Q(m-1,j))^2)./(nominal(j))^2;
                end
                constraints = [constraints, 0 <= Q(m,j) <= nominal(j),
X(m+1,j) <= TSETPOINT+2];
            end
        end
    end
end

```

```

        optimize(constraints,objective,options);

        qMPC(k,j) = value(Q(1,j));
        uMPC(k,j) = qMPC(k,j)/nominal(j);
        T_MPC(k,j) = value(X(2,j));

        X(1,j) = X(2,j);
    end

    % Send inputs to EnergyPlus
    ep.write(uMPC(k,:),t);

    % Get outputs from EnergyPlus
    [TT, t] = ep.read;

    T_EPLUS(k,:) = TT(2:end) + 273.15;      % [K]
    X(1,:) = TT(2:end) + 273.15;          % [K]
    k = k+1

    TsetpointPLOT = [TsetpointPLOT,TSETPOINT];
else
    % Send inputs to EnergyPlus
    ep.write(zeros(1,7),t);

    % Get outputs from EnergyPlus
    [TTJanuary1, t] = ep.read;
end

end

%Stop the communication process
ep.stop;

figure(9)
plot([1:1:168],T_EPLUS(1:end-1,:)-273.15,'linewidth',1)
title(['Indoor Air Temperature computed by the MPC with ? = ',num2str(lambda),' ',
January 2^nd to 8^th]);
xlabel('Time [h]');
ylabel('Temperature [°C]');
grid on
box on
set(gca,'fontsize',20,'FontName','Palatino Linotype');
hold on
legend('ZT 1 Kitchen', 'ZT 2 Living Room', 'ZT 3 Night Area', 'ZT 4 Studio', 'ZT
5 Bathroom 1', 'ZT 6 Bathroom 2', 'ZT 7 Bathroom 3','location', 'best');
xlim([1 168]);
xticks([0:24:168]);
plot([1:1:168],TsetpointPLOT(2:end)-273.15-2,'--r','linewidth',1);
plot([1:1:168],TsetpointPLOT(2:end)-273.15+2,'--r','linewidth',1);

figure(10)
plot([1:1:168],qMPC(1:end-1,:), 'linewidth',1)
title(['Heating demand computed by the MPC with ? = ',num2str(lambda),' ', January
2^nd to 8^th]);
xlabel('Time [h]');
ylabel('Thermal Power [W]');
grid on
box on
set(gca,'fontsize',20,'FontName','Palatino Linotype');
legend('ZT 1 Kitchen', 'ZT 2 Living Room', 'ZT 3 Night Area', 'ZT 4 Studio', 'ZT
5 Bathroom 1', 'ZT 6 Bathroom 2', 'ZT 7 Bathroom 3', 'location', 'best');
xlim([1 168]);
xticks([0:24:168]);

```

```

% Radiation data
Ibeam = xlsread('CorTauResults_Original.xlsx','D26:D193');
Idiff = xlsread('CorTauResults_Original.xlsx','C26:C193');
Irefl = xlsread('CorTauResults_Original.xlsx','E26:E193');
Itot = Ibeam+Idiff+Irefl;

figure(11)
hold on

yyaxis left
plot(TOUTDOOR(25:192)-273.15,'linewidth',1.5);           % Outdoor temperature
[°C]
plot(T_EPLUS(1:end-1,1)-273.15,'linewidth',1.5);       % Indoor temperature
[°C]
ylabel('Temperature [°C]');

yyaxis right
plot([1:1:168],Itot,'r','linewidth',1.5)
ylabel('Total Irradiance [W/m^2]');

xlim([1 168]);
xticks([0:24:168]);
title('Influence of the outdoor temperature and solar radiation on T_i_n_d_o_o_r
in free-running conditions');
grid on
box on
set(gca,'fontsize',20,'FontName','Palatino Linotype');

legend('Outdoor air temperature','ZT1 Kitchen Indoor air temperature')

hold off

qpersurface = zeros(169,7);
for j = 1:7
    qpersurface(:,j) = qMPC(:,j)/surface(j);
end

figure(12)
plot([1:1:168],qpersurface(1:end-1,:), 'linewidth',1)
title(['Heating demand computed by the MPC with ? = ',num2str(lambda),' January
2^n^d to 8^t^h']);
xlabel('Time [h]');
ylabel('Thermal Power [W/m^2]');
grid on
box on
set(gca,'fontsize',20,'FontName','Palatino Linotype');
legend('ZT 1 Kitchen', 'ZT 2 Living Room', 'ZT 3 Night Area', 'ZT 4 Studio', 'ZT
5 Bathroom 1', 'ZT 6 Bathroom 2', 'ZT 7 Bathroom 3', 'location', 'best');
xlim([1 168]);
xticks([0:24:168]);

%% NEDSTACK FCS 7-XXL

I = [40,80,120,160,200,230]';      % [A]
V = [39,37,35,33,31,30]';          % [V]
Area = 200;                        % Fuel Cell cross surface [cm2]
j = I/Area;                        % Current Density [A/cm2]

% Polarization curve fitting parameters
a = 7.157;      % [V]
b = 0.5747;     % [V]
R = 8.639;      % [ohm/cm2]

```

```

% Polarization curve plot
Iplot = [0:10:230]; % [A]
jplot = Iplot/Area; % [A/cm2]
Vplot = 47-(a+b*log(jplot))-R*jplot; % [V]
Vplot(1) = 47;

figure(13)
plot(jplot,Vplot,'linewidth',1.5)
hold on
plot(j,V,'o','linewidth',1.5)
hold on
plot((0:0.1:1.2),47*ones(13,1),'k--','linewidth',1.5)
title('V-I Polarization curve fitting for the NEDSTACK FCS 7-XXL stack')
xlabel('Stack current density j (A/cm^2)');
ylabel('Stack voltage (V)');
grid on
box on
set(gca,'fontsize',20,'FontName','Palatino Linotype');

figure(14)
plot(Iplot,Iplot.*Vplot/1000,'linewidth',1.5)
title('Power curves for the NEDSTACK FCS 7-XXL stack')
hold on
plot(Iplot,(47-Vplot).*Iplot/1000,'linewidth',1.5);
xlabel('Fuel cell stack current I_s_t_a_c_k (A)');
ylabel('Fuel cell stack power (kW)');
legend('Stack electrical power','Stack thermal power')
grid on
box on
set(gca,'fontsize',20,'FontName','Palatino Linotype');
xlim([0 230])

Qth_total = sum(qMPC,2); %Sum up the contributions to the demand from all the
thermal zones

% Evaluation of the cell stack current from the thermal power
for k = 1:length(Qth_total)

    syms jj

    % Qthermal = ((a+b*log(j))+R*j)*jj*Area;
    eqn = ((a+b*log(jj))+R*jj)*jj*Area - Qth_total(k) == 0;

    S(k) = solve(eqn,jj); % [A/cm2]

end

Electrical_Power = S.*Area.*(47-(a+b*log(S))-R*S); % [W] One stack
Vcell = (47-(a+b*log(S))-R*S)/48; % [V/cell] Voltage
of a single cell (as this stack has 48 cells)

H2Rate = 1.05*1e-8*(Electrical_Power)./Vcell.*3600; % [kg/h/cell]
H2Rate = H2Rate/0.07078*48; % [lt/h]

figure(15)
bar(H2Rate)
title('Total Hydrogen consumption rate for one NEDSTACK FCS 7-XXL fuel cells'
stack')
xlabel('Time (h)');
ylabel('H_2 rate (lt/h)');
grid on
box on
set(gca,'fontsize',20,'FontName','Palatino Linotype');

```

```
xlim([1 168]);
xticks([0:24:168]);

ElectricityDemand = xlsread('CorTauResults_Original.xlsx','AU26:AU193');

figure(16)
bar(Electrical_Power)
hold on
bar(ElectricityDemand)
title('Building electrical demand and NEDSTACK FCS 7-XXL fuel cells'' stack
generation')
xlabel('Time [h]');
ylabel('Power [W]');
legend('Stack generation','Building demand');
grid on
box on
set(gca,'fontsize',20,'FontName','Palatino Linotype');
xlim([1 168]);
xticks([0:24:168]);

figure(17)
bar(Qth_total)
title('Thermal power production from one NEDSTACK FCS 7-XXL fuel cells'' stack')
xlabel('Time [h]');
ylabel('Power [W]');
grid on
box on
set(gca,'fontsize',20,'FontName','Palatino Linotype');
xlim([1 168]);
xticks([0:24:168]);
```